UNIVERSITY OF THE PHILIPPINES
OPEN UNIVERSITY

MASTER OF ENVIRONMENT AND NATURAL RESOURCES MANAGEMENT

KHIM CATHLEEN M. SADDI

BIOLOGICAL PUMP POTENTIAL: A PLANKTON SPATIO-TEMPORAL MODELING IN THE PHILIPPINE SEA WITH EMPHASIS ON THE EFFECTS OF TYPHOONS

Special Problem Adviser:

LENI YAP-DEJETO, Ph.D.
Faculty of Management and Development Studies

21 August 2025

Permission is given for the following people to have access to this Special Problem, subject to the provisions of applicable laws, the provisions of the UP IPR policy and any contractual obligations:

Invention (I)	□ Yes or □ No
Publication (P)	□ Yes or □ No
Confidential (C)	□ Yes or □ No
Free (F)	✓ Yes or □ No

Student's signature:

Special Problem adviser's signature:

University Permission Page

BIOLOGICAL PUMP POTENTIAL: A PLANKTON SPATIO-TEMPORAL MODELING IN THE PHILIPPINE SEA WITH EMPHASIS ON THE EFFECTS OF TYPHOONS

I hereby grant the University of the Philippines a non-exclusive, worldwide, royalty-free license to reproduce, publish and publicly distribute copies of this Academic Work in whatever form subject to the provisions of applicable laws, the provisions of the UP IRR policy and any contractual obligations, as well as more specific permission marking on the Title Page.

Specifically, I grant the following rights to the University:

a. *Upload a copy of the work in the special problem database of the college/school/institute/department and in any other databases available on the public internet;*
b. *Publish the work in the college/school/institute/department journal, both in print and electronic or digital format and online; and*
c. *Give open access to the work, thus allowing "fair use" of the work in accordance with the provisions of the Intellectual Property Code of the Philippines (Republic Act No. 8293), especially for teaching, scholarly and research purposes."*

08/21/25
KHIM CATHLEEN M. SADDI

Acceptance Page

This Special Problem titled: **"BIOLOGICAL PUMP POTENTIAL: A PLANKTON SPATIO-TEMPORAL MODELING IN THE PHILIPPINE SEA WITH EMPHASIS ON THE EFFECTS OF TYPHOONS"** is hereby accepted by the Faculty of Management and Development Studies, U.P. Open University, in partial fulfillment of the requirements for the degree Master of Environment and Natural Resources Management.

_____ 08/22/2025

PROF. LENI YAP-DEJETO, Ph.D.
Faculty-in-Charge, ENRM 290 (Special Problem) (Date)

_____ 9 September 2025

ASST. PROF. KARL ABELARD L. VILLEGAS, JR.
Program Chair (Date)

ASSOC. PROF. FINAFLOR F. TAYLAN, DProfSt
Dean
Faculty of Management and Development Studies

09 September 2025
(Date)

DECLARATION

This is to certify that:

I. The Special Problem comprises only my original work towards the MENRM except where indicated in the Preface.

II. Due acknowledgment has been made in the text to all other material used.

III. The Special Problem is fewer than 25,000 words in length, exclusive of tables, maps, bibliographies and appendices.

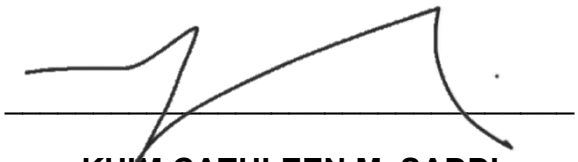

KHIM CATHLEEN M. SADDI

Acknowledgment

The author would like to express deep gratitude to Dr. Leni Yap-Dejeto for extending all the support as the adviser. It all started that semester when COVID-19 hit, and the rest is history.

To the author's family, and friends, for all the love and unending cheering on the side.

Special thanks to Nerona and Floridiana who served as my lucky charms during the final edit of this manuscript.

The author also wishes to thank Dr. Mari for the never-ending inspiration. She will meet you soon.

Dedication

Dedicated to:

All the girls who dream to sail.

Table of Contents

List of Figures

List of Tables

List of Appendices

Abstract

Current carbon sequestration technologies are not meeting targets to deliver the 2050 global net zero goal. Hence, there is an increase in campaigns for nature-based solutions (NBS) rather than depending on engineered sequestration technologies, which is by far harder to scale up. Though amplifying the NBS that are already inherent in the environment is a matter of increased activities, the current changing climatic conditions complicates this, such as site-targeted mangrove rehabilitation, regenerative forestry, and restorative agriculture. These land-based solutions comprise approximately half of the global total carbon sequestered, while the other 50% are the materials that naturally sink in the depths of the ocean.

Harnessing the potential of ocean productivity is a huge leap in the world's carbon sequestration thrust. Not only does this process happen in the natural world, but quantification, monitoring, and forecasting activities can aid future policymaking to amplify productivity in our ocean–which is also expected to serve as a driver to the placement of programs geared toward water quality preservation, conservation, and treatment in inland waters. This study focuses on the quantification and forecasting of the Biological Pump potential in the Philippine Sea, specifically inside the Exclusive Economic Zone (EEZ). Variabilities and disturbances such as increased sea surface temperature, and considering the geographic location of the Philippines, receiving high frequency of annual typhoons, were investigated to affect ocean productivity. Spatio-temporal maps were generated to provide visualization for the trends and phenomena before, during, and after typhoon occurrence for the years 2019 until 2021. The normal scenario for typhoons was reflected in 2019 while both 2020 and 2021 recorded rare high-intensity super typhoons Rolly (Goni) and Odette (Rai), respectively. NASA Ocean Biology Processing Group (OBPG) Ocean Color data were used to produce

spatiotemporal maps for both chlorophyll (CHL) and Sea surface temperature (SST). Correlating these maps with typhoon occurrence, and SST, the Biological Pump potential annual estimate was generated.

Keywords: image processing, biological pump potential, environmental monitoring, remote sensing, forecasting planktons, plankton carbon sequestration

I. INTRODUCTION

One of the main challenges of the climate crisis is the available carbon sequestration technologies which currently fail to meet targets. Still, the global ambition to achieve a net-zero by 2050 is continuously being pushed by different sectors throughout the world. However, despite the increase in renewables in the global energy mix, it was recorded that just the past decade, the global energy-related emissions increased by about 5 percent (1.7 $GTCO_2$) which can be mainly attributed to growing energy demand (McKinsey, 2023). Though there are already various policies to cut emissions and green economy transition plans which were laid out through the Nationally Determined Contributions (NDCs) submitted by each country after the Paris Agreement, these are still 0.99 and 2.92 GT CO_2 lower than their previous pledges for 2025 and 2030 (UNCC, 2021). There is an urgent need to ramp up NDCs with new carbon sequestration technologies that are inherent in the environment already. However, the huge potential of the ocean's blue carbon is often overlooked.

Background of the Study

In regulating the atmospheric CO_2 concentration, the ocean plays a vital role in the Earth's carbon cycle (Brewin et. al., 2021). There are six (6) ocean biological carbon pumps (OBCPs) that comprise the downward pumping of biogenic carbon to the deep ocean (Claustre et al., 2021), estimated to be between 5 and 14 Pg C y^{-1} (Laws et al., 2000; Najjar and Keeling, 2000). These include the Mixed layer pump, the Eddy Subduction pump, the Large-scale Subduction pump, the Ekman pumping, and animal mediated pumps, and the vertical migration of zooplankton (Boyd et al.,

2019). Some animals like fish and jellyfish, which are larger than zooplankton may also contribute to these animal-mediated pumps (Pinti et al., 2023).

Apart from fisheries-related activities, plankton plays an active role in the natural carbon sequestration framework by providing primary services to the global carbon and nutrient cycle (Behrenfeld et al., 2001). Often called "drifter", plankton relates to all organisms inhabiting aquatic environments which are not capable of horizontal maneuver in the water column. Specifically, phytoplankton are photosynthetic organisms with a large variety of taxa (Merz et al., 2021) which can serve as a bioindicator for water quality. Hence, the importance in conducting assessments of the plankton composition to forecast potential algal blooms which cause huge ecological and economic losses (Huisman et al., 2018) which seems to be globally increasing because of climate change (Ho et al., 2019; Chorus and Welker, 2021). Since ocean warming may fast-track growth and decomposition of microorganisms which could lead to direct export of carbon into the atmosphere (Laws et al., 2000), it is important to develop advanced carbon cycle satellite methods (Siegel et al., 2016), which could be effectively understood with space and time scales.

Phytoplankton often estimated using chlorophyll-a (CHL-a) photopigment (Wright et al., 1991), also serves as a key indicator of at least half of the globally photosynthetically carbon comprising the net primary production (NPP) which drives the biogeochemical cycle (Falkowski et al., 1998). This productivity that happens near the ocean surface exports carbon into the seafloor which is generally considered as blue carbon. Interest in the dynamics of NPP in the context of climate change (Tagliabue et al., 2021) has brought the focus on monitoring NPP using advanced methods such as remote sensing (Kulk et al., 2020).

Presently, various techniques have been conducted to monitor and understand the dynamics of these processes in space and time, which is also critical in global climate processes (Bianchi et al., 2005). In addition, the potential of using remote sensing to expand monitoring, as seen in traditional ship-based NPP measurements (Carr et al., 2006; Milutinović and Bertino, 2011), from points to the entire surface ocean (Brewin et. al., 2021), presents a viable and low-cost option as such in other environmental monitoring applications.

In addition, the frequency of typhoons, such as in the Philippines brought by its geographical location, can also have positive effects on biodiversity (Kubota et al., 2004; Wang et al., 2008). However, the exacerbating effects of climate change are driving climate extremes including increased typhoon intensity (27-38% of tropical cyclones in 2019-2021 are classified as typhoons, cyclones with wind speed of 118-184 kph) and lower return period of super typhoons (e.g. Typhoon Yolanda in 2013 and Rolly in 2020) (PAGASA-DOST, 2023). The effects of this phenomenon under a changing climate are yet to be fully understood in order to optimize marine productivity monitoring and development efforts.

Significance of the Study

The ocean carbon sequestration takes off in the primary production as CO_2 is converted to phytoplankton tissues through photosynthesis. This is the engine of the OBCP that occurs in the euphotic zone, the surface ocean that receives light (Field et al., 1998), hence the main focus of this study. This study is important to various stakeholders and the world in tackling the climate crisis, specifically to the following:

Academe/Researchers - The insights generated from this study may contribute to the present carbon sequestration study gaps.

PAGASA-DOST - The insights from this study may open new avenues for the research agenda on Blue Carbon and nature-based solutions which may fuel the green economy in the Philippines.

Government/LGUs - The Philippine government may develop new policies that may support blue carbon sequestration from the results of this study, especially localized community-based interventions.

Coastal Communities - The activities and projects that may arise from the insights of this study may benefit in capacitating local communities to push for sustainable practices and overall coastal resilience.

Conceptual Framework

There have been previous studies that successfully presented sophisticated models of marine productivity using Satellite-Derived Phytoplankton Absorption data like in the studies of Milutinović and Bertino (2011) and Ma et al. (2014). Despite these models, it was well affirmed that Chlorophyll-a reflects the green pigment while carotenoids reflect the red pigment in plants (Clementson and Wojtasiewicz, 2019), hence CHL-a data still presents a good initial indicator of productivity with less complexity. This study utilized NASA Satellite data, machine learning, and image processing techniques to produce the spatio-temporal maps and explore NPP estimation in the Philippine Sea.

Figure 1. Conceptual framework.

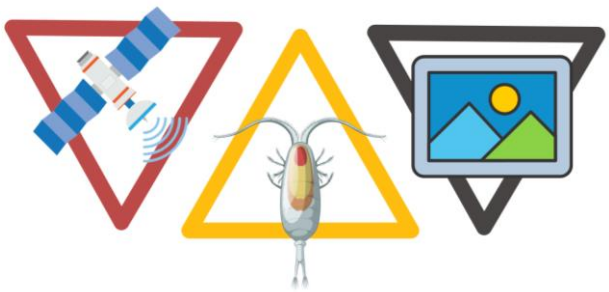

II. REVIEW OF RELATED LITERATURE

This chapter presents a literature review about plankton and remote sensing, as well as highlighting the knowledge gaps that need to be addressed in the identification of plankton productivity in space and time.

Remote Sensing Plankton

A global study on hyperspectral remote sensing reflectance groups five pigments and were assumed to represent various phytoplankton species such as diatoms, dinoflagellates, haptophytes, green algae, and cyanobacteria. It was found that the resulting thirteen (13) pigments from the reflectance dataset can be grouped into the original five (5) pigment groups. Accordingly, the spectral gap hypothesis that phytoplankton signals are useful for characterizing the pigment was affirmed and that principal components regression modeling posed as an effective tool to retrieve phytoplankton pigment composition from hyperspectral remote sensing data (Kramer et al., 2022).

One study automated in-situ measurements of zooplanktons and phytoplankton by incorporating a Dual Scripps Plankton Camera (DSPC). Except for zooplankton properties, using a dark-field microscope, data gathered through DSPC were found to be similar with data from traditional sampling. Further, it was found that due to the high temporal resolution available, this approach performed better in gathering the dynamics and demography of heterogeneously distributed zooplanktons. Least-squares linear regressions were used to correlate the data from DSPC and lab measured data (Merz et al., 2021).

In another study, the impact of the COVID-19 lockdown to the phytoplankton development using chlorophyll-a concentrations in Kuwait Bay (Persian Gulf) were

assessed using Sentinel data from 2018 to 2020 as compared to *in situ* data. It was also affirmed that the use of remote sensing provided an opportunity for fast analysis that could aid decision making processes specifically in times of crisis. However, the study pointed out that there shall be a region-specific remote sensing infrastructure present to sustain and validate global data models (Polikarpov et al., 2021).

Another study on the Persian Gulf highlighted the spatio-temporal variability of phytoplankton for a period of 23 years. It was found that generally, the wind mixings and the stratification of water layers during the summer affects the phytoplankton penology. This further puts emphasis on the vulnerability of productivity to global warming. Satellite-derived Ocean color chlorophyll-a data from 1998 to 2020 was generated and k-means clustering was performed. There were two clusters identified at the end of the study, 1) minimum in April-July and maximum in December-February, and 2) a minimum in March and maximum in September-October (Zoljoodi et al., 2022).

Global ocean net primary production (NPP) a proposed phytoplankton pigment absorption a_{ph}-based model was derived from satellite data and was later compared to existing NPP models which are chlorophyll-based and carbon-based. Surprisingly, the proposed model improved the accuracy in describing NPP variation and which is more similar with the carbon-based than the chlorophyll-based model (Ma et al., 2014).

Further, the uncertainties in using the Vertically Generalized Productivity Model for NPP quantification were analyzed in another study. A minimal overestimation of around 6% of the global NPP was observed. This is highly attributed to the physiological state description of phytoplankton and the depth variability of the normalized photosynthesis, since the ocean color data is restricted to a limited

threshold in the water column, which were highly recommended to improve in future work (Milutinović and Bertino, 2011).

Advantages of Remote Sensing Ocean Data

Remote sensing has the capacity to monitor the global ocean considering space and time for years already (Brewin et al., 2021), with at least 30-m (Landsat 8), and 10-m (Sentinel 2) at most, available resolutions (NASA, 2012; ESA, 2020), which are readily available and free. These sensors collect spectral data from the ocean surface and provide characteristics which can be discriminated against water, such as the presence of phytoplankton (Kirk, 1994). Literature suggests that the NPP quantification based on remote sensing data provides a better representation of space and time variability of plankton productivity than interpolating traditional *in situ* data (Friedrichs et al., 2009). In addition, the introduction of Sentinel 2 twin satellites, in coordinated orbits, narrows the time gap of revisit, providing more coverage and better time scale insight.

Limitations of Remote Sensing Ocean Data

However, the accuracy of remote sensing data is currently limited to the spatial resolution of the sensors available. Since even though there is an increased presence of commercial satellite data with higher spatial resolution, such as GeoEye (0.41 m for panchromatic data and 1.65 m for 4-band multispectral) (ESA, 2012), NASA and ESA products remain to be the widely used data due to its historical coverage and wide availability at no cost.

The use of satellite data is widely used in ocean monitoring. However, regional biases might arise depending on the calibration source used for the product data

(Franz et al., 2012), in this case CHL and SST. This can be improved with setting up a regional ground truth dataset which can be used for localized data calibration.

Synthesis

Spatio-temporal mapping provides a better visualization of environmental phenomena in space and time. This approach was made possible by online repositories of time series satellite data which is freely available. There are dynamics that can only be visually observed in space and time, such as in this case, the extent of typhoon effects on ocean productivity. Hence, the importance of establishing spatio-temporal maps for qualitative, and later quantitative analyses.

There are numerous factors affecting PP such as level of pollution, salinity, SST, and water quality parameters like Phosphorus (P), Dissolved Oxygen (DO), and Nitrogen (N) content (Radwan, 2005). The portion of the Primary Production (PP) which sinks to the ocean interior or the Export Production (XP) is critical of the variability in annual and interannual seasonality (Berger and Wefer, 1990). Accordingly, analysis in space and time is required to identify the carbon fluxes in the oceanic setting (Lévy et al., 2013; Omand et al., 2015). In addition, significant increase in productivity was theorized to be associated with increased wind and mixing of warm surface waters with nutrient-rich deep cold waters during upwelling (Berger and Wefer, 1990), which is especially higher during pulse upwelling (Boyle and Keigwin, 1987). In fact, in an experimental study which simulates pulse upwelling (increased nutrient concentrations), the phytoplankton responded immediately with a 50% increase in productivity (Ferreira et al., 2020). Since it was observed that there exists a higher intermittency in regions above the equator than below, which supported the low CO_2 content in polar ice cores (Neftel et al., 1982; Barnola et al., 1987), hence, the focus of this study is in the seasonality more than ocean current processes–due to the high

frequency of typhoons in the country which also generates higher upwelling occurrences.

Moreover, there are numerous studies which developed models for ocean productivity estimation. The aim of this study is to provide an alternative labor- and cost-effective estimation methodology to initially identify hotspots for future intensive management and regenerative OBCP studies.

III. STATEMENT OF THE STUDY

The analysis of the recent literature in the domain of marine productivity reveals the current knowledge gap in ocean productivity estimation. In addition, the effects of local phenomena in ocean productivity, such as high typhoon occurrence, are still yet to be understood in different times and spatial scales.

IV. OBJECTIVES OF THE STUDY

This study aims to assess the Biological Pump Potential as a long-term natural carbon sequestration technology for the Philippines. Specifically, the study will address the following:

1. Establish Spatio-temporal maps of Phytoplankton in the Philippines using satellite images for the years 2019, 2020 and 2021.
2. Compare the Phytoplankton response to different seasonal variability in the Philippines specific to pre- and post-typhoon seasons.
3. Generate potential productivity forecast for the Philippine Biological Pump.

V. RATIONALE

There is an urgency to device action plans to reach net-zero targets by 2050, and this is mostly shared globally. But, current carbon sequestration efforts, and cutting-edge technologies still fail to deliver targets. Therefore, increased understanding of natural carbon processes, like the quantification of blue carbon, provides a huge potential boost to current carbon sequestration efforts.

VI. SCOPE AND LIMITATIONS

Utilizing remote sensing techniques, this work provided ocean productivity estimate using CHL and SST satellite data from NASA Ocean Biology Processing Group limited to the Philippine Exclusive Economic Zone (EEZ) for the period 2019-2021. Machine learning was used in data processing using Matlab and python. Qualitative analysis was also employed to understand the variability of productivity with respect to pre- and post-typhoon seasons.

VII. DESCRIPTION OF STUDY AREA

The study area covers the marine surface waters inside the Philippine Exclusive Economic Zone (EEZ). EEZ covers 200 nautical miles (370.4 km) extending from the shoreline of the land territory where a country has jurisdictions for all resources (NOOA, 2025). In the context of PH EEZ, this covers part of three seas: 1) Philippine Sea, 2) Sulu Sea, and 3) West Philippine Sea. A map showing the Region of Interest (ROI) is presented in Figure 4.

VIII. METHODOLOGY

Satellite data was extracted to visualize potential phytoplankton productivity in the Philippine Sea using Spatio-temporal maps from the NASA Ocean Biology Processing Group, an online global ocean data repository such as Chlorophyll-a (CHL) abundance, and Sea Surface Temperature (SST). Abundance was compared with climate variability specific to pre- and post-typhoon seasons. Only the Philippine Exclusive Economic Zone was considered and adjusted during data cleaning. Image Processing using Python and Matlab was conducted to generate the Spatio-Temporal 8-day maps for the years 2019-2021. Machine Learning algorithm k-nearest neighbor (KNN) was used to classify the map data and extract both the CHL and SST values based on NASA color scale.

NASA CHL & SST Data

False color representations of satellite data were extracted from the NASA Ocean Biology Processing Group (OBPG) Ocean Color website. Specifically, the maps used were 8-day data of both CHL and SST from the Level 1 & 2 browser (NASA Goddard Space Flight Center, Ocean Ecology Laboratory, Ocean Biology Processing Group, 2018). These data were produced under NASA's Earth Observing System Data and Information System (EOSDIS). NASA's CHL uses an algorithm derived from the *in-situ* measurements of CHL-a and remote sensing reflectance (Rrs) captured by satellite sensors using the band range 440 - 670 nm (NASA Goddard Space Flight Center, Ocean Ecology Laboratory, Ocean Biology Processing Group, 2018). Shown in Figure 2 and 3 the online repository of ocean color satellite data captured by Landsat 8.

Figure 2. Sample global Chlorophyll-a concentration, NASA Ocean Color data browser (2019).

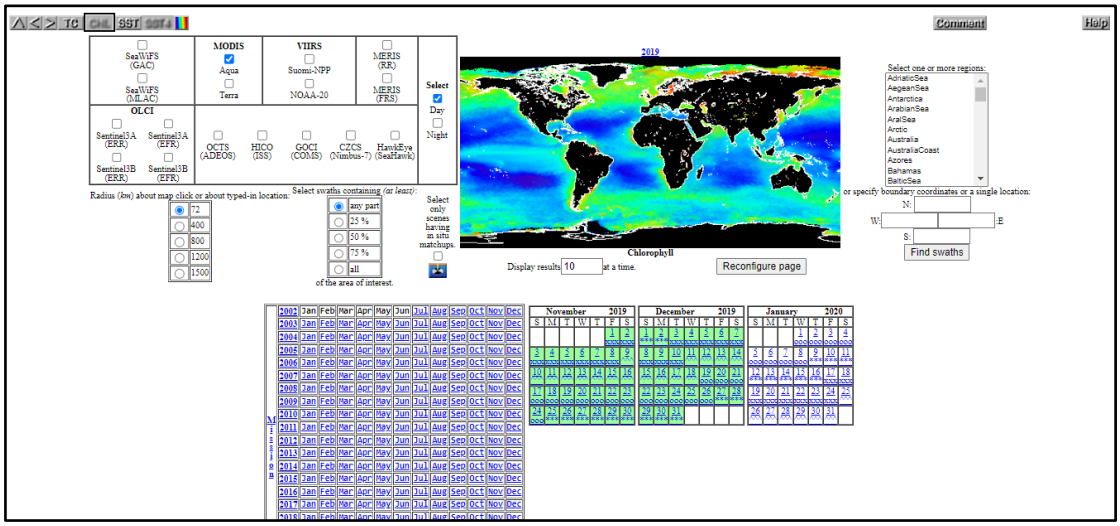

While the SST was derived from long-wave infrared (LWIR) bands in MODIS and VIIRS sensors with an algorithm based on a modified nonlinear SST algorithm developed by Walton et al. (1998) and recently, Kilpatrick et al. (2015) (NASA Goddard Space Flight Center, Ocean Ecology Laboratory, Ocean Biology Processing Group, 2018).

Figure 3. Sample global sea surface temperature, NASA Ocean Color data browser (2019).

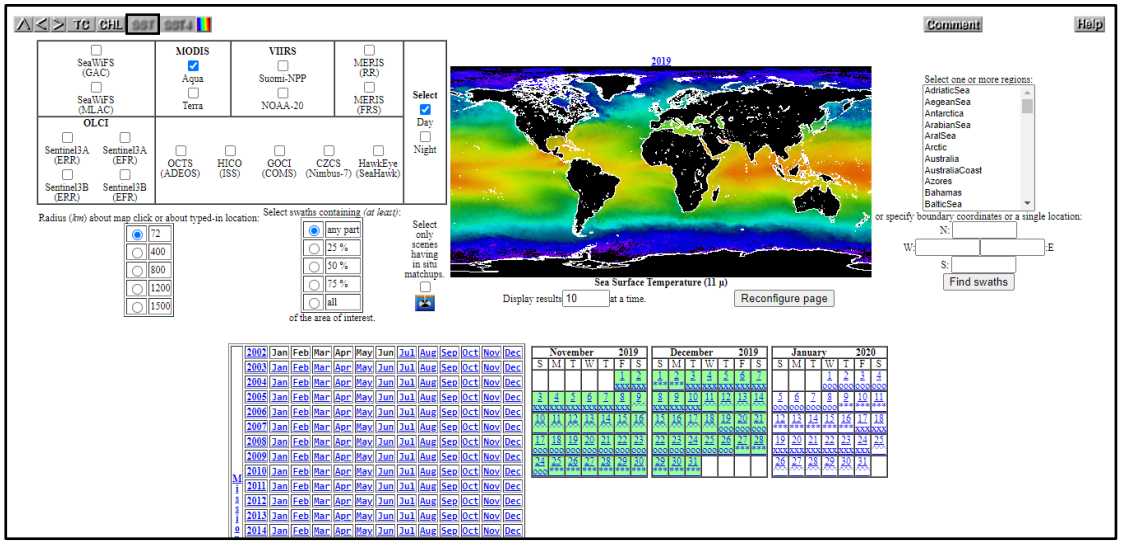

A total of 276 images (CHL and SST) for 2019-2021 were downloaded from the NASA website.

Image Processing

In order to harmonize the data capture, the Philippine Map was overlaid all through the downloaded false color images. The Region of Interest (ROI) was chosen as a square area enclosing the Philippine EEZ, thus the rectangular images were cropped. The coordinates of the four (4) transect lines (also representing four quadrants, Q1-Q4) were used to extract the RGB data of all PH 75x75 px images for both CHL and SST as shown in Figure 4. In addition, the cloud cover, represented by black pixels, were all replaced by non-black neighboring pixels, limited to the PH EEZ ROI only, as shown in Figure 5.

Figure 4. Map showing the Region of interest (ROI), transect lines, and PH EEZ.

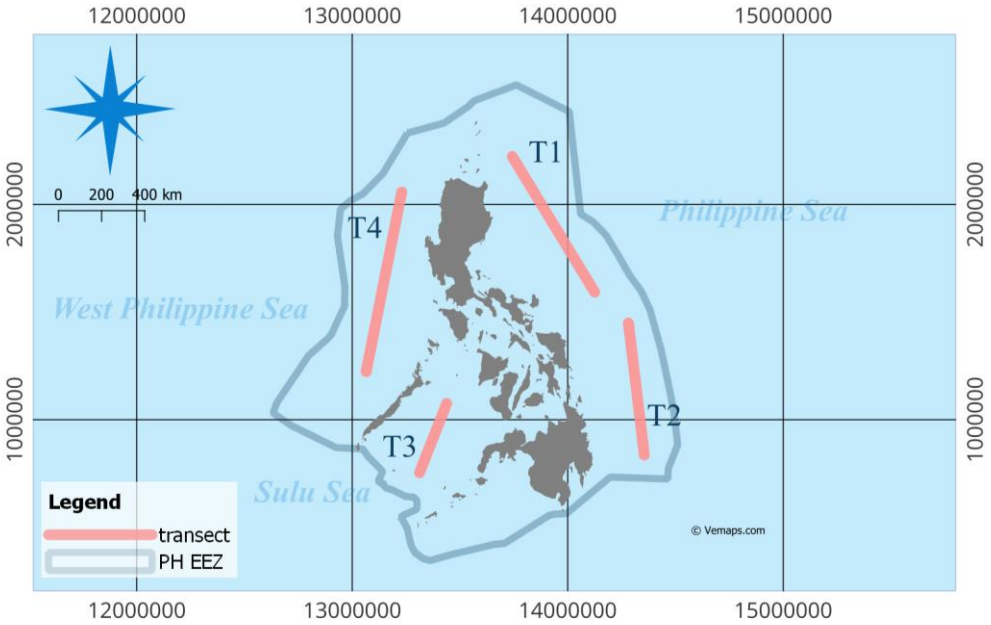

Figure 5. Sample 75x75 CHL spatio-temporal map a) original, and b) cleaned cloud cover.

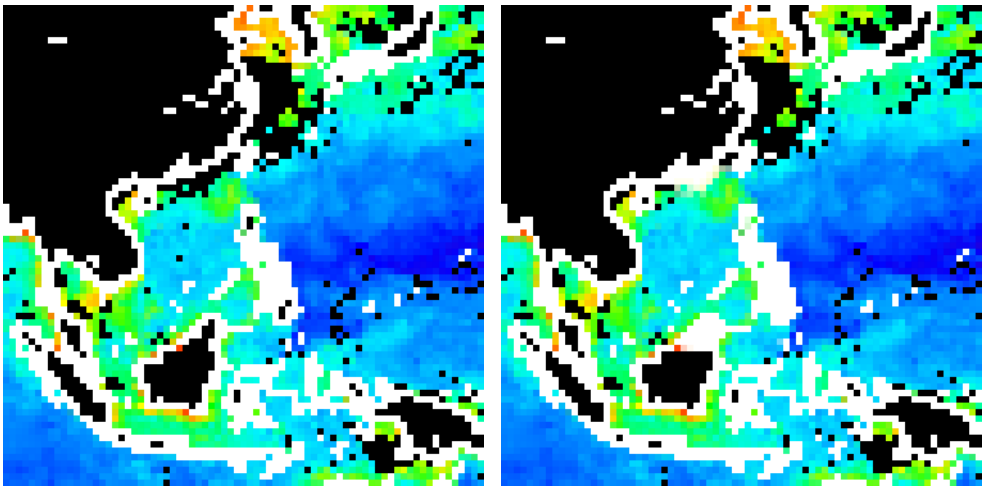

(a) (b)

These RGB data served as the input data for the KNN classifier which returns the nearest CHL and SST values of each RGB combination, based on the NASA colorscales. Matlab and Python were used for image processing and machine learning. The workflow of the image processing and KNN classification is shown in Figure 6.

Figure 6. Image processing and classification workflow.

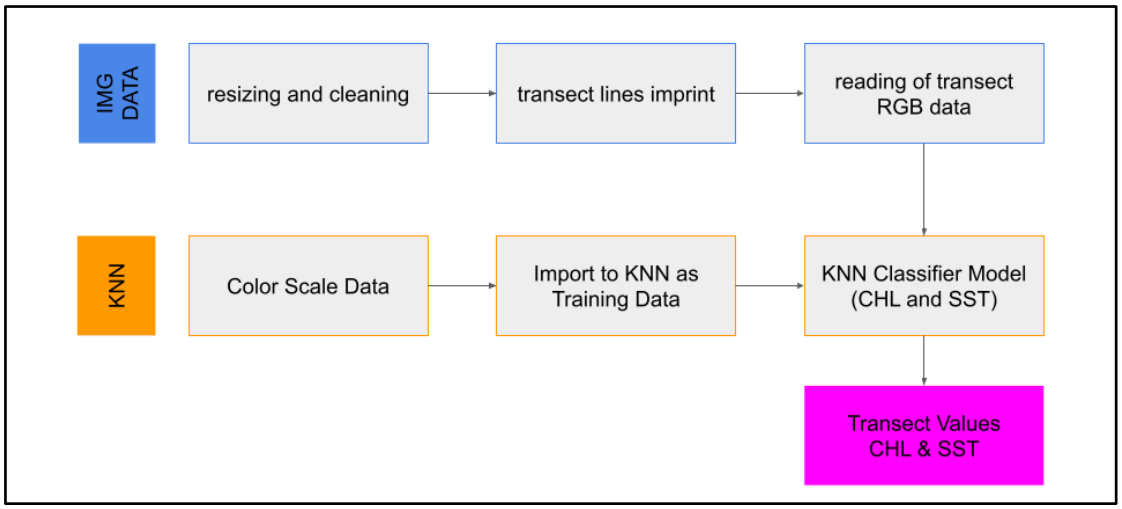

Classifying CHL and SST using KNN

The false colors reference maps are already Level 2 and 3 products. These representations of satellite data are not directly the data itself, hence the need to use KNN to retrieve both CHL and SST values based on the NASA color scales as shown in Figure 7.

Figure 7. NASA Ocean Color CHL and SST color scale.

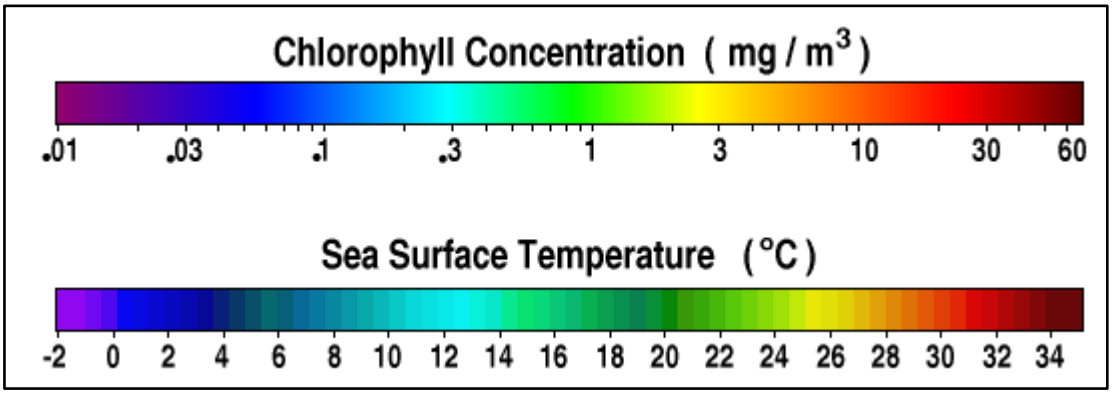

This color bar was used to derive the CHL concentration and SST of the images using a KNN classifier coded in python through Google colab notebook. The color bar RGB data serves as training data of the KNN model and uses the RGB band combination to determine the nearest value of both CHL and SST respectively (for full code, check Appendix K).

In the case of other marine productivity sources like the seagrass, there have been quantification efforts using remote sensing utilizing band indices such as the Normalized Difference Vegetation Index (NDVI), and Leaf Area Index (LAI) (Dierssen et al., 2003).

Mapping of Philippine Typhoons for 2019-2021

To simplify analysis of the plankton productivity the perimeter of the archipelago was represented by 4 transect lines (T1-T4) representing four quadrants covering the Philippine Sea, West Philippine Sea and Sulu Sea as shown in Figure 4.

Table 1

Notable Typhoons for 2019-2021

Year	Cyclone Classification	Name	Period		Wind Speed (Kph)
2019	T	HANNA	8/3/2019	8/9/2019	250
2019	T	LIWAYWAY	9/1/2019	9/5/2019	220
2019	T	TISOY	12/1/2019	12/5/2019	215
2020	T	JULIAN	8/28/2020	8/31/2020	205
2020	T	KRISTINE	8/31/2020	9/5/2020	230
2020	T	QUINTA	10/23/2020	10/27/2020	305
2020	ST	ROLLY	10/27/2020	11/3/2020	315
2020	T	ULYSSES	11/8/2020	11/13/2020	205
2021	T	BISING	4/12/2021	4/24/2021	315
2021	T	KIKO	9/7/2021	9/12/2021	280
2021	T	ODETTE	12/12/2021	12/19/2021	280

Typhoon track maps for years 2019-2021 were created using QGIS Firenze version 3.28 from PAGASA-DOST typhoon tracks bulletin (PAGASA-DOST, 2023), sample shown in Figure 8.

Figure 8. Sample typhoon data, PAGASA-DOST (2023).

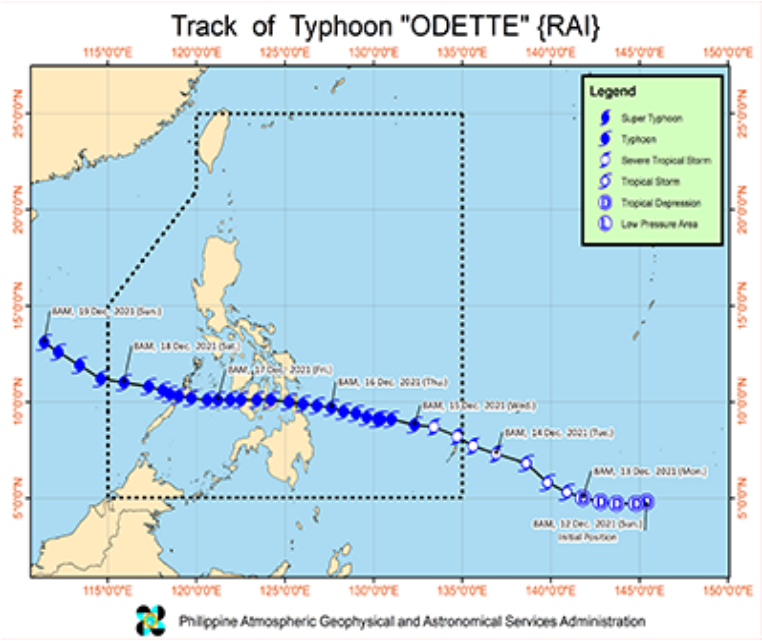

Relationship of CHL with SST and Typhoon Occurrence

Spatio-Temporal CHL abundance was compared with SST variability and typhoon occurrence (before, during and after) to look for trends, both short- and long-term periods. CHL and SST linear relationships were also checked for possible correlations. Then, the CHL and SST correlations were generated using a linear regression data tool in MS Excel.

Validating the NASA CHL product with in-situ data

To understand the limitations of utilizing remote sensing for NPP Estimation, the NASA CHL product data were compared with in-situ measurements taken in 2011 from a global CHL in situ dataset (Valente et al., 2022). The search coordinates from the global dataset were 25°N 105°E and 1°N, 135°E respectively. Since the sentinel mission was not yet commissioned by this time, all Copernicus products are also based with the Landsat MODIS and other related missions, hence, other satellite product comparisons would be irrelevant.

Estimating NPP using CHL, SST and Vertically Generalized Production Model (VGPM)

The Vertically Generalized Production Model (VGPM), a widely used NPP model, was utilized to generate the NPP in all four quadrants of the Philippine EEZ following the transect assignment. VGPM was first described by (Behrenfeld and Falkowski, 1997), and since then, this model was utilized and further improved such with the development of carbon-based NPP (Westberry et al., 2008). The NPP model used follows the convention of the original VGPM model, represented by equation 1.

$$npp = chl\ x\ pb\_opt\ x\ day\ length\ x\ f(irr)\ x\ z\_eu \qquad [equation\ 1]$$

Both the CHL and SST data were already previously generated. The f(irr) is the photosynthetically active radiation (PAR) function which was downloaded from the Ocean Color website (Ocean Productivity, 2024) while pb_opt is a polynomial of 7th order which varies depending on the sea surface temperature (°C) represented by equation 2. Z_eu is the euphotic depth.

$$\begin{aligned} pb\_opt = {} & -3.27x10^{-8} * sst^7 + 3.4132x10^{-6} * sst^6 \\ & - 1.348x10^{-4} * sst^5 + 2.462x10^{-3} * sst^4 \\ & -2.05x10^{-2} * sst^3 + 6.17x10^{-2} * sst^2 \\ & + 2.749x10^{-1} * sst + 1.2956 \end{aligned} \qquad [equation\ 2]$$

IX. RESULTS

This chapter discusses the findings and summarizes the results of the study, providing emphasis on the Spatio-Temporal Maps and its relationship with Typhoon tracks and SST. The NPP estimation was also presented.

Spatio-Temporal Maps

High productivity occurs mainly in the West Philippine Sea, near Palawan and in land waters between Mindanao as shown in the sample map in Figure 8 (for complete CHL and SST maps, check Appendix B-G).

Figure 9. Sample CHL spatio-temporal map, 2020.

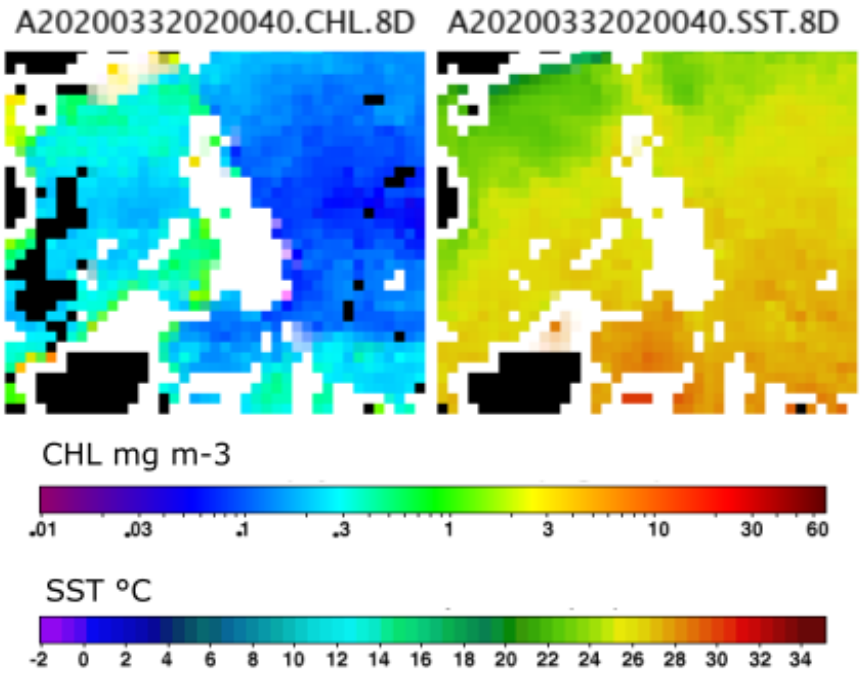

Interestingly, in the deeper oceans (Philippine Sea, along Q1 and Q2) with high salinity, productivity is less than the shallower oceans (West Philippine Sea, along Q3 and Q4), though, in the case of the Baltic Sea, there seems to be a coupled upwelling-downwelling zone just off the coast (Myrberg and Andrejev, 2003).

Typhoon Track Maps

Shown in Figure 10 and 11 the Philippine Tropical Cycle tracks for the years 2019-2021. The typhoon season in the Philippines usually begins by June but typhoons may occur as early as January, just like in the year 2019. However, in 2020, PAGASA started naming local typhoons starting only in the month of May, with high intensity typhoons occurring in the last quarter of the year and primarily in Luzon and Visayas. The opposite can be said for 2021 with typhoons both for 3rd and 4th quarter but mostly in the Visayas and Mindanao area. High intensity Typhoons occur in Luzon (2019), Luzon and Visayas (2020) and Visayas and Mindanao (2021) with as fast as over 250 kph, 315 kph, and 280 kph respectively. In fact, back in 2020, there was even a series of typhoons which hit the Bicol Region in a span of only 3 weeks, led by the infamous Super Typhoon Rolly.

Time series plots for CHL, SST, and Typhoon occurrence

Presented in Figure 12, the time series plots showing CHL, SST, and typhoons for period 2019-2021 in the four transects (T1-T4). Contextualizing with the Dry and Rainy Seasons in the Philippines, peak CHL levels was generally observed in all transects in the cool dry season (December-February), decreasing levels during hot dry season (March – May), and lowest levels occurred during the rainy season (June to November). Variabilities in these trends occurred mostly during the rainy season specifically in T3 and T4. A boost in CHL levels was observed in T3 for 2019 during the rainy season without a related typhoon occurrence. Which is also similar in T4 for 2021, also during the rainy season.

SST levels in T3 and T4 are generally higher than T1 and T2. Lowest levels for all transect were observed during the cool dry season, increasing levels during the hot dry season, and peak levels during the rainy season in all transects.

Figure 10. Philippine tropical cyclone tracks classified by quarter occurrence (2019-2021).

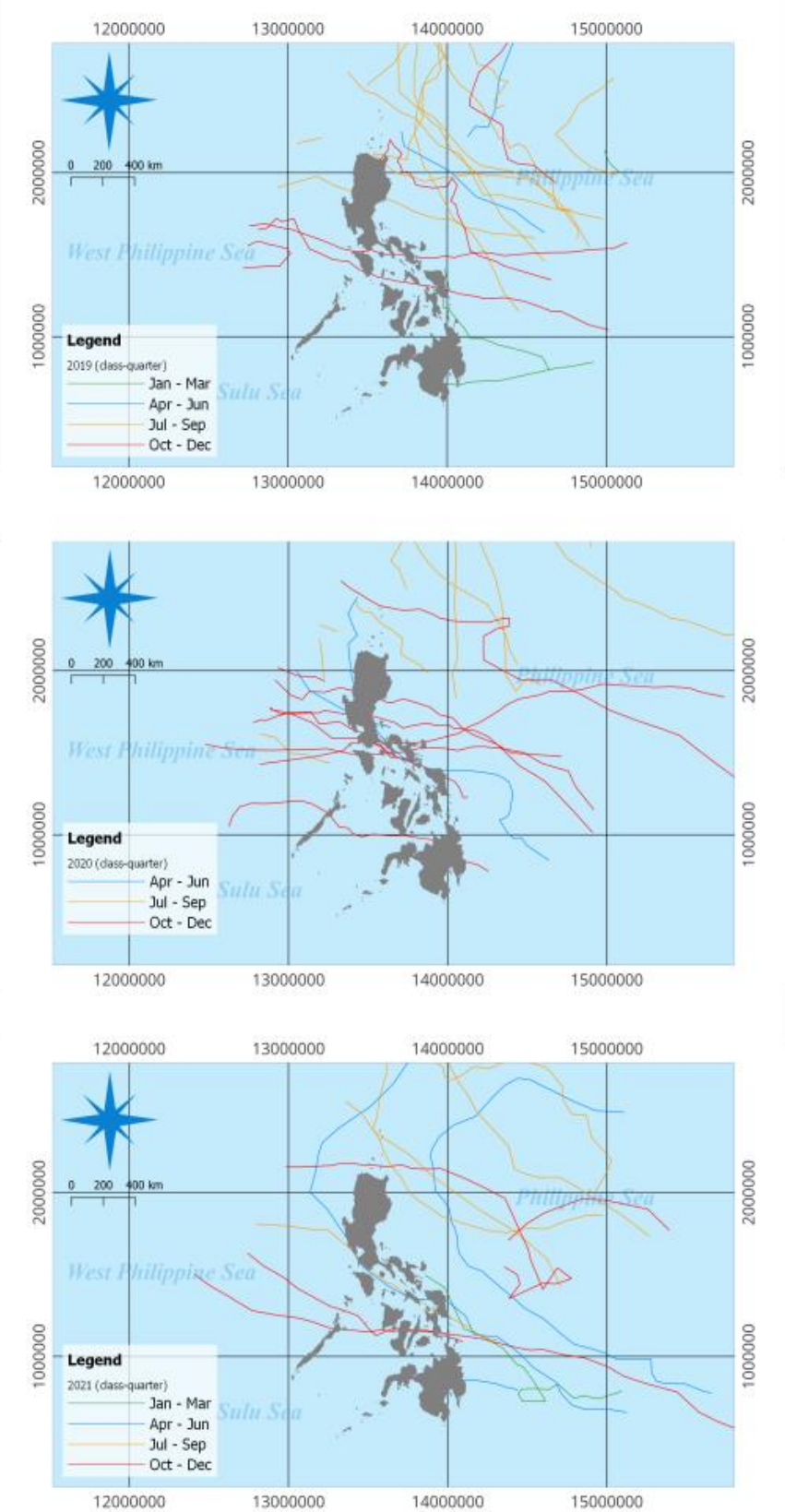

Figure 11. Philippine tropical cyclone tracks classified by maximum wind speed (2019-2021).

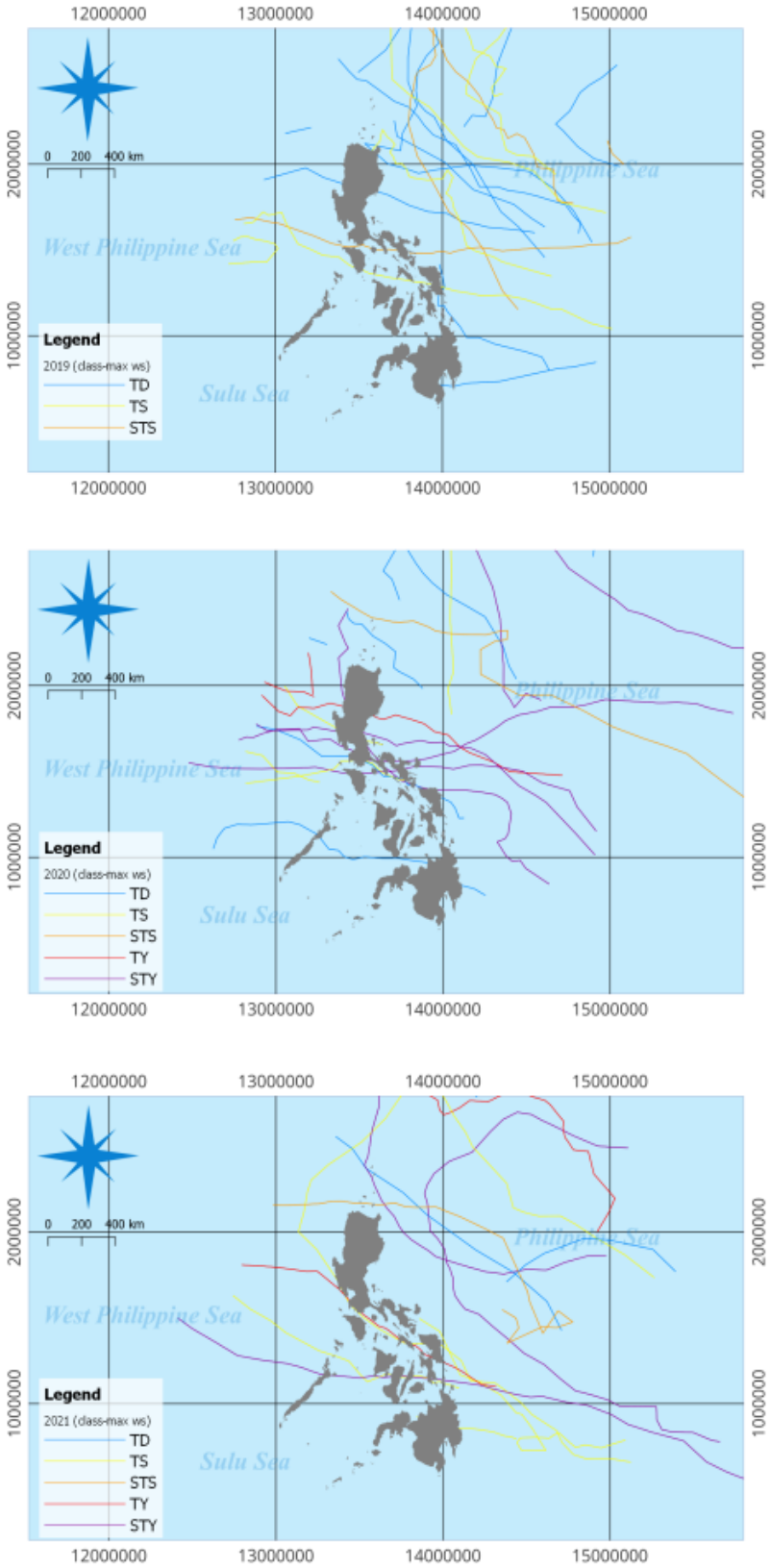

Figure 12. Time series plot of CHL, SST and typhoons for all transect lines for 2019–2021.

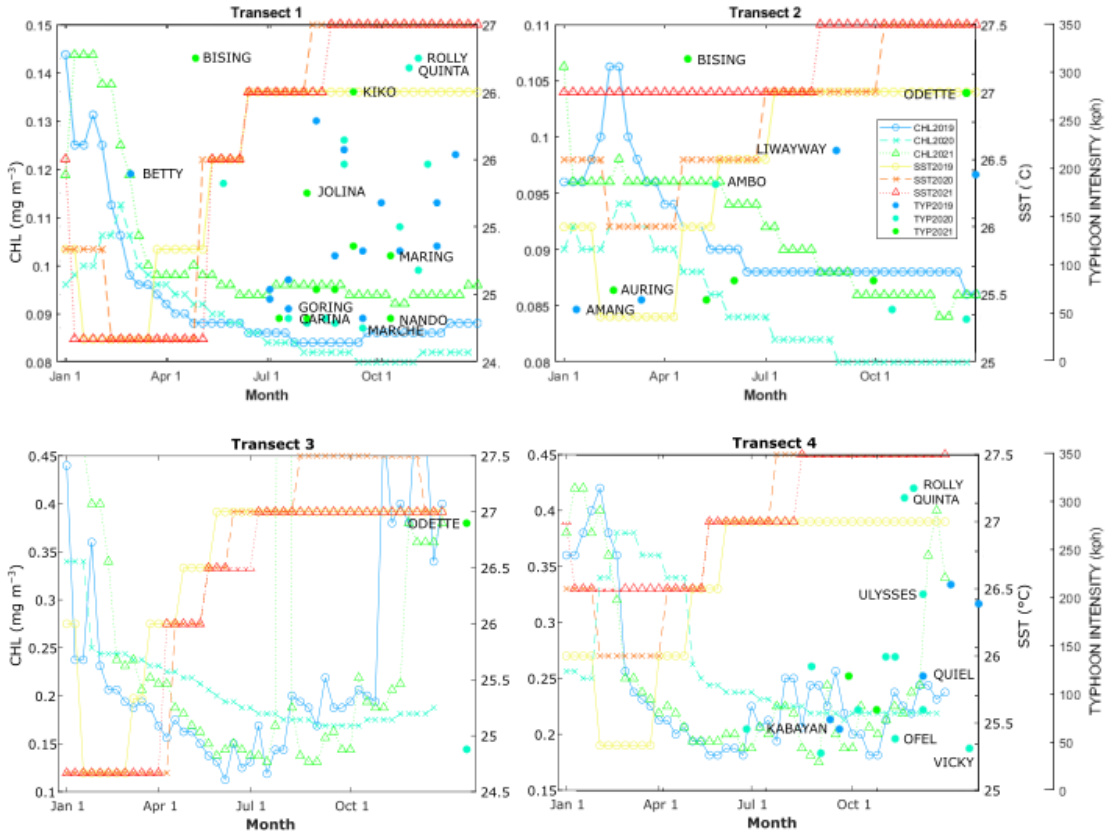

Net Primary Production Estimation

There is a general trend of the high levels of NPP during December-January (Q1-Q3), which are rainy and cold months in the Philippines. However, a peak anomaly was recorded for July of 2021 ($NPPPeak_{2021}$=2,235.5 mgC m-2 day-1). There is a single downward curve in July-August (Q1-Q3) while a double downward curve can be observed May-June, November-December (Q4). Without removing the anomaly, NPP annual for 2021 was estimated at approximately 0.34 PgC y-1 (see Figure 13).

Figure 13. Net primary production estimate for 2019-2021.

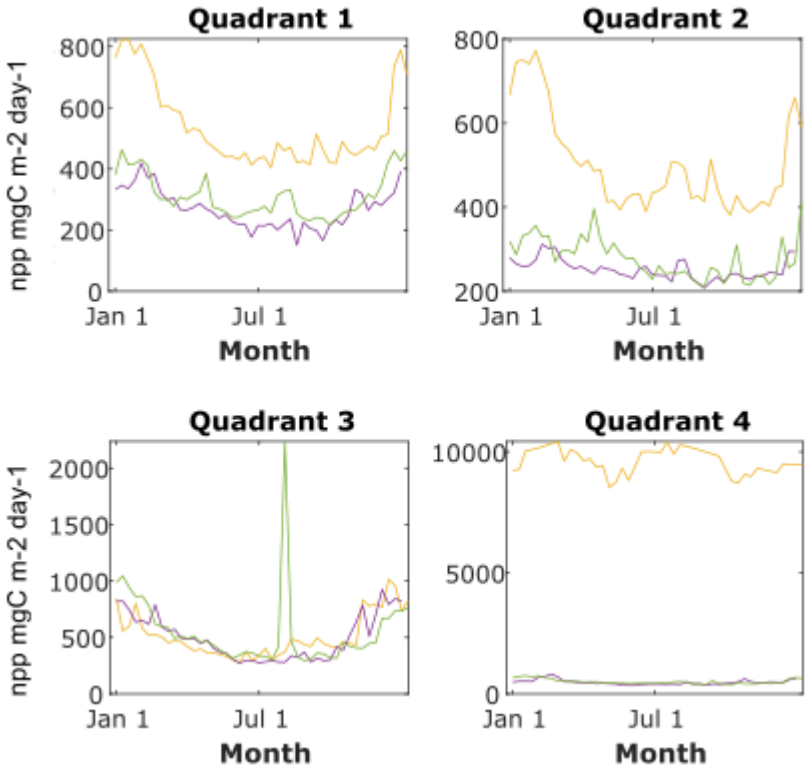

Linear Relationship of CHL and SST

The Regression results with varying values of R^2 are shown in Table 2 considering different data groups. Using all the data from 2019-2021 resulted with R^2=0.42, quite near with the individual annual result for 2019 and 2021.

Table 2

Regression Results for Different Data Input of CHL and SST (2019-2021)

Data Year	R^2	Adj R^2	STD Error	Data Range Error
2019	0.497350775	0.485926929	0.010314718	0.172631256
2020	0.813471554	0.809133683	0.003874051	0.11920158
2021	0.420219238	0.407042402	0.011789143	0.227809524
2019-2021	0.423529973	0.419227958	0.010920877	0.171307876

Results reflect total ungrouped data.

Validation of NASA CHL Product

There were 26 data points inside the Philippine EEZ utilized for in-situ validation covering the 8-day NASA CHL data of 2011 (November 25-December 2). Out of these, only seven points (about 27%) presented an overestimate of one order of magnitude, while the rest provided a correct CHL threshold as shown in Figure 14.

Figure 14. Comparison of the NASA CHL product with in-situ for the 8-day raster of November 25-December 2, 2011.

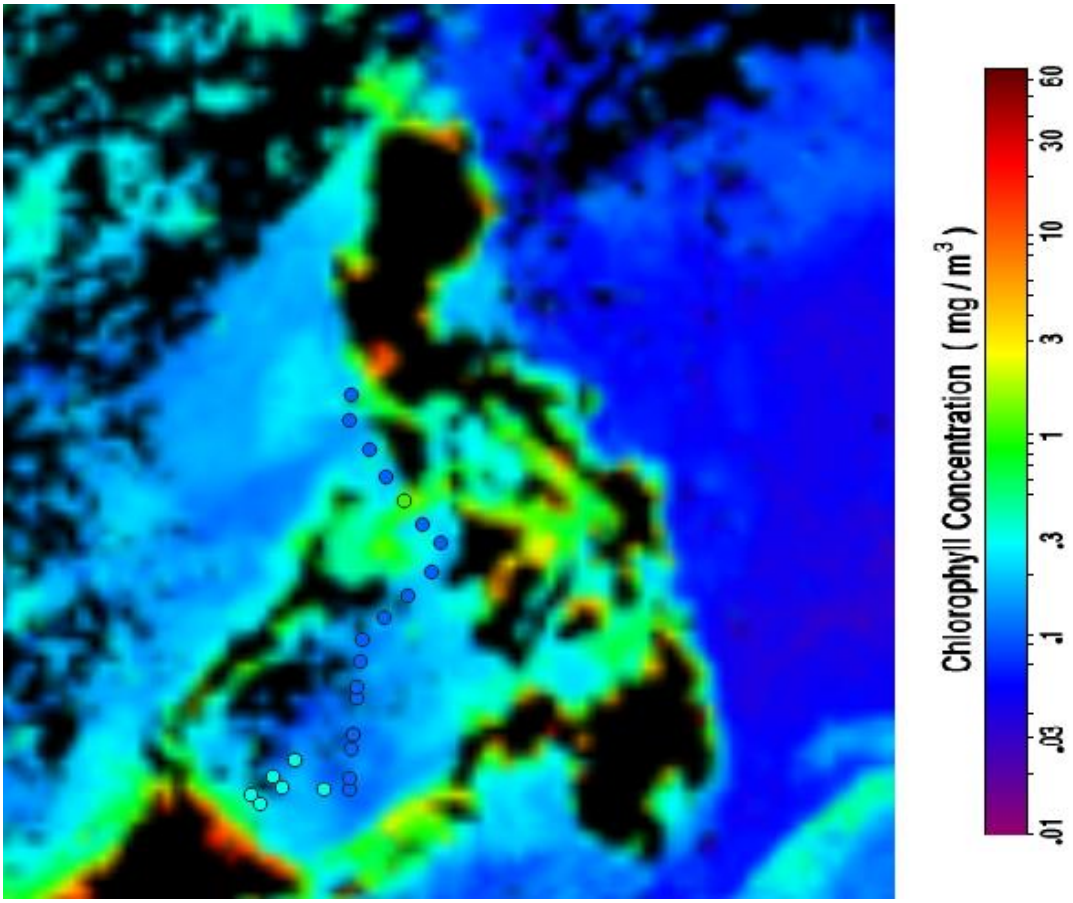

X. ANALYSIS AND DISCUSSION

Spatio-Temporal Relationship of CHL and Typhoons in the Philippines

It was highly evident that when typhoons Goring and Betty (2019), Marce and Carina (2020), and Kiko, Jolina, Maring, and Nando (2021) traversed near transect 1, the CHL value dropped, as shown in Figure 11. This is also true with Ambo (2020), but when Liwayway (2019) and Odette (2021) there was no change in the CHL value, even though they are both high intensity typhoons. While it was surprising to observe that when typhoons Amang (2019) and Auring (2021) traversed near transect 2, the CHL value increased.

Transect 3 is rather peculiar since the CHL value increased after the occurrence of Quiel (2019), and Ofel, Ulysses, and Vicky (2020), while dropping after Lanie (2021). There was no observable effect in CHL related to the typhoons crossing transect 4 (complete typhoon track maps in Appendices H-J).

This can be attributed to the ocean mixing brought by the wind-driven upwelling (He and Mahadevan, 2021), which presents a potential in harnessing our productivity despite the high frequency of typhoon occurrence. Despite that in some studies (Jacox and Edwards, 2011; deCastro et al., 2016) this effect was countered by the increase in stratification brought by warming oceans, in this study, the high frequency of typhoons appears to be affecting productivity, more than the negating effect of SST as shown in Figures 12 and 13.

Spatio-Temporal Relationship of CHL and SST

In Transect 1, a steep decrease in CHL was observed with decreasing SST for January-March (2019-2021) while a steady decrease in CHL with increasing SST from April onwards for 2019-2020 and almost no change in CHL for 2021.

In Transect 2, with decreasing SST comes an interesting increase and decreasing CHL for February-March (2019-2020) and decreasing CHL with increasing SST for April onwards. The year 2021 has a different behavior since the decrease in SST was observed from January-June with also decreasing CHL while July onwards, SST increased with almost no change in the CHL.

Transect 3 did not show a clear trend between CHL and SST.

There are three different trends that can be observed in transect 4. In 2019, CHL markedly decreased with decreasing SST from February to March, while the opposite was observed in 2020, with CHL increasing and decreasing SST. On the other hand, in 2021, increasing and decreasing CHL correlated with decreasing SST for January–April. However, for the second threshold of the year, increasing SST and decreasing CHL went together from April/May onwards (2019–2020).

Weak Linear Relationship between CHL and SST

The CHL and SST regression results showed a weak linear relationship between CHL and SST using all the data from 2019-2021, and individual yearly data (true for 2019 and 2021). Yet, it was surprising that a high R^2 (R^2_{2020}=0.81) was observed in the same year super typhoon Rolly occurred. This may be explained by the typhoon passage which only started in May 2020 (around the summer period), which avoided the data class imbalance as can be observed for 2019 and 2021

(typhoon presence all year round with negating effects), which most machine learning algorithms face.

XI. RECOMMENDATION AND CONCLUSIONS

Conclusion

This study presented a low-cost methodology to provide an overview of the "where" and "when" of ocean productivity in response to typhoon occurrences in the PH, which is one of the hardest hits in the world in terms of cyclones. It is encouraging that typhoon frequency is not heavily affecting productivity, as much as SST in the Philippine Seas, which were not observed in a recent study with period overlap for the year 2020 (Cordero-Bailey et al., 2022). In fact, there are instances that productivity increases after typhoon occurrences due to the upwelling effect. A similar observation in China was recorded which may be attributed to the nutrient mixing and upwelling after typhoon passage (Zeng and Tang, 2007). However, the counter-effect of stratification dependent on warming oceans cannot be at all ignored since this also has implications on the variations in the upwelling source depth (Lei et al., 2023), affecting the nutrient transfer in the euphotic zone. Also, the possible release of sunk CO_2 in the atmosphere during ocean mixing needs more understanding and further research.

Interestingly, a strong linear relationship between CHL and SST was observed for the year 2020. Since it is the year of the pandemic, it is possible that less anthropogenic activities might have minimized the CHL variability. The varying value of R2 considering different data groups of CHL and SST suggested that other factors may influence CHL variability, such as anthropogenic activities. Moreover, the importance of close monitoring in the Quadrant 3 (Sulu Sea), and Quadrant 4 (West Philippine Sea) should be prioritized given the relatively high productivity in these regions.

Only about 27% of in situ validation data points reflect an overestimate of only 1 order of magnitude, in the 2011 8-day NASA CHL data which presents a high confidence in utilizing this remote sensing data. Current models estimate that approximately between 1% and 40% of the primary production is being exported out of the euphotic zone, which settles in different areas of the water column, and roughly 1% sinks to the ocean seafloor (Passow and Carlson, 2012; Turner, 2015).

Recommendations

Limited to the spatial resolution of the Landsat 8 (30m swath width), the results may represent an underestimate or overestimate of the actual phytoplankton productivity depending on location. Hence, it is highly recommended to explore the use of Sentinel-2 data to improve the spatial resolution in the analysis. Specifically, the use of ground truths for future satellite remote sensing is highly recommended. Though typhoon occurrence poses no major threat to planktonic productivity, recent literature suggests that fast transport of organic compounds typhoon induced urban runoff could potentially make the ocean a carbon source (Lao et al., 2023). This coupling effect of typhoons is not yet extensively understood (Chen et al., 2023) opening more research in this direction. The NPP annual estimate suggests that the PH EEZ is providing a carbon sink, however, the NPP VGPM product from the ocean productivity website says otherwise (NPPOP2021= -0.64 PgC y-1 based on monthly scale) despite using the same model. It would be beneficial to provide an NPP validation with ground truths, which was not present in this paper.

Moreover, the importance of close monitoring in the Transect 3 (West Philippine Sea) and Transect 4 (Sulu Sea) should be prioritized given that continued disputes in commercial fishing activities in municipal waters persist in both Palawan and Zamboanga (Oceana, 2021). Though there is a low probability that NASA data is

measuring seagrass in Sulu Sea for CHL instead of phytoplankton due to the bathymetric conditions of this area, it is still early to say that this is not the case since the spatial coverage of the seagrass mapping in the Philippines is still scarce.

These uncertainties should be explored in future work including bioindicators for stress in the ocean, and potentially activities in the river corridor, to better understand micro processes that influence planktonic activity both in the macro and microscale.

Finally, there is a need to better understand upwelling dynamics in order to have a system insight about the ocean carbon which is crucial for long-term management strategies on nature-based carbon sequestration. Moreover, this paper presents a low-cost methodology to jumpstart ocean carbon estimation for future intensive ocean carbon monitoring.

References

Barnola, J. M., Raynaud, D. Y. S. N., Korotkevich, Y. S., & Lorius, C. (1987). Vostok ice core provides 160,000-year record of atmospheric CO2. *Nature*, 329(6138), 408-414.

Behrenfeld, M.J. & Falkowski, P.G. (1997). A Consumer's Guide to Phytoplankton Primary Productivity Models. *Limnology and Oceanography,* 42(7), 1479-1491.

Behrenfeld, M. J., Randerson, J. T., McClain, C. R., Feldman, G. C., Los, S. O., Tucker, C. J., Falkowski, P. G., Field, C. B., Frouin, R., Esaias, W. E., Kolber, D. D., & Pollack, N. H. (2001). Biospheric primary production during an ENSO transition. *Science*, *291*(5513), 2594–2597. https://doi.org/10.1126/science.1055071.

Berger, W., & Wefer, G. (1990). Export production: seasonality and intermittency, and paleoceanographic implications. *Paleogeography, Paleoclimatology, Paleoecology (Global and Planetary Change Section)*, *89*, 245–254. https://doi.org/10.1016/0031-0182(90)90065-f.

Bianchi, A. A., Bianucci, L., Piola, A. R., Pino, D. R., Schloss, I., Poisson, A., & Balestrini, C. F. (2005). Vertical stratification and air-sea CO2 fluxes in the Patagonian shelf. *Journal of Geophysical Research: Oceans*, *110*(7), 1–10. https://doi.org/10.1029/2004JC002488.

Boyd, P.W., Claustre, H., Levy, M., Siegel, D., & Weber, T. (2019). Multi-faceted particle pumps drive carbon sequestration in the ocean. *Nature*, 568, 327–335. https://doi.org/10.1038/s41586-019-1098-2.

Boyle, E.A. & Keigwin, L., 1987. North Atlantic thermo- haline circulation during the past 20,000 years linked to high-latitude surface temperature. *Nature*, 330, 35-40.

Brewin, R. J. W., Sathyendranath, S., Platt, T., Bouman, H., Ciavatta, S., Dall'Olmo, G., Dingle, J., Groom, S., Jönsson, B., Kostadinov, T. S., Kulk, G., Laine, M., Martínez-Vicente, V., Psarra, S., Raitsos, D. E., Richardson, K., Rio, M. H., Rousseaux, C. S., Salisbury, J., Shutler, J.; & Walker, P. (2021). Sensing the ocean biological carbon pump from space: A review of capabilities, concepts, research gaps and future developments. *Earth-Science Reviews*, 217 (March). https://doi.org/10.1016/j.earscirev.2021.103604.

Carr, M. E., Friedrichs, M. A. M., Schmeltz, M., Noguchi Aita, M., Antoine, D., Arrigo, K. R., Asanuma, I., Aumont, O., Barber, R., Behrenfeld, M., Bidigare, R., Buitenhuis, E. T., Campbell, J., Ciotti, A., Dierssen, H., Dowell, M., Dunne, J., Esaias, W., Gentili, B., … Yamanaka, Y. (2006). A comparison of global estimates of marine primary production from ocean color. *Deep-Sea Research Part II: Topical Studies in Oceanography*, *53*(5–7), 741–770. https://doi.org/10.1016/j.dsr2.2006.01.028.

Chen, F., Lao, Q., Lu, X., Wang, C., Chen, C., Liu, S., & Zhou, X. (2023). A review of the marine biogeochemical response to typhoons. *Marine Pollution Bulletin*, 194 (Part B), 115408.

Chorus, I., & Welker, M. (2021). *Toxic cyanobacteria in water: a guide to their public health consequences, monitoring and management.* Taylor & Francis. https://doi.org/10.1201/9781003081449

Claustre, H., Legendre, L., Boyd, P. W. & Levy, M. (2021). The Oceans' Biological Carbon Pumps: Framework for a Research Observational Community Approach. *Front. Mar. Sci.*, https://doi.org/10.3389/fmars.2021.780052

Clementson, L. A., & Wojtasiewicz, B. (2019). Dataset on the absorption characteristics of extracted phytoplankton pigments. *Data in Brief,* 24. https://doi.org/10.1016/j.dib.2019.103875.

Cordero-Bailey, K. S., Almo, A. T., David, L. T., & Yñiguez, A. T. (2022). Estimation of the vertical phytoplankton distribution in the Philippine Sea: Influence of turbulence following passage of typhoons. *Regional Studies in Marine Science*, 56, 102659. https://doi.org/10.1016/j.rsma.2022.102659

deCastro, M., Sousa, M. C., Santos, F., Dias, J. M., & Gómez-Gesteira, M. (2016). How will Somali coastal upwelling evolve under future warming scenarios? *Scientific Reports*, 6(1). https://doi.org/10.1038/srep30137

Dierssen, H. M., Zimmerman, R. C., Leathers, R. A., Downes, T. V., Davis, C. O. (2003). Ocean color remote sensing of seagrass and bathymetry in the Bahamas Banks by high-resolution airborne imagery. *Limnology and oceanography*, 48 (1part2), 444-455. https://doi.org/10.4319/lo.2003.48.1_part_2.0444

ESA. (2012). GeoEye-1 (OrbView-5). https://www.eoportal.org/satellite-missions/geoeye-1#mission-capabilities.

ESA. (2020), Sentinel-2 Mission Guide, https://sentinel.esa.int/web/sentinel/missions/sentinel-2.

Falkowski, P. G., Barber, R. T., & Smetacek, V. (1998). Biogeochemical controls and feedbacks on ocean primary production. *Science*, 281(5374), 200-206. https://doi.org/10.1126/science.281.5374.200

Ferreira, A., Sá, C., Silva, N., Beltrán, C., Dias, A. M., & Brito, A. C. (2020). Phytoplankton response to nutrient pulses in an upwelling system assessed through a microcosm experiment (Algarrobo Bay, Chile). *Ocean and Coastal Management*, *190*. https://doi.org/10.1016/j.ocecoaman.2020.105167

Field, C.B., Behrenfeld, M.J., Randerson, J.T., and Falkowski, P.G. (1998). Primary production of the biosphere: integrating terrestrial and oceanic components. *Science*, 281, pp. 237-240. https://doi.org/10.1126/science.281.5374.237

Franz, B. A., Bailey, S. W., Meister, G., & Werdell, P. J. (2012). Quality and consistency of the NASA ocean color data record. *Proc. Ocean Optics XXI,* Glasgow, Scotland.

Friedrichs, M. A. M., Carr, M. E., Barber, R. T., Scardi, M., Antoine, D., Armstrong, R. A., Asanuma, I., Behrenfeld, M. J., Buitenhuis, E. T., Chai, F., Christian, J. R., Ciotti, A. M., Doney, S. C., Dowell, M., Dunne, J., Gentili, B., Gregg, W., Hoepffner, N., Ishizaka, J., … Winguth, A. (2009). Assessing the uncertainties of model estimates of primary productivity in the tropical Pacific Ocean. *Journal of Marine Systems*, *76*(1–2), 113–133. https://doi.org/10.1016/j.jmarsys.2008.05.010

He, J., & Mahadevan, A. (2021). How the source depth of coastal upwelling relates to stratification and wind. *Journal of Geophysical Research: Oceans*, 126(12), e2021JC017621.

Ho, J. C., Michalak, A. M., & Pahlevan, N. (2019). Widespread global increase in intense lake phytoplankton blooms since the 1980s. *Nature*, *574*(7780), 667–670. https://doi.org/10.1038/s41586-019-1648-7

Huisman, J., Codd, G. A., Paerl, H. W., Ibelings, B. W., Verspagen, J. M. H., & Visser, P. M. (2018). Cyanobacterial blooms. In *Nature Reviews Microbiology* (Vol. 16,

Issue 8, pp. 471–483). Nature Publishing Group. https://doi.org/10.1038/s41579-018-0040-1.

Jacox, M. G., & Edwards, C. A. (2011). Effects of stratification and shelf slope on nutrient supply in coastal upwelling regions. *Journal of Geophysical Research: Oceans*, 116(C3).

Kilpatrick, K. A., Podestá, G., Walsh, S., Williams, E., Halliwell, V., Szczodrak, M., ... & Evans, R. (2015). A decade of sea surface temperature from MODIS. *Remote Sensing of Environment,* 165, 27-41.

Kirk, J. T. O. (1994). *Light and photosynthesis in aquatic ecosystems*. Cambridge University Press: London.

Kubota, Y., Murata, H., & Kikuzawa, K. (2004). Effects of topographic heterogeneity on tree species richness and stand dynamics in a subtropical forest in Okinawa Island, southern Japan. *Journal of Ecology,* 92, 230–240.

Kulk, G., Platt, T., Dingle, J., Jackson, T., Jönsson, B. F., Bouman, H. A., ... & Sathyendranath, S. (2020). Primary production, an index of climate change in the ocean: satellite-based estimates over two decades. *Remote Sensing*, 12(5), 826.

Kramer, S. J., Siegel, D. A., Maritorena, S., & Catlett, D. (2022). Modeling surface ocean phytoplankton pigments from hyperspectral remote sensing reflectance on global scales. *Remote Sensing of Environment*, 270(September 2021). https://doi.org/10.1016/j.rse.2021.112879.

Laws, E.A., Falkowski, P.G., Smith Jr., W.O., Ducklow, H., McCarth, J.J., 2000. Temperature effects on export production in the open ocean. *Glob. Biogeochem. Cycles*, 14, 1231–1246. https://doi.org/10.1029/1999GB001229.

Lao, Q., Chen, F., Jin, G., Lu, X., Chen, C., Zhou, X., & Zhu, Q. (2023). Characteristics and Mechanisms of Typhoon-Induced Decomposition of Organic Matter and Its Implication for Climate Change. *Journal of Geophysical Research: Biogeosciences*, 128, e2023JG007518.

Lei, F., Dai, H., Shang, S., He, Z., & Yang, S. (2023). Analysis of the dynamic mechanisms of upwelling in deep ocean water caused by typhoons. *Ocean Dynamics*, 73(8), 517-529.

Lévy, M., Bopp, L., Karleskind, P., Resplandy, L., Ethe, C., & Pinsard, F. (2013). Physical pathways for carbon transfers between the surface mixed layer and the ocean interior. *Global Biogeochem. Cycles,* 27, 1001–1012. doi:10.1002/gbc.20092.

Ma, S., Tao, Z., Yang, X., Yu, Y., Zhou, X., Ma, W., & Li, Z. (2014). Estimation of marine primary productivity from satellite-derived phytoplankton absorption data. *IEEE Journal of Selected Topics in Applied Earth Observations and Remote Sensing*, *7*(7), 3084–3092. https://doi.org/10.1109/JSTARS.2014.2298863.

McKinsey (2023). A more orderly transition: Navigating energy in 2023. https://www.mckinsey.com/industries/electric-power-and-natural-gas/our-insights/a-more-orderly-transition-navigating-energy-in-2023.

Merz, E., Kozakiewicz, T., Reyes, M., Ebi, C., Isles, P., Baity-Jesi, M., Roberts, P., Jaffe, J. S., Dennis, S. R., Hardeman, T., Stevens, N., Lorimer, T., & Pomati, F. (2021). Underwater dual-magnification imaging for automated lake plankton monitoring. *Water Research*, *203*, 117524. https://doi.org/10.1016/J.WATRES.2021.117524

Milutinović, S., & Bertino, L. (2011). Assessment and propagation of uncertainties in input terms through an ocean-color-based model of primary productivity. *Remote Sensing of Environment*, *115*(8), 1906–1917. https://doi.org/10.1016/j.rse.2011.03.013.

Myrberg, K., & Andrejev, O. (2003). Main upwelling regions in the Baltic Sea—a statistical analysis based on three-dimensional modelling. *Boreal Environment Research*, 8(2), 97.

Najjar, R. G., & Keeling, R. F. (2000). Mean annual cycle of the air-Sea oxygen flux: A global view. *Global Biogeochemical Cycles*, *14*(2), 573–584. https://doi.org/10.1029/1999GB900086

NASA. (2012). Landsat Data Continuity Mission, Continuously Observing Your World, https://landsat.gsfc.nasa.gov/wp-content/uploads/2012/12/LDCM_Brochure_Dec2012.pdf.

NASA Goddard Space Flight Center, Ocean Ecology Laboratory, Ocean Biology Processing Group. Moderate-resolution Imaging Spectroradiometer (MODIS) Aqua Ocean Color Data. (2018) Reprocessing. NASA OB.DAAC, Greenbelt, MD, USA. doi: 10.5067/AQUA/MODIS/L2/OC/2018. (Accessed on 01 September 2023).

NASA Ocean Biology Processing Group. (2018). Sea-viewing Wide Field-of-view Sensor (SeaWiFS) Level-2 Ocean Color Data, version R2018.8, NASA Ocean Biology Distributed Active Archive Center. doi: 10.5067/ORBVIEW-2/SEAWIFS/L2/OC/2018. (Accessed on 01 September 2023).

Neftel, A., Oeschger, H., Schwander, J., Stauffer, B., & Zumbrunn, R. (1982). Ice core sample measurements give atmospheric CO2 content during the past 40,000 yr. *Nature*, 295(5846), 220-223.

NOOA. (2025). What is the “EEZ”? Available online: https://oceanexplorer.noaa.gov/facts/useez.html (Accessed on 21 August 2025).

Ocean Productivity. (2024). Ocean Productivity. Available online: https://sites.science.oregonstate.edu/ocean.productivity/index.php (Accessed on 01 September 2023).

Oceana. (2021). Ostensible commercial fishing in municipal waters pervades despite COVID19 pandemic; Full implementation of vessel monitoring pushed. https://ph.oceana.org/press-releases/ostensible-commercial-fishing-in-municipal-waters-pervades-despite-covid19-pandemic-full-implementation-of-vessel-monitoring-pushed/. (Accessed on 01 September 2023).

Omand, M. M., D’Asaro, E. A., Lee, C. M., Perry, M. J., Briggs, N., Cetinić, I., & Mahadevan, A. (2015). Eddy-driven subduction exports particulate organic carbon from the spring bloom. *Science*, 348(6231), 222-225. https://doi.org/10.1126/science.1260062

PAGASA-DOST, (2023). Annual Tropical Cyclone Tracks. https://www.pagasa.dost.gov.ph/information/annual-cyclone-track

Passow, U., & Carlson, C. A. (2012). The biological pump in a high CO2 world. *Marine Ecology Progress Series*, 470, 249-271.

Pinti, J., DeVries, T., Norin, T., Serra-Pompei, C., Proud, R., Siegel, D. A., Kiørboe, T., Petrik, C. M., Andersen, K. H., Brierley, A. S., Visser, A. W. (2023). Model estimates of metazoans' contributions to the biological carbon pump. *Biogeosciences*, 20(5), 997-1009.

Polikarpov, I., Al-Yamani, F., Petrov, P., Saburova, M., Mihalkov, V., & Al-Enezi, A. (2021). Phytoplankton bloom detection during the COVID-19 lockdown with

remote sensing data: Using Copernicus Sentinel-3 for north-western Arabian/Persian Gulf case study. *Marine Pollution Bulletin,* 171(June), 112734. https://doi.org/10.1016/j.marpolbul.2021.112734.

Radwan, A. M. (2005). Some factors affecting the primary production of phytoplankton in Lake Burullus Item Type Journal Contribution. *Egyptian Journal of Aquatic Research*, *31*(2), 72–88.

Siegel, D. A., Buesseler, K. O., Behrenfeld, M. J., Benitez-Nelson, C. R., Boss, E., Brzezinski, M. A., Burd, A., Carlson, C. A., D'Asaro, E. A., Doney, S. C., Perry, M. J., Stanley, R. H. R., & Steinberg, D. K. (2016). Prediction of the export and fate of global ocean net primary production: The exports science plan. *Frontiers in Marine Science*, *3*(MAR). https://doi.org/10.3389/fmars.2016.00022.

Tagliabue, A., Kwiatkowski, L., Bopp, L., Butenschön, M., Cheung, W., Lengaigne, M., & Vialard, J. (2021). Persistent uncertainties in ocean net primary production climate change projections at regional scales raise challenges for assessing impacts on ecosystem services. *Frontiers in Climate*, 3.

Turner, J. T. (2015). Zooplankton fecal pellets, marine snow, phytodetritus and the ocean's biological pump. *Progress in Oceanography*, 130, 205-248.

UNCC (2021). Nationally Determined Contributions (NDCs). https://unfccc.int/process-and-meetings/the-paris-agreement/nationally-determined-contributions-ndcs/nationally-determined-contributions-ndcs.

Valente, A., Sathyendranath, S., Brotas, V., Groom, S., Grant, M., Jackson, T., Chuprin, A., Taberner, M., Airs, R., Antoine, D., Arnone, R., Balch, W.M., Barker, K., Barlow, R., Bélanger, S., Berthon, J.F., Beşiktepe, Ş., Borsheim, Y., Bracher, A., Brando, V., Brewin, R. J. W., Canuti, E., Chavez, F. P., Cianca, A., Claustre, H., Clementson, L., Crout, R., Ferreira, A., Freeman, S., Frouin, R.,

García-Soto, C., Gibb, S. W., Goericke, R., Gould, R., Guillocheau, N., Hooker, S. B., Hu, C., Kahru, M., Kampel, M., Klein, H., Kratzer, S., Kudela, R., Ledesma, J., Lohrenz, S., Loisel, H., Mannino, A., Martinez-Vicente, A., Matrai, P., McKee, D., Mitchell, B. G., Moisan, T., Montes, E., Muller-Karger, F., Neeley, A., Novak, M., O'Dowd, L., Ondrusek, M., Platt, T., Poulton, A. J., Repecaud, M., Röttgers, R., Schroeder, T., Smyth, T., Smythe-Wright, D., Sosik, H. M., Thomas, C., Thomas, R., Tilstone, G., Tracana, A., Twardowski, M., Vellucci, V., Voss, K., Werdell, J., Wernand, M., Wojtasiewicz, B., Wright, S., & Zibordi, Z. (2022). A compilation of global bio-optical in situ data for ocean-colour satellite applications–version three. *Earth System Science Data Discussions*, 1-61. https://doi.org/10.5194/essd-14-5737-2022

Walton, C. C., Pichel, W. G., Sapper, J. F., & May, D. A. (1998). The development and operational application of nonlinear algorithms for the measurement of sea surface temperatures with the NOAA polar-orbiting environmental satellites. *Journal of Geophysical Research:* Oceans, 103(C12), 27999-28012.

Wang, Q., Yu, D., Li, Z., & Wang, L. (2008). The effect of typhoons on the diversity and distribution pattern of aquatic plants on Hainan Island, *South China. Biotropica*, 40(6), 692-699.

Westberry, T., Behrenfeld, M. J., Siegel, D. A., & Boss, E. (2008). Carbon-based primary productivity modeling with vertically resolved photoacclimation. *Global Biogeochem. Cycles*, 22, GB2024.

Wright, S. W., Jeffrey, S. W., Mantoura, R. F. C., Llewellyn, C. A., Bjørnland, T., Repeta, D., & Welschmeyer, N. (1991). Improved HPLC method for the analysis of chlorophylls and carotenoids from marine phytoplankton. *Marine ecology progress series*, 183-196.

Zeng, G. M., & Tang, D. (2007). Offshore and nearshore chlorophyll increases induced by typhoon winds and subsequent terrestrial rainwater runoff. Marine Ecology Press Series, 333, 61-74.

Zoljoodi, M., Moradi, M., & Moradi, N. (2022). Seasonal and interannual cycles of total phytoplankton phenology metrics in the Persian Gulf using ocean color remote sensing. *Continental Shelf Research*, 237 (February), 104685. https://doi.org/10.1016/j.csr.2022.104685.

Appendices

Appendix A.
Philippine Cyclone List (2019-2021)

YEAR	CYCLONE CLASSIFICATION	NAME	PERIOD		WIND SPEED (kph)
2019	TD	AMANG	1/19/2019	1/21/2019	55
2019	TS	BETTY	2/28/2019	3/1/2019	195
2019	TD	CHEDENG	3/17/2019	3/19/2019	65
2019	TD	DODONG	6/25/2019	6/26/2019	75
2019	TD	EGAY	6/29/2019	7/1/2019	65
2019	TS	FALCON	7/15/2019	7/18/2019	85
2019	TD	GORING	7/19/2019	7/19/2019	55
2019	T	HANNA	8/3/2019	8/9/2019	250
2019	STS	INENG	8/20/2019	8/24/2019	110
2019	TS	JENNY	8/26/2019	8/28/2019	75
2019	TD	KABAYAN	9/1/2019	9/1/2019	65
2019	T	LIWAYWAY	9/1/2019	9/5/2019	220
2019	TD	MARILYN	9/12/2019	9/14/2019	45
2019	STS	NIMFA	9/17/2019	9/21/2019	115
2019	T	ONYOK	9/28/2019	10/1/2019	165
2019	T	PERLA	10/16/2019	10/20/2019	115

YEAR	CYCLONE CLASSIFICATION	NAME	PERIOD		WIND SPEED (kph)
2019	T	QUIEL	11/5/2019	11/9/2019	120
2019	T	RAMON	11/12/2019	11/20/2019	165
2019	TS	SARAH	11/19/2019	11/23/2019	120
2019	T	TISOY	12/1/2019	12/5/2019	215
2019	T	URSULA	12/23/2019	12/28/2019	195
2020	T	AMBO	5/10/2020	5/17/2020	185
2020	TS	BUTCHOY	6/11/2020	6/12/2020	65
2020	TD	CARINA	7/13/2020	7/14/2020	45
2020	STS	DINDO	7/31/2020	8/3/2020	40
2020	TS	ENTENG	8/8/2020	8/9/2020	75
2020	TD	FERDIE	8/9/2020	8/10/2020	130
2020	TD	GENER	8/13/2020	8/13/2020	45
2020	TD	HELEN	8/17/2020	8/18/2020	40
2020	STS	IGME	8/21/2020	8/22/2020	40
2020	T	JULIAN	8/28/2020	8/31/2020	205
2020	T	KRISTINE	8/31/2020	9/5/2020	230
2020	TS	LEON	9/15/2020	9/17/2020	85

YEAR	CYCLONE CLASSIFICATION	NAME	PERIOD		WIND SPEED (kph)
2020	TS	MARCE	9/20/2020	9/21/2020	35
2020	TS	NIKA	10/11/2020	10/12/2020	140
2020	TD	OFEL	10/13/2020	10/16/2020	55
2020	T	PEPITO	10/19/2020	10/22/2020	140
2020	T	QUINTA	10/23/2020	10/27/2020	305
2020	ST	ROLLY	10/27/2020	11/3/2020	315
2020	STS	SIONY	10/29/2010	11/6/2020	95
2020	TS	TONYO	11/7/2020	11/9/2020	85
2020	T	ULYSSES	11/8/2020	11/13/2020	205
2020	TS	VICKY	12/18/2020	12/21/2020	45
2021	STS	AURING	2/17/2021	2/22/2021	75
2021	T	BISING	4/12/2021	4/24/2021	315
2021	TS	CRISING	5/13/2021	5/14/2021	65
2021	TS	DANTE	5/29/2021	6/5/2021	85
2021	TD	EMONG	7/4/2021	7/6/2021	45
2021	T	FABIAN	7/16/2021	7/24/2021	175
2021	TD	GORIO	8/4/2021	8/4/2021	45

YEAR	CYCLONE CLASSIFICATION	NAME	PERIOD		WIND SPEED (kph)
2021	TS	HUANING	8/7/2021	8/7/2021	75
2021	TS	ISANG	8/19/2021	8/22/2021	75
2021	T	JOLINA	9/6/2021	9/9/2021	120
2021	T	KIKO	9/7/2021	9/12/2021	280
2021	TD	LANNIE	10/4/2021	10/6/2021	85
2021	STS	MARING	10/7/2021	10/12/2021	110
2021	TD	NANDO	10/8/2021	10/9/2021	45
2021	T	ODETTE	12/12/2021	12/19/2021	280

Appendix B.
Spatio-Temporal Maps of CHL (2019)

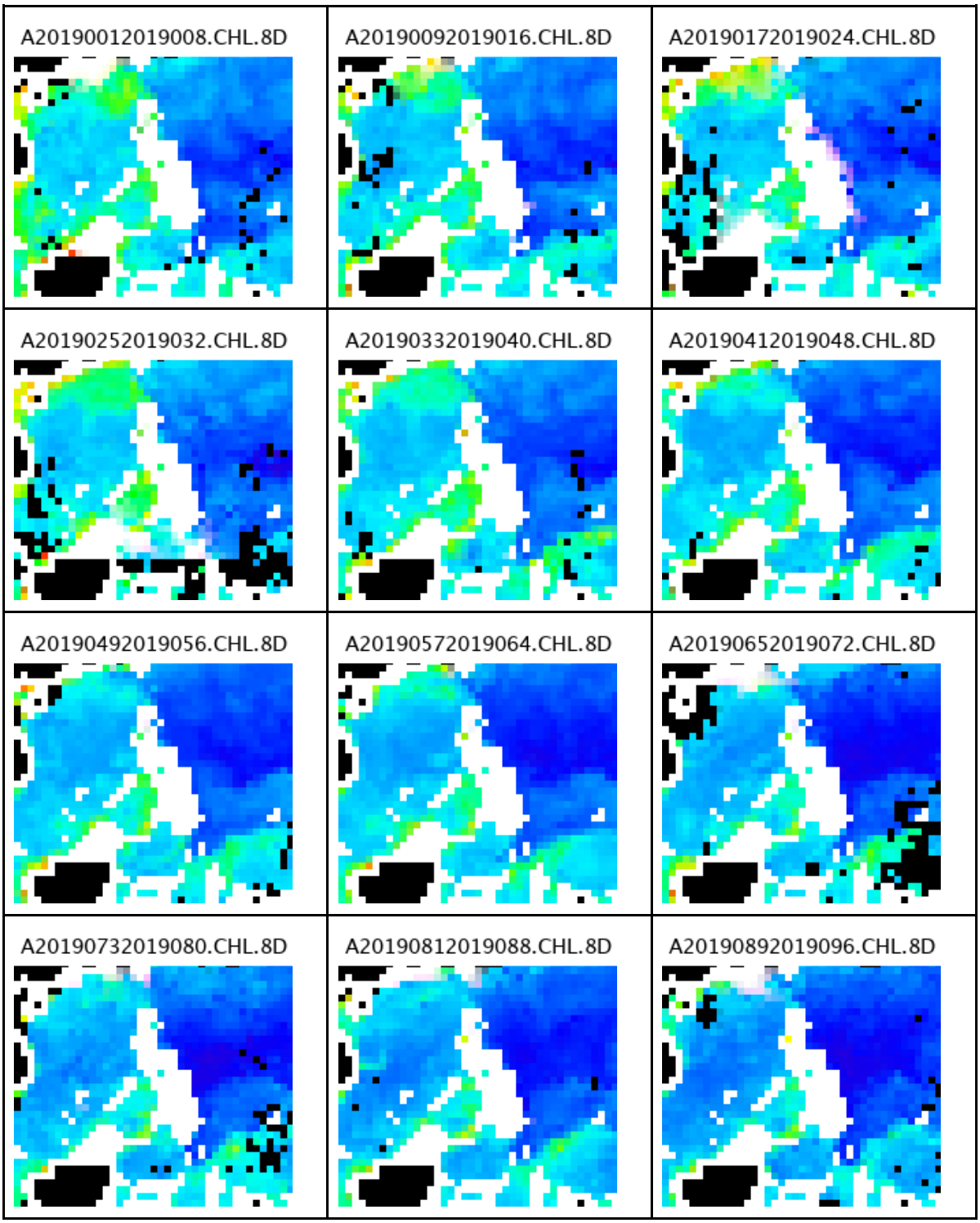

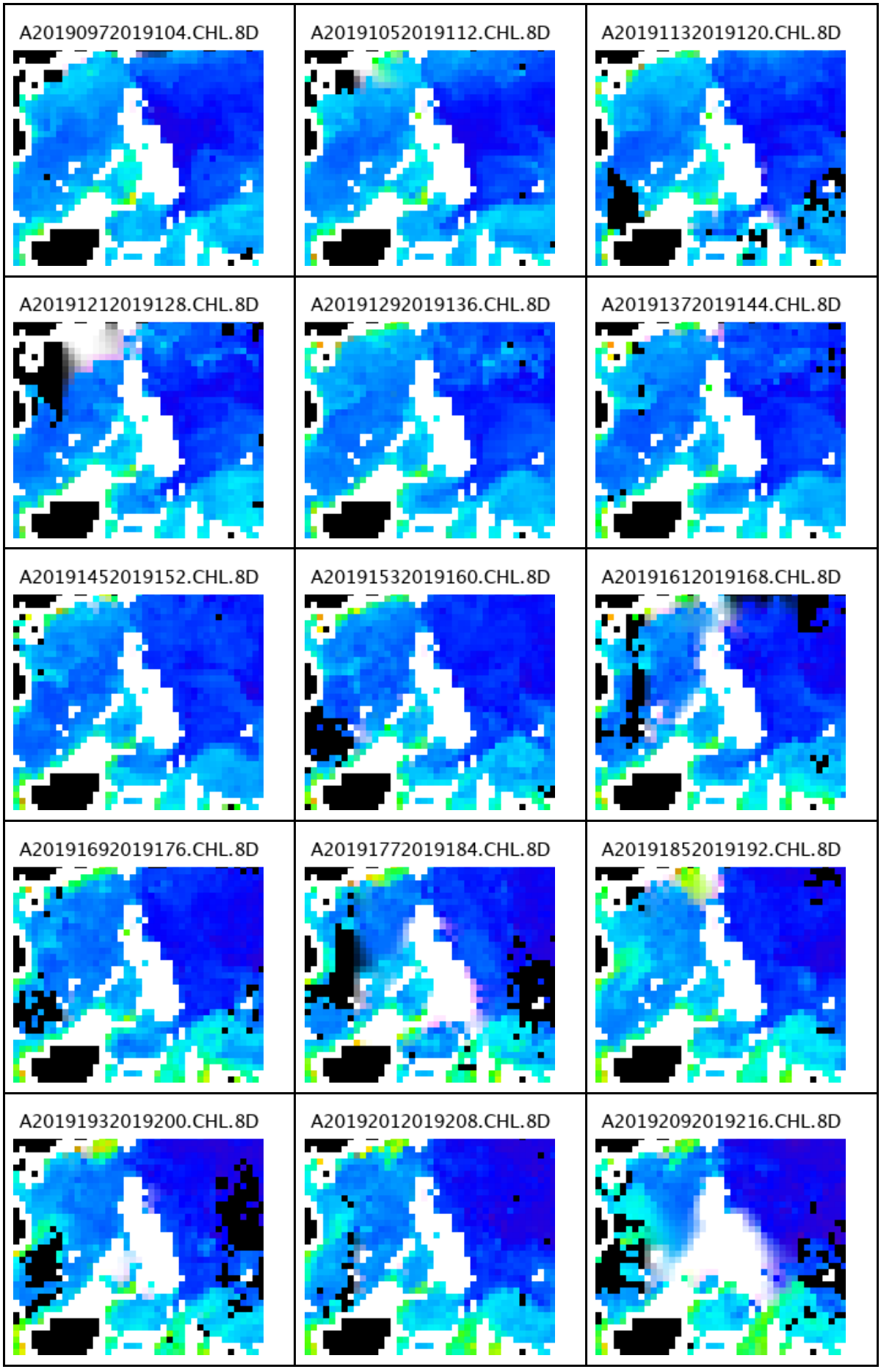
A20190972019104.CHL.8D
A20191052019112.CHL.8D
A20191132019120.CHL.8D
A20191212019128.CHL.8D
A20191292019136.CHL.8D
A20191372019144.CHL.8D
A20191452019152.CHL.8D
A20191532019160.CHL.8D
A20191612019168.CHL.8D
A20191692019176.CHL.8D
A20191772019184.CHL.8D
A20191852019192.CHL.8D
A20191932019200.CHL.8D
A20192012019208.CHL.8D
A20192092019216.CHL.8D

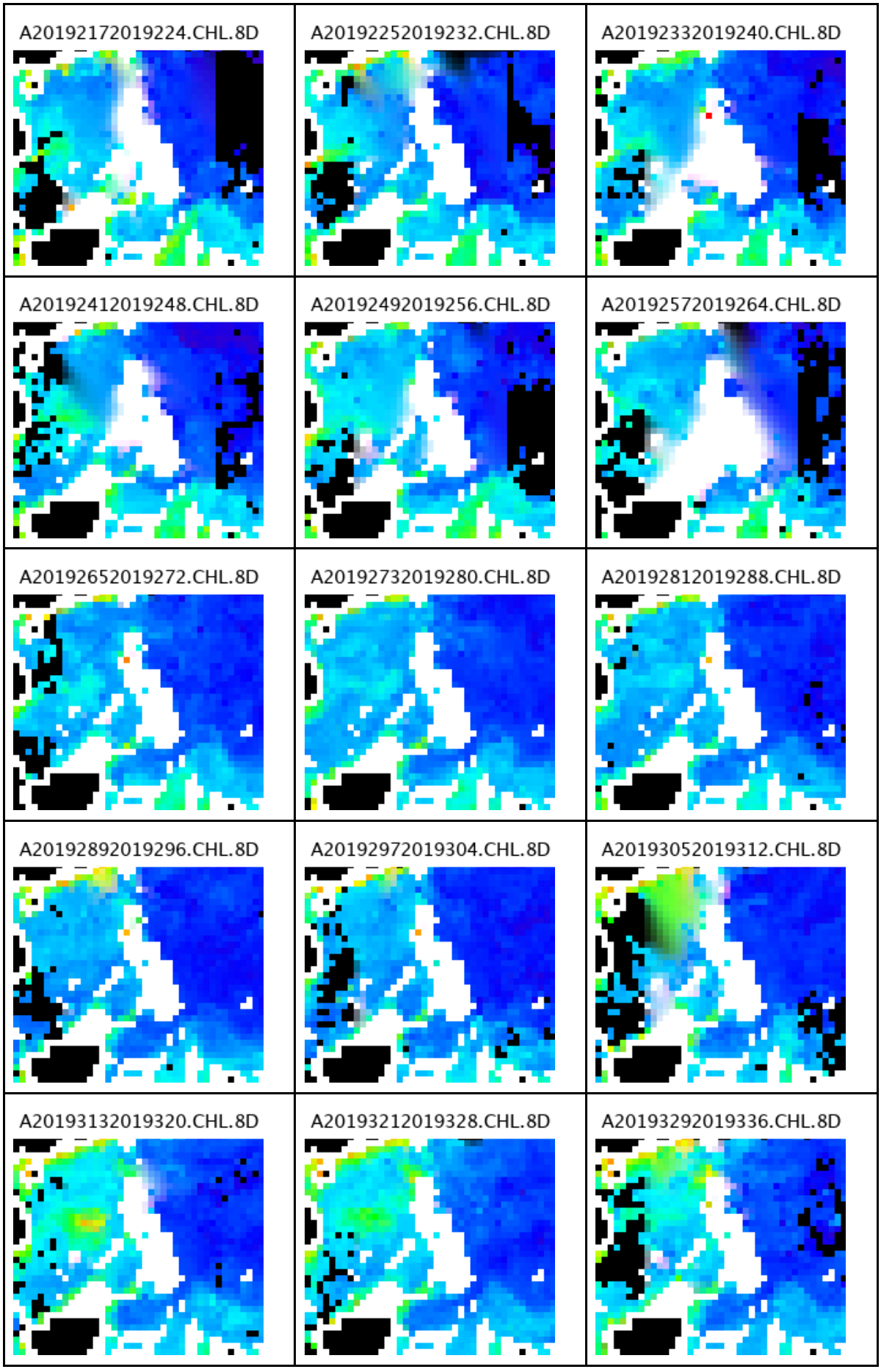
A20192172019224.CHL.8D
A20192252019232.CHL.8D
A20192332019240.CHL.8D
A20192412019248.CHL.8D
A20192492019256.CHL.8D
A20192572019264.CHL.8D
A20192652019272.CHL.8D
A20192732019280.CHL.8D
A20192812019288.CHL.8D
A20192892019296.CHL.8D
A20192972019304.CHL.8D
A20193052019312.CHL.8D
A20193132019320.CHL.8D
A20193212019328.CHL.8D
A20193292019336.CHL.8D

A20193372019344.CHL.8D 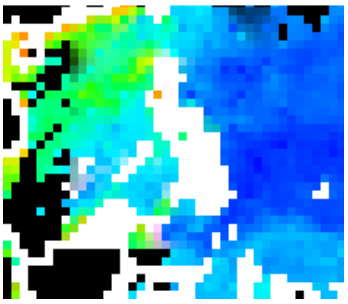	A20193452019352.CHL.8D 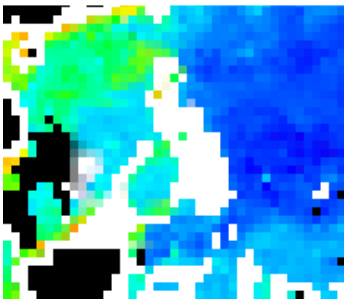	A20193532019360.CHL.8D 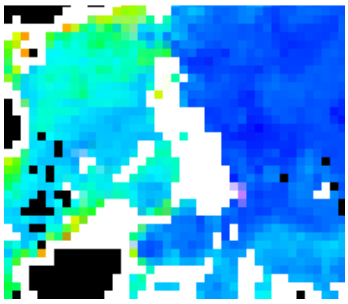
A20193612019365.CHL.8D 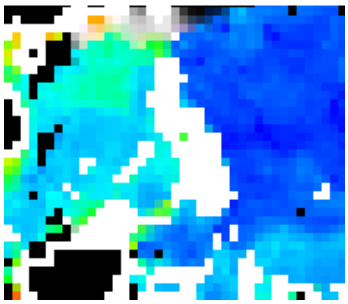		

Appendix C.
Spatio-Temporal Maps of CHL (2020)

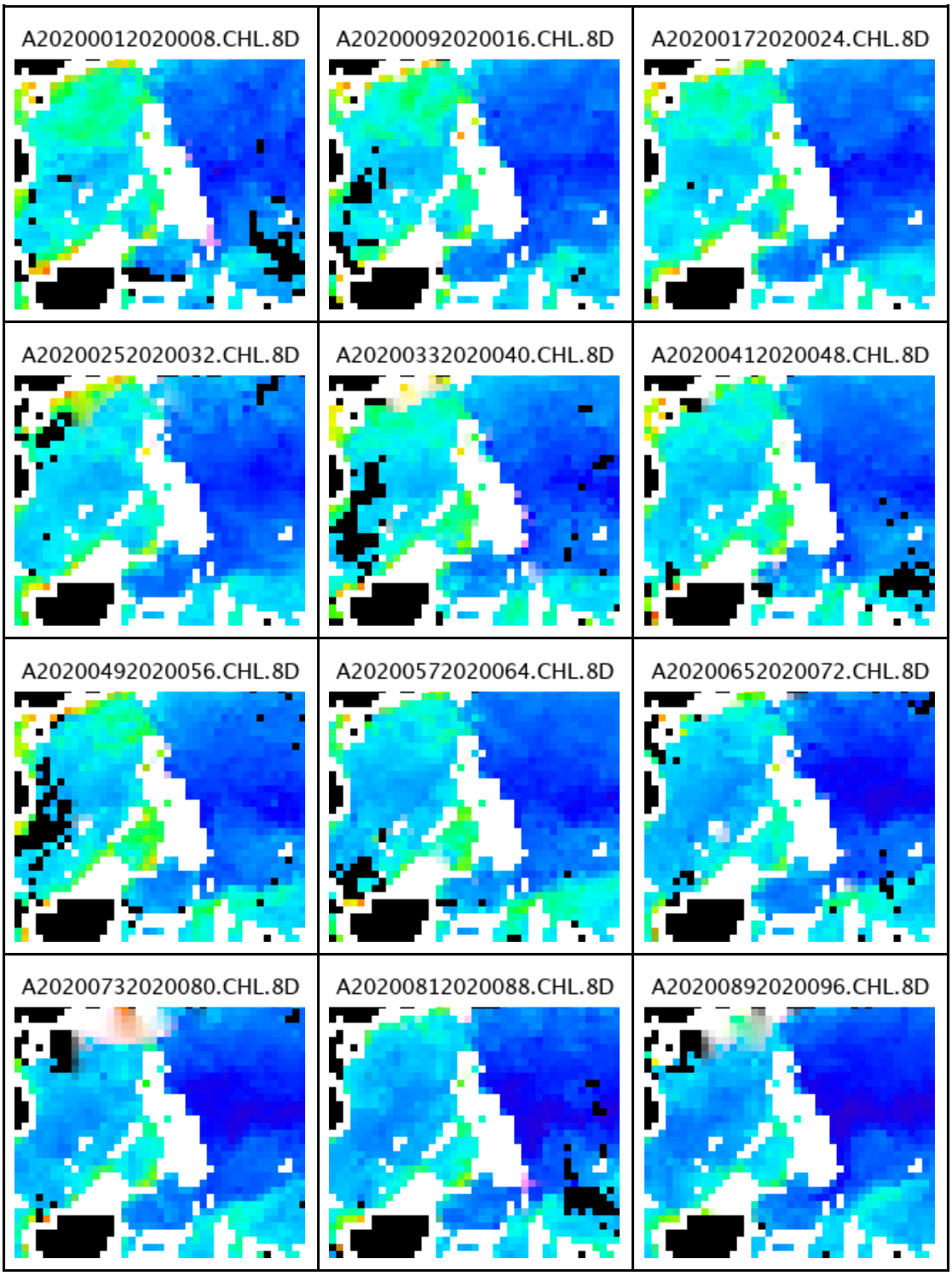

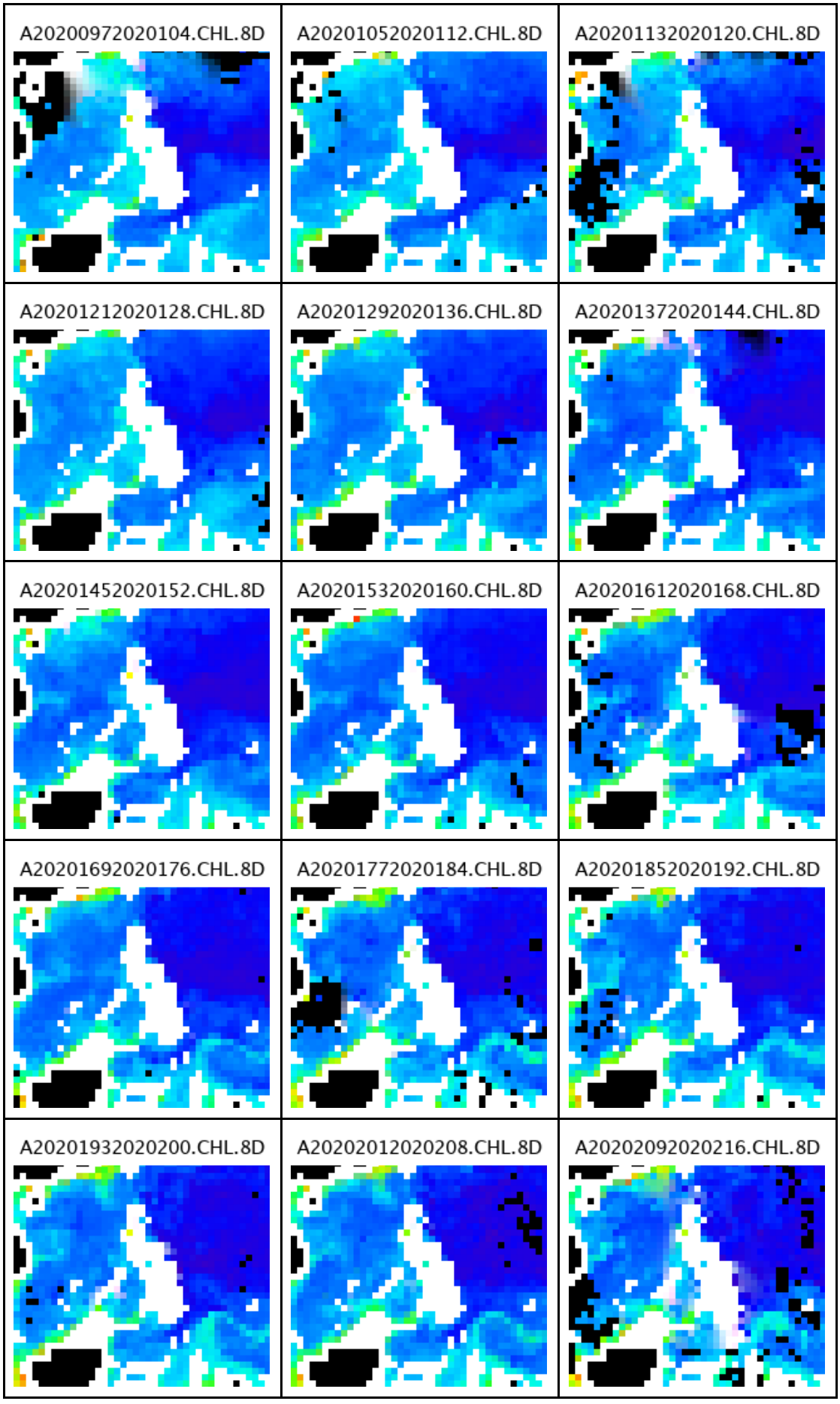
A20200972020104.CHL.8D
A20201052020112.CHL.8D
A20201132020120.CHL.8D
A20201212020128.CHL.8D
A20201292020136.CHL.8D
A20201372020144.CHL.8D
A20201452020152.CHL.8D
A20201532020160.CHL.8D
A20201612020168.CHL.8D
A20201692020176.CHL.8D
A20201772020184.CHL.8D
A20201852020192.CHL.8D
A20201932020200.CHL.8D
A20202012020208.CHL.8D
A20202092020216.CHL.8D

A20202172020224.CHL.8D 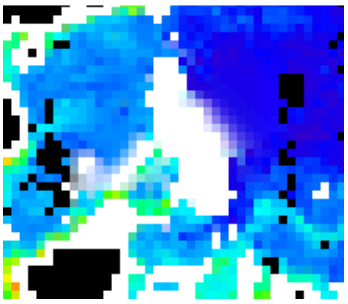	A20202252020232.CHL.8D 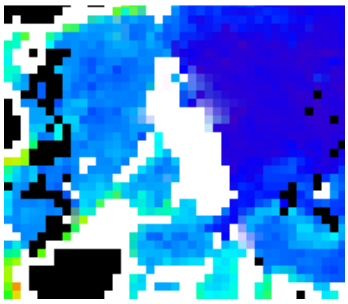	76TH
A20202412020248.CHL.8D 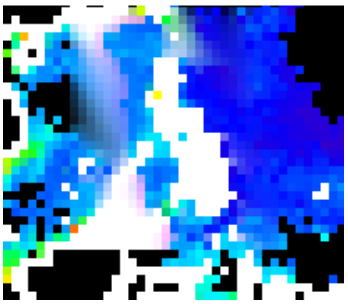	A20202492020256.CHL.8D 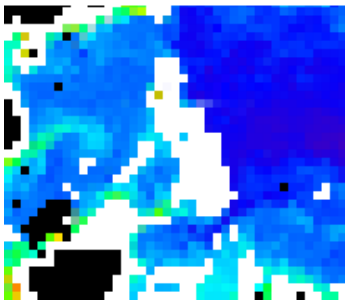	A20202572020264.CHL.8D 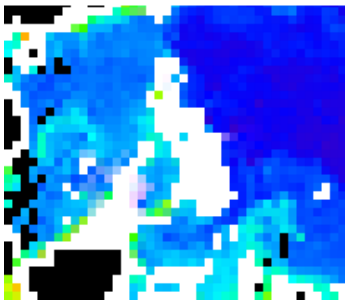
A20202652020272.CHL.8D 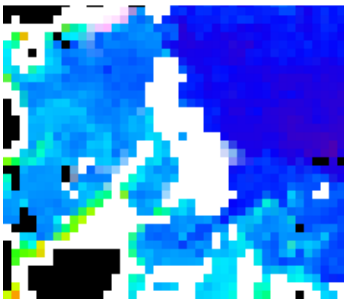	A20202732020280.CHL.8D 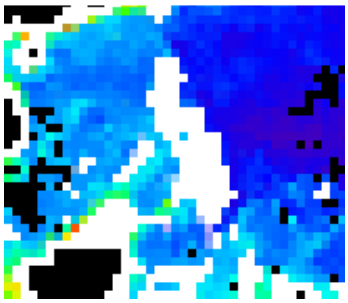	A20202812020288.CHL.8D 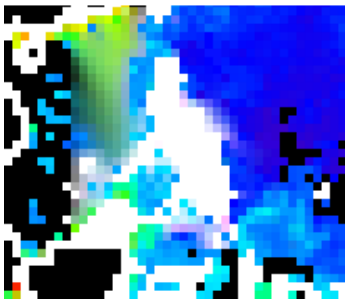
A20202892020296.CHL.8D 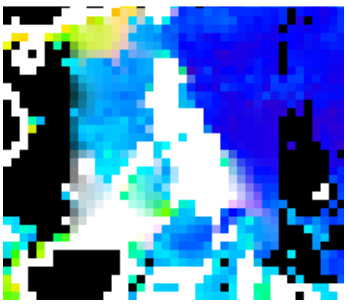	A20202972020304.CHL.8D 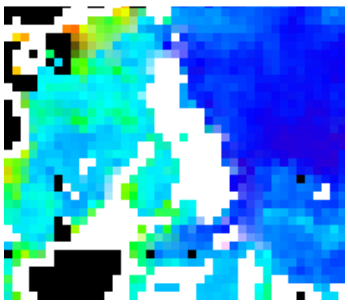	A20203052020312.CHL.8D 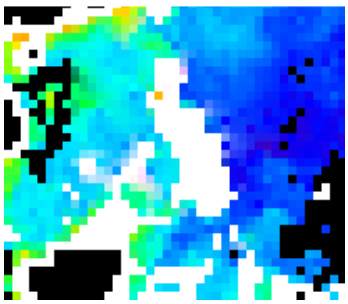
A20203132020320.CHL.8D 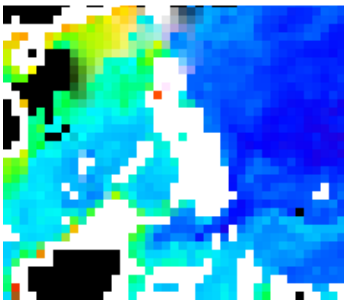	A20203212020328.CHL.8D 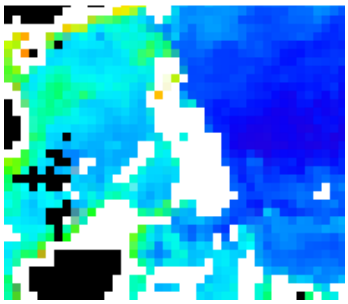	A20203292020336.CHL.8D 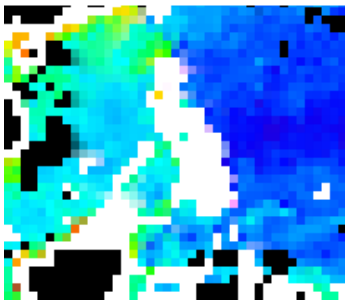

A20203372020344.CHL.8D 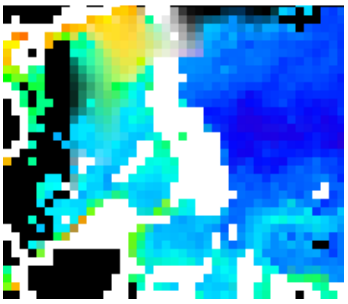	A20203452020352.CHL.8D 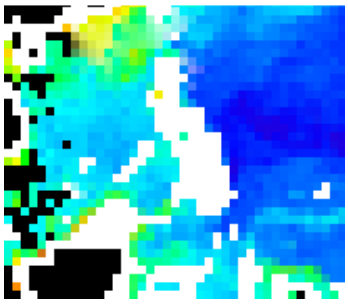	A20203532020360.CHL.8D 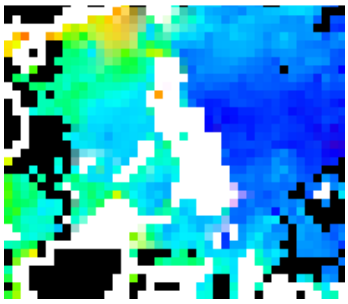
A20193612019365.CHL.8D 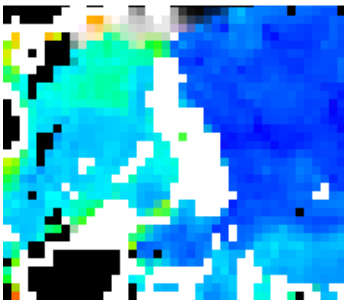		

Appendix D.
Spatio-Temporal Maps of CHL (2021)

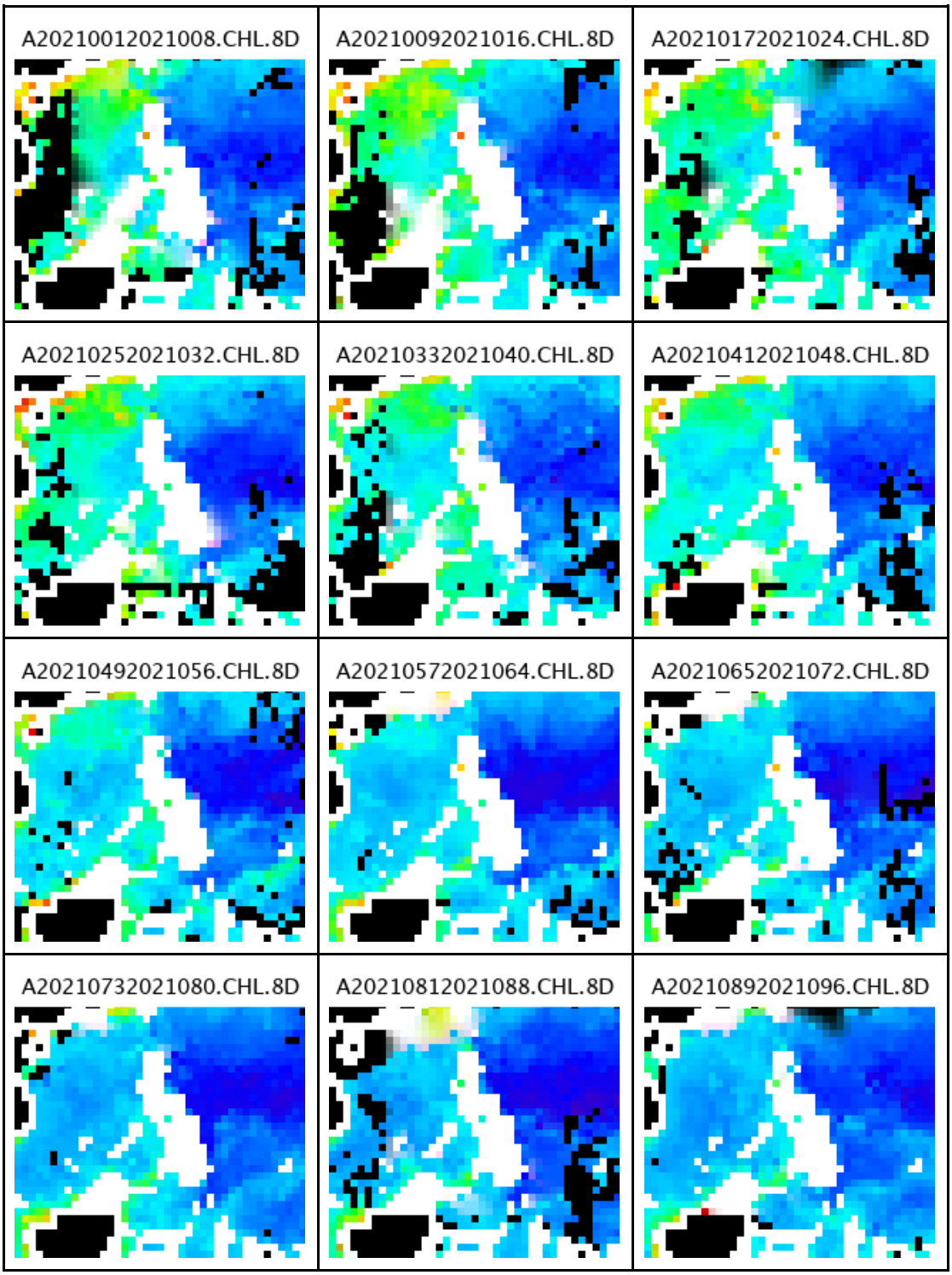

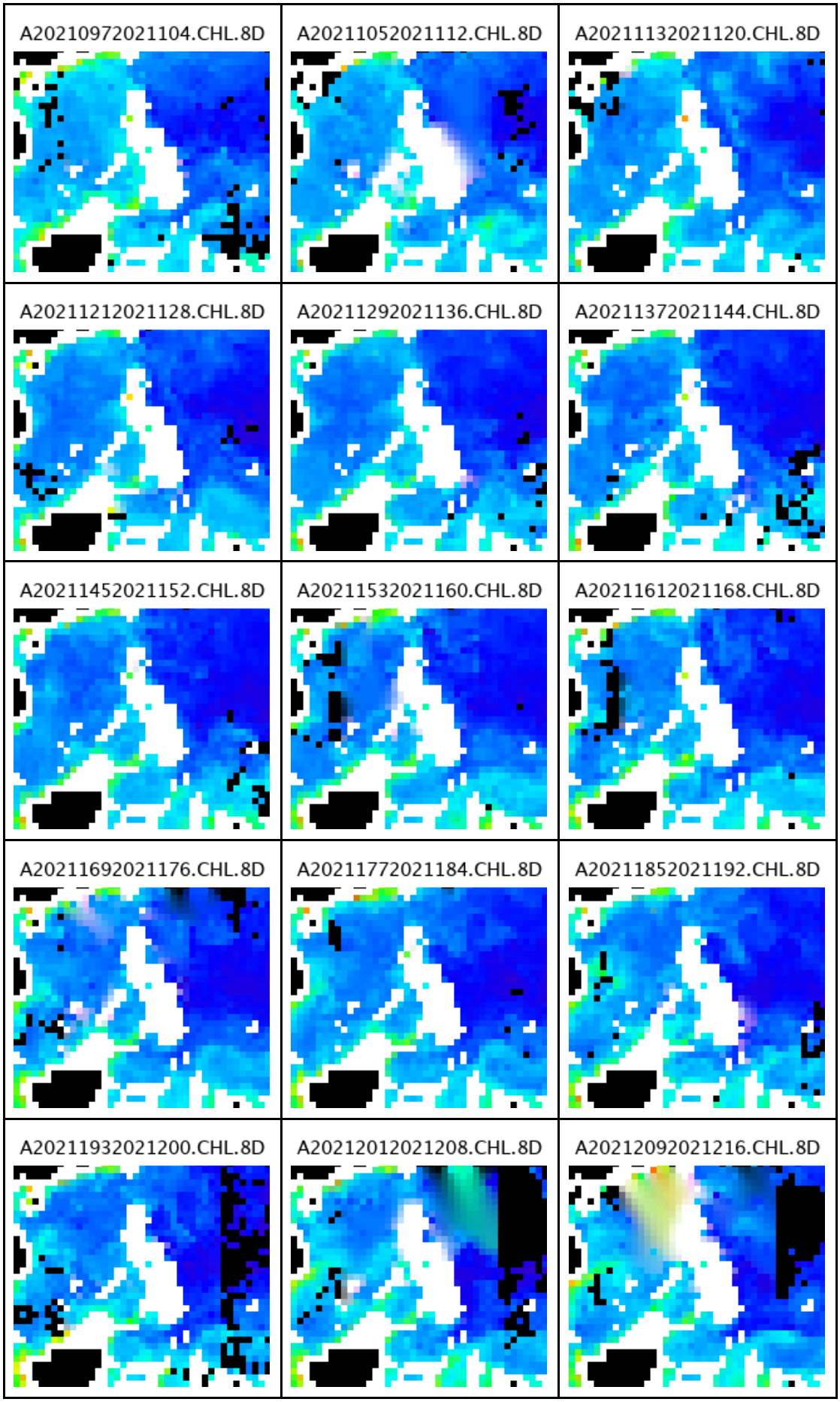
A20210972021104.CHL.8D
A20211052021112.CHL.8D
A20211132021120.CHL.8D
A20211212021128.CHL.8D
A20211292021136.CHL.8D
A20211372021144.CHL.8D
A20211452021152.CHL.8D
A20211532021160.CHL.8D
A20211612021168.CHL.8D
A20211692021176.CHL.8D
A20211772021184.CHL.8D
A20211852021192.CHL.8D
A20211932021200.CHL.8D
A20212012021208.CHL.8D
A20212092021216.CHL.8D

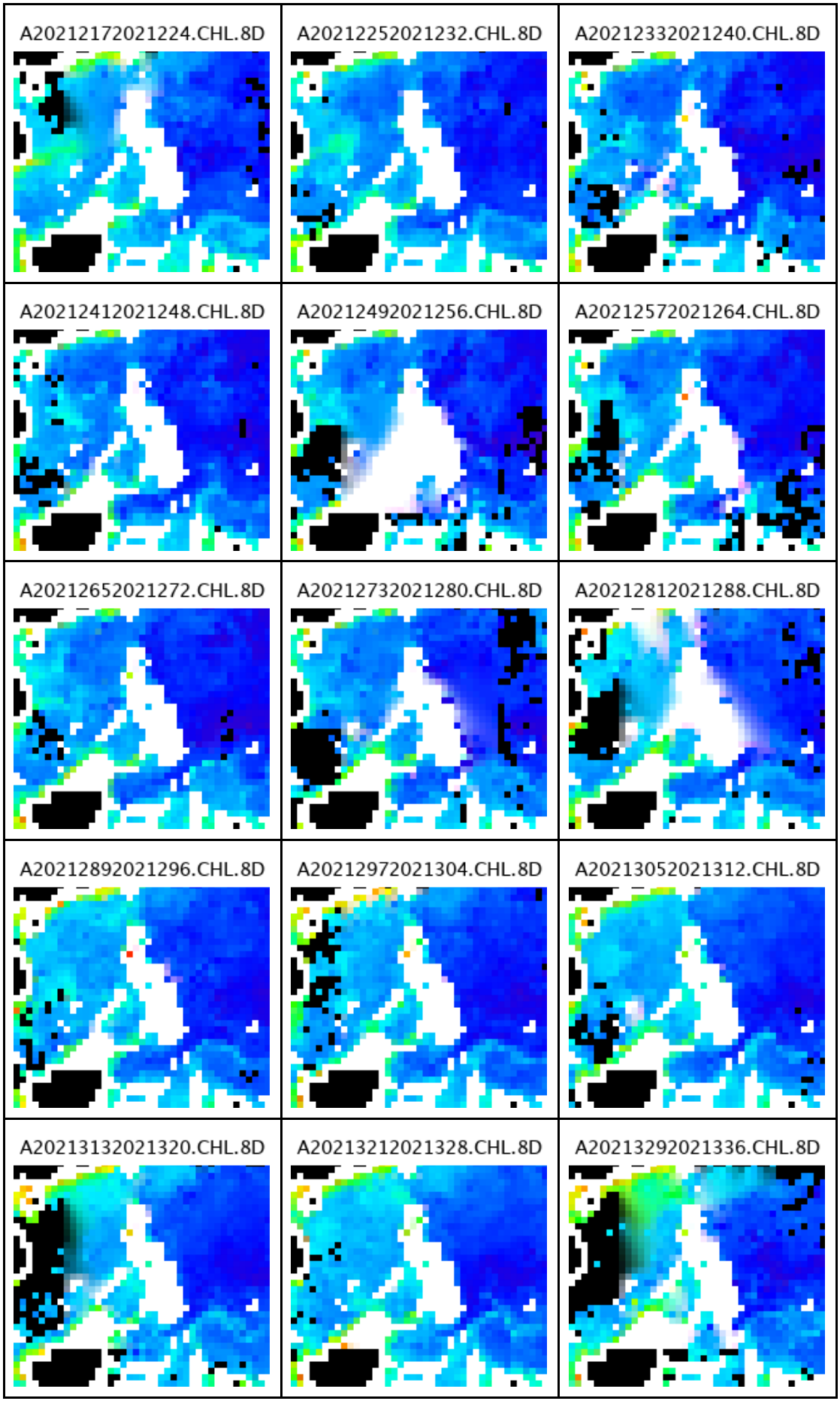
A20212172021224.CHL.8D
A20212252021232.CHL.8D
A20212332021240.CHL.8D
A20212412021248.CHL.8D
A20212492021256.CHL.8D
A20212572021264.CHL.8D
A20212652021272.CHL.8D
A20212732021280.CHL.8D
A20212812021288.CHL.8D
A20212892021296.CHL.8D
A20212972021304.CHL.8D
A20213052021312.CHL.8D
A20213132021320.CHL.8D
A20213212021328.CHL.8D
A20213292021336.CHL.8D

A20213372021344.CHL.8D 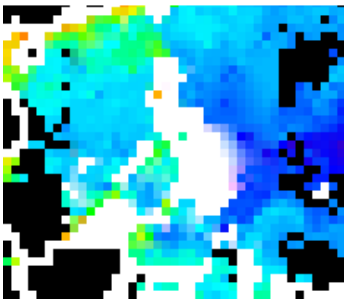	A20213452021352.CHL.8D 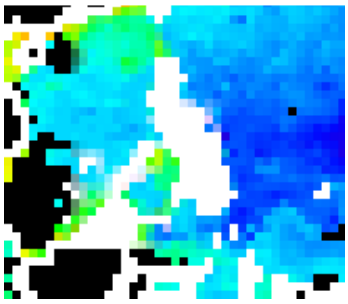	A20213532021360.CHL.8D 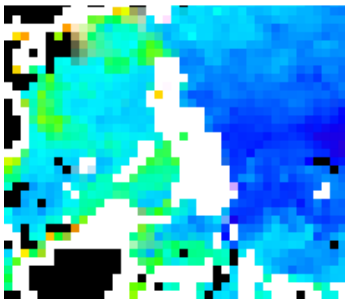
A20213612021365.CHL.8D 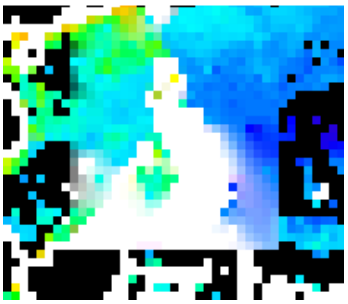		

Appendix E.
Spatio-Temporal Maps of SST (2019)

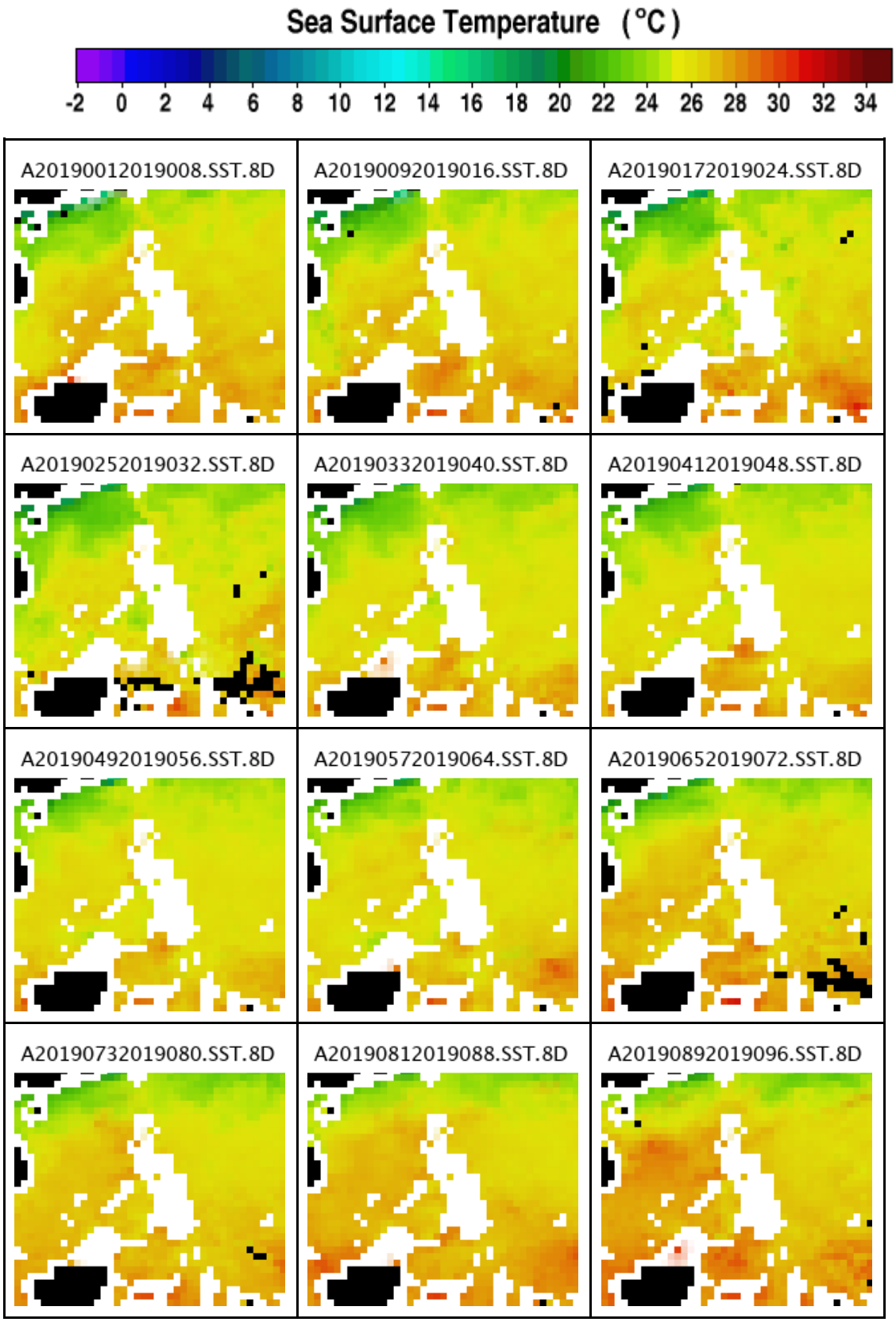

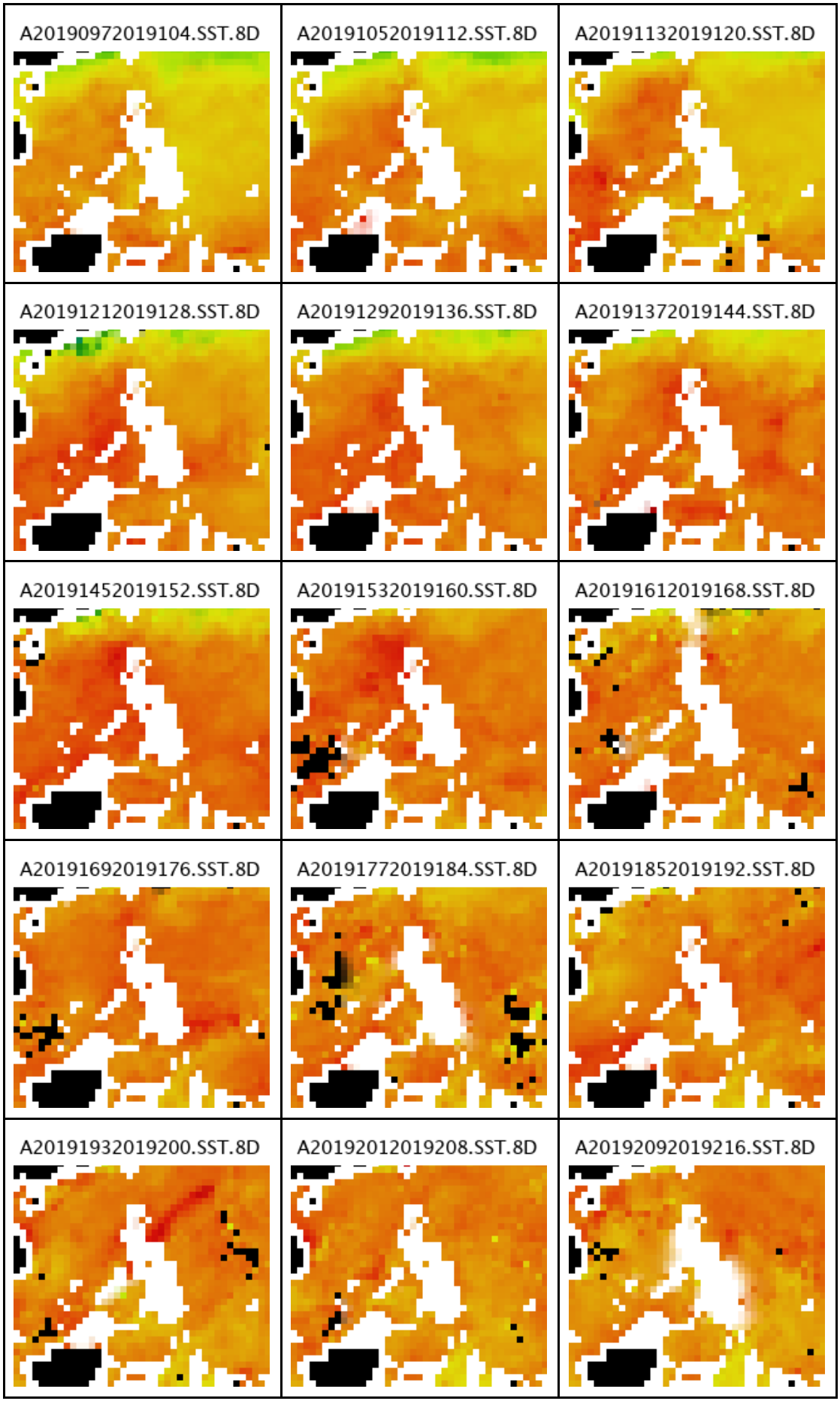
A20190972019104.SST.8D
A20191052019112.SST.8D
A20191132019120.SST.8D
A20191212019128.SST.8D
A20191292019136.SST.8D
A20191372019144.SST.8D
A20191452019152.SST.8D
A20191532019160.SST.8D
A20191612019168.SST.8D
A20191692019176.SST.8D
A20191772019184.SST.8D
A20191852019192.SST.8D
A20191932019200.SST.8D
A20192012019208.SST.8D
A20192092019216.SST.8D

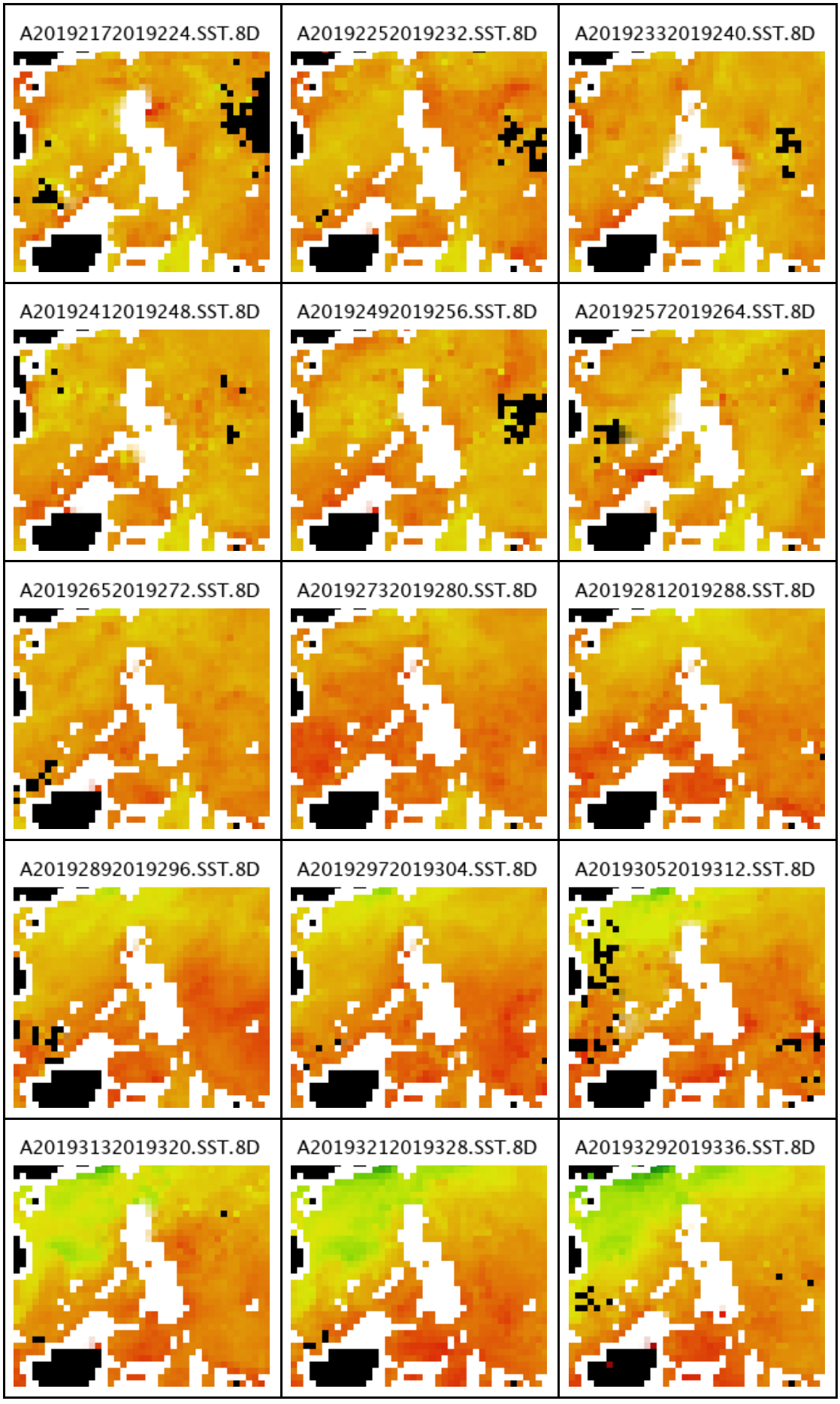
A20192172019224.SST.8D
A20192252019232.SST.8D
A20192332019240.SST.8D
A20192412019248.SST.8D
A20192492019256.SST.8D
A20192572019264.SST.8D
A20192652019272.SST.8D
A20192732019280.SST.8D
A20192812019288.SST.8D
A20192892019296.SST.8D
A20192972019304.SST.8D
A20193052019312.SST.8D
A20193132019320.SST.8D
A20193212019328.SST.8D
A20193292019336.SST.8D

A20193372019344.SST.8D 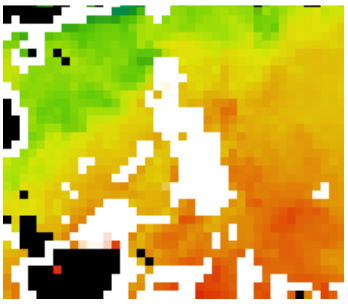	A20193452019352.SST.8D 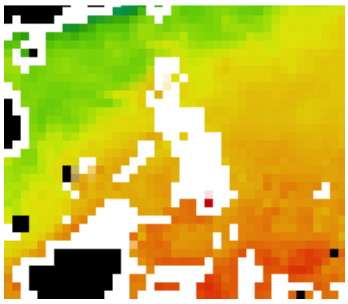	A20193532019360.SST.8D 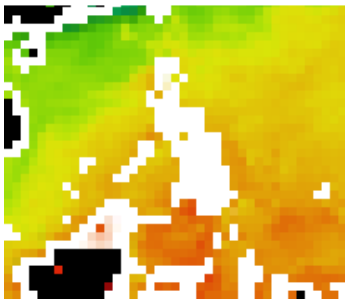
A20193612019365.SST.8D 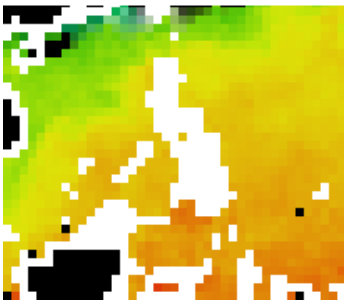		

Appendix F.
Spatio-Temporal Maps of SST (2020)

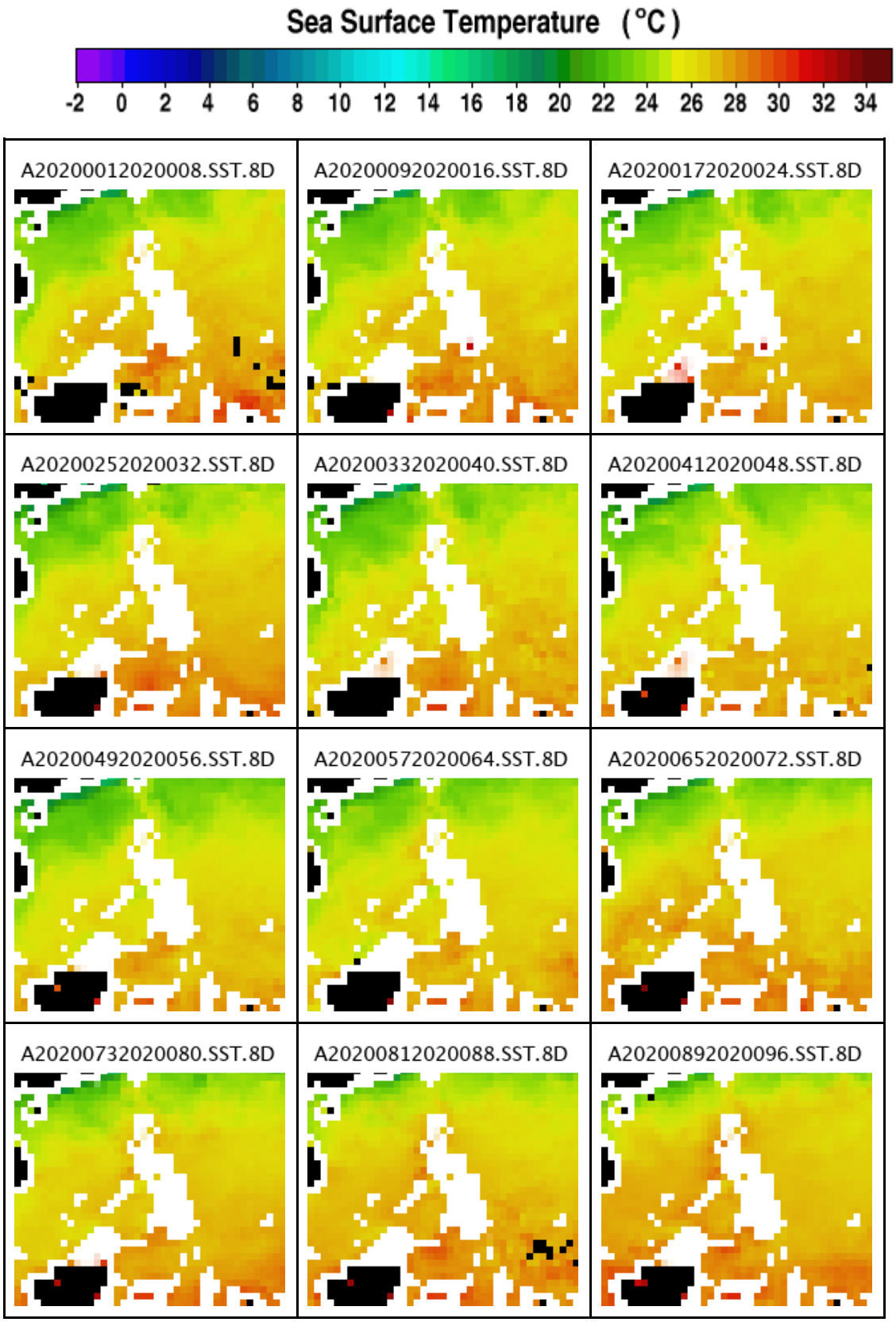

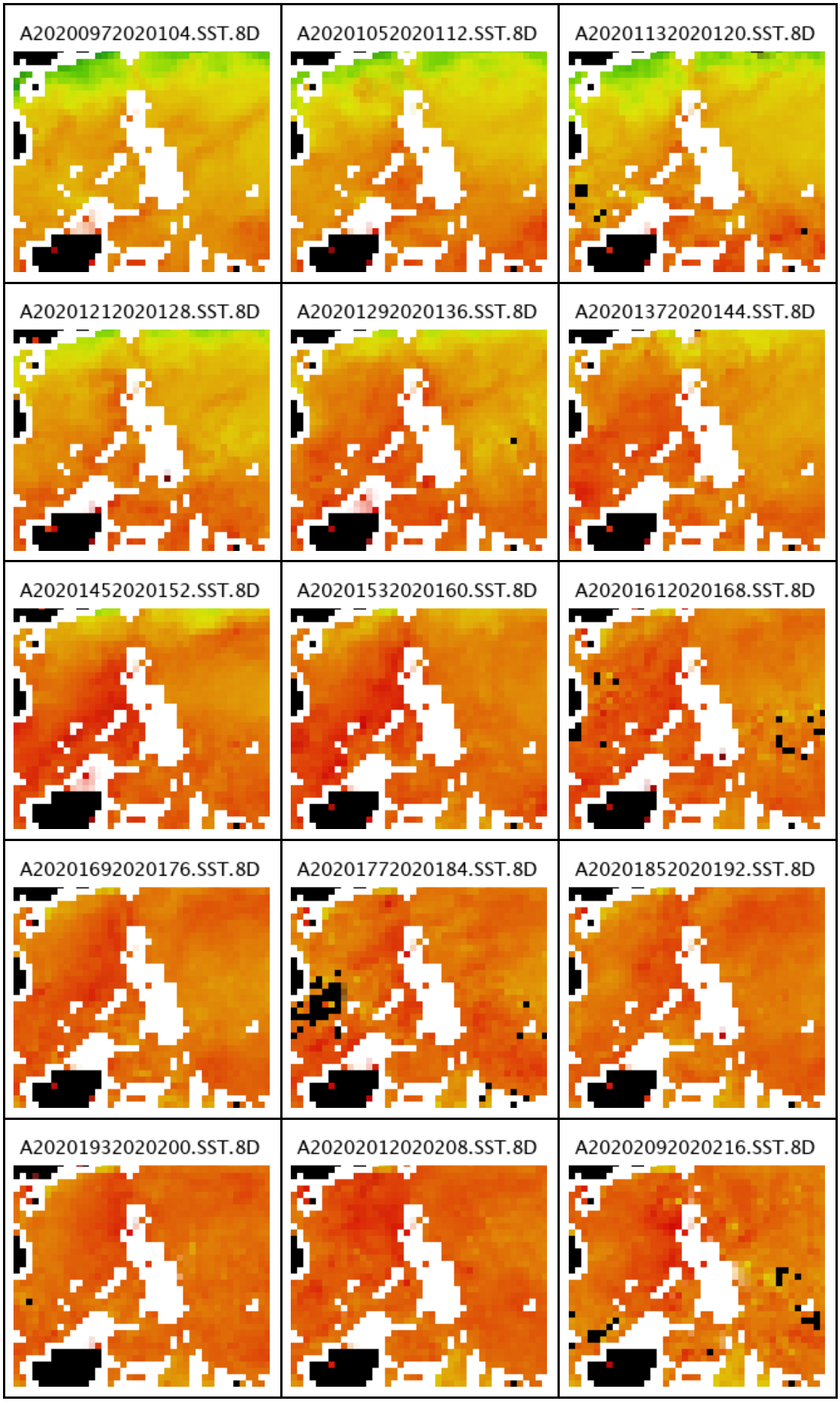
A20200972020104.SST.8D
A20201052020112.SST.8D
A20201132020120.SST.8D
A20201212020128.SST.8D
A20201292020136.SST.8D
A20201372020144.SST.8D
A20201452020152.SST.8D
A20201532020160.SST.8D
A20201612020168.SST.8D
A20201692020176.SST.8D
A20201772020184.SST.8D
A20201852020192.SST.8D
A20201932020200.SST.8D
A20202012020208.SST.8D
A20202092020216.SST.8D

A20202172020224.SST.8D 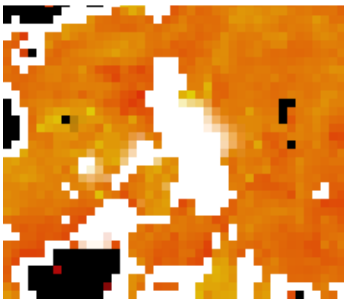	A20202252020232.SST.8D 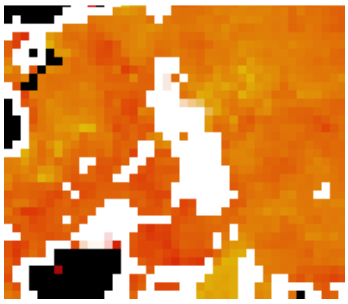	76TH
A20202412020248.SST.8D 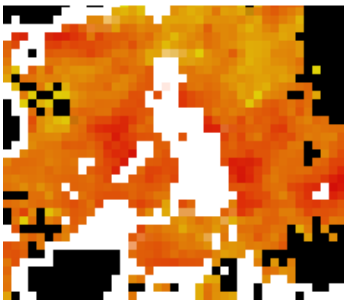	A20202492020256.SST.8D 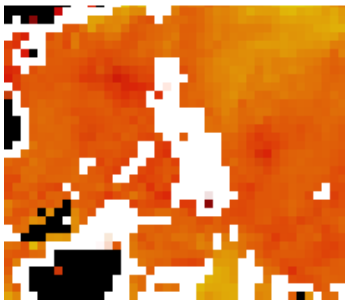	A20202572020264.SST.8D 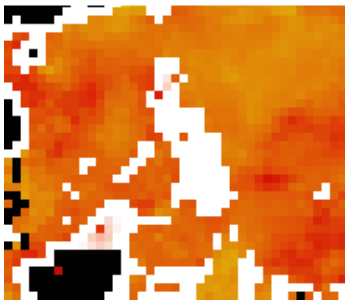
A20202652020272.SST.8D 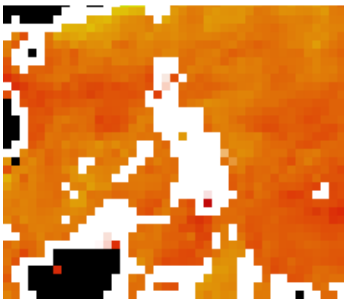	A20202732020280.SST.8D 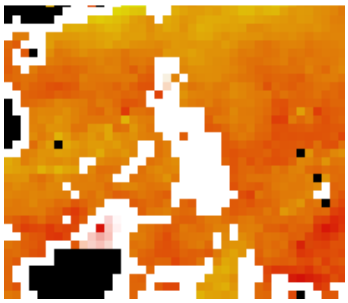	A20202812020288.SST.8D 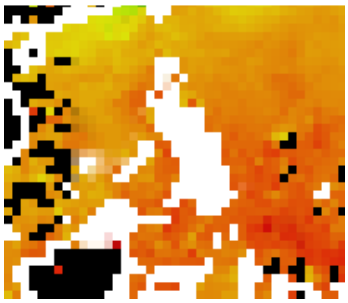
A20202892020296.SST.8D 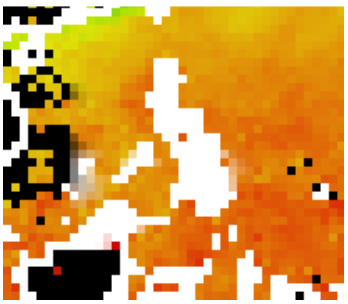	A20202972020304.SST.8D 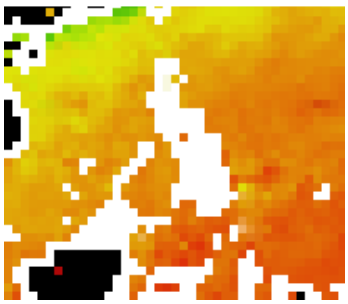	A20203052020312.SST.8D 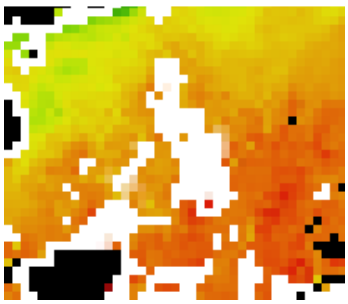
A20203132020320.SST.8D 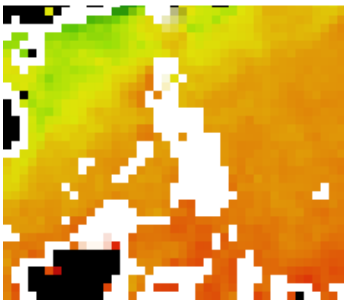	A20203212020328.SST.8D 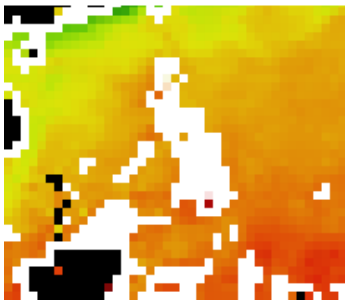	A20203292020336.SST.8D 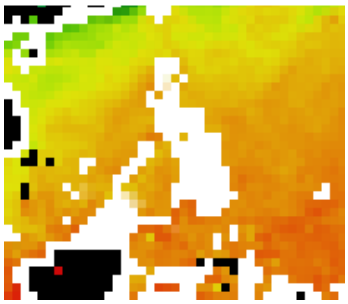

A20203372020344.SST.8D 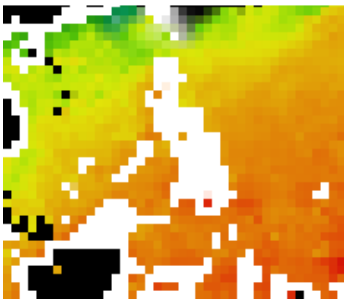	A20203452020352.SST.8D 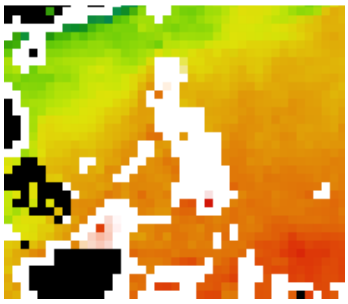	A20203532020360.SST.8D 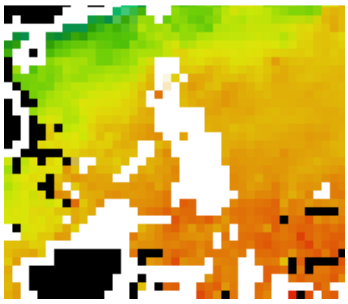
A20203612020366.SST.8D 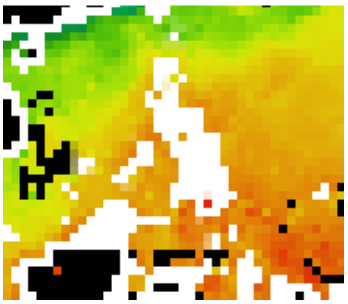		

Appendix G.
Spatio-Temporal Maps of SST (2021)

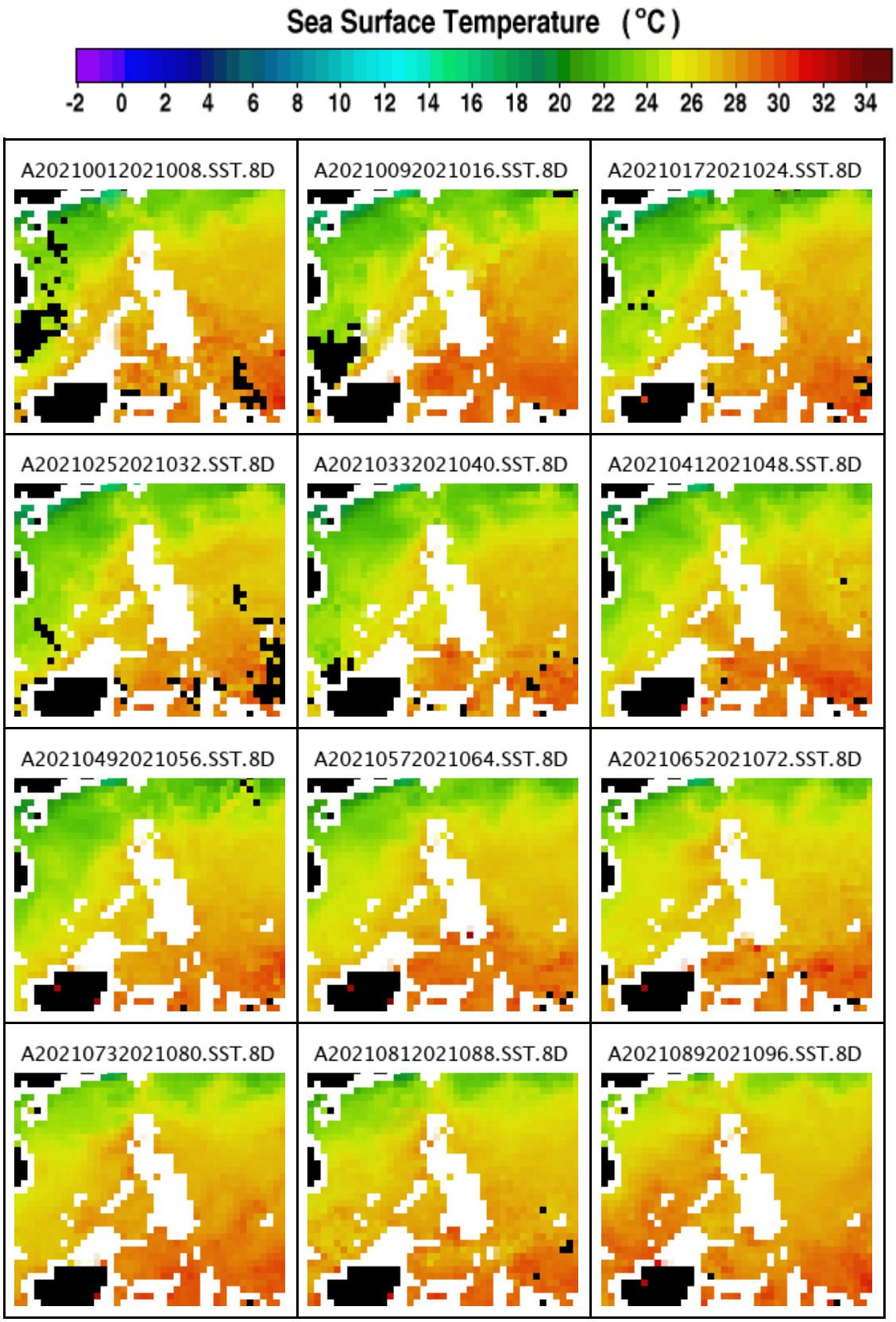

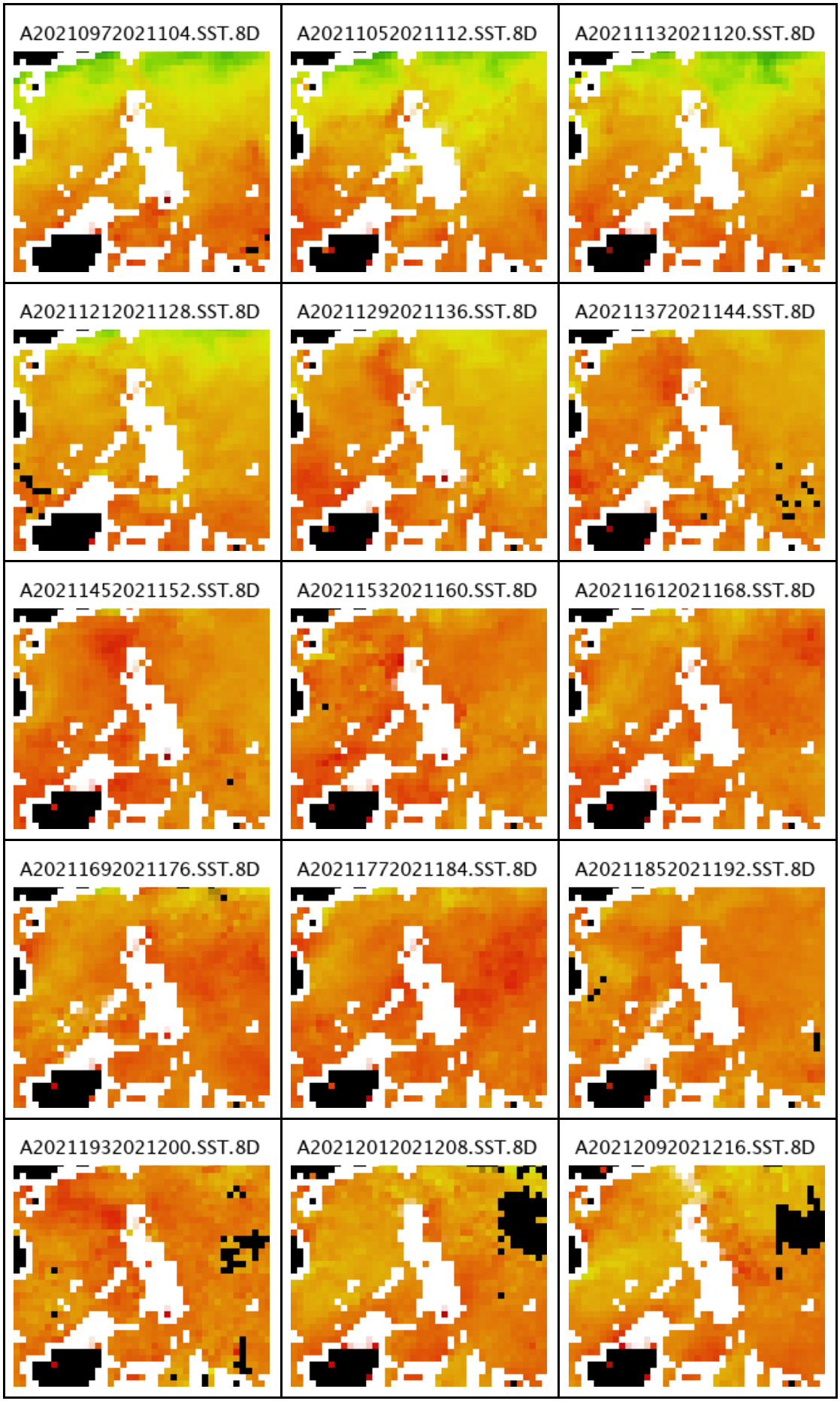
A20210972021104.SST.8D
A20211052021112.SST.8D
A20211132021120.SST.8D
A20211212021128.SST.8D
A20211292021136.SST.8D
A20211372021144.SST.8D
A20211452021152.SST.8D
A20211532021160.SST.8D
A20211612021168.SST.8D
A20211692021176.SST.8D
A20211772021184.SST.8D
A20211852021192.SST.8D
A20211932021200.SST.8D
A20212012021208.SST.8D
A20212092021216.SST.8D

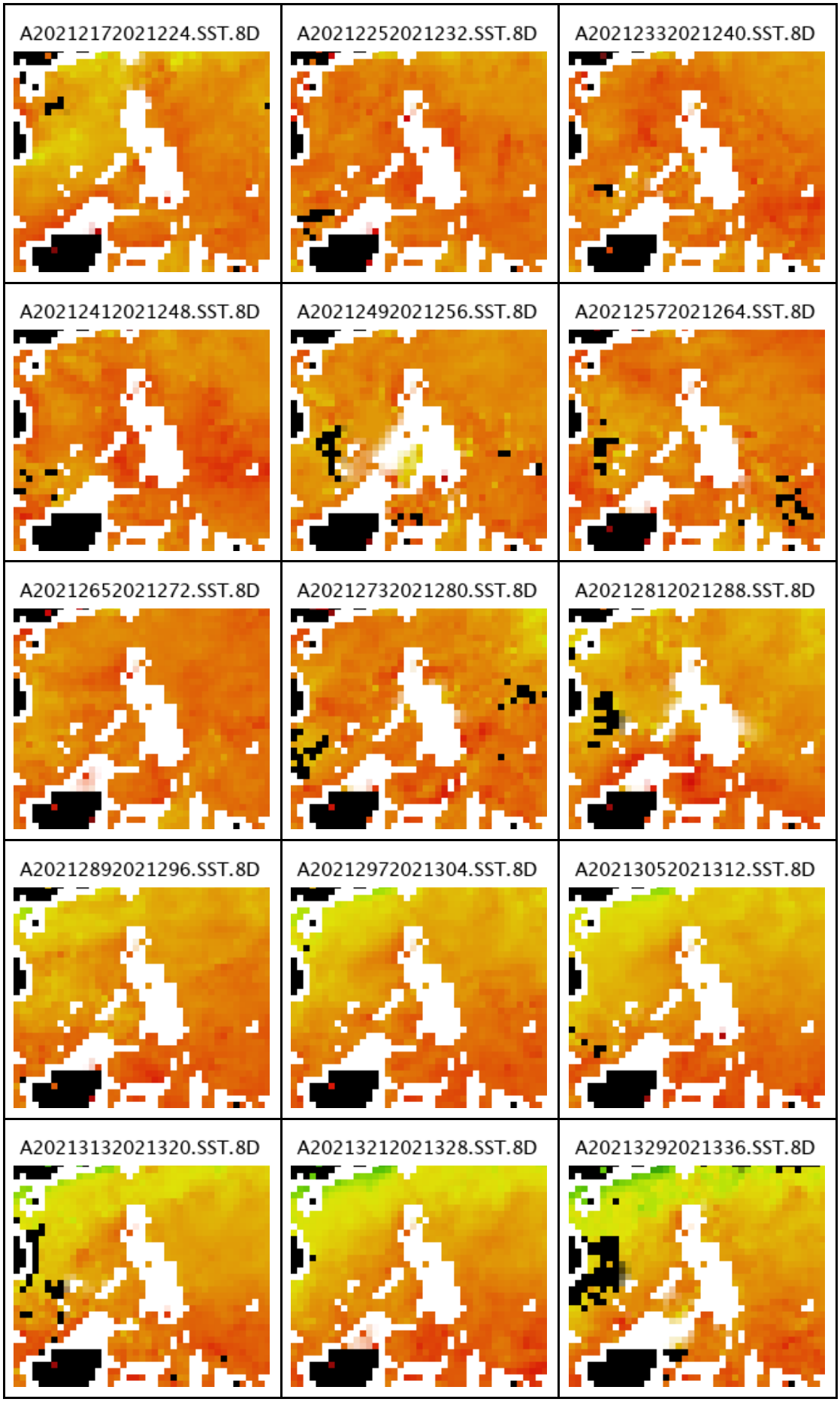
A20212172021224.SST.8D
A20212252021232.SST.8D
A20212332021240.SST.8D
A20212412021248.SST.8D
A20212492021256.SST.8D
A20212572021264.SST.8D
A20212652021272.SST.8D
A20212732021280.SST.8D
A20212812021288.SST.8D
A20212892021296.SST.8D
A20212972021304.SST.8D
A20213052021312.SST.8D
A20213132021320.SST.8D
A20213212021328.SST.8D
A20213292021336.SST.8D

A20213372021344.SST.8D 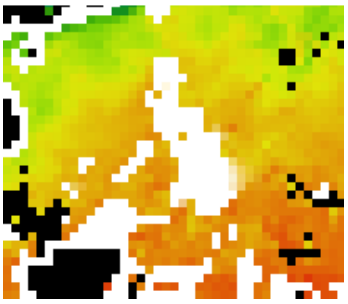	A20213452021352.SST.8D 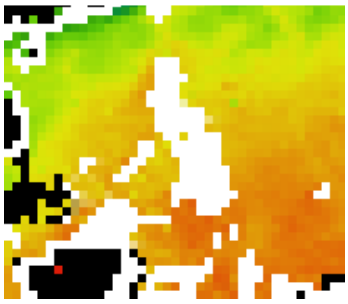	A20213532021360.SST.8D 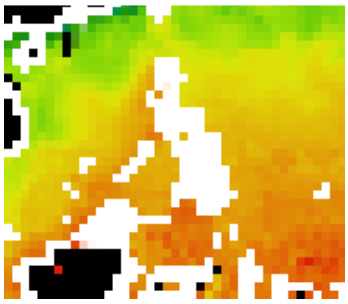
A20213612021365.SST.8D 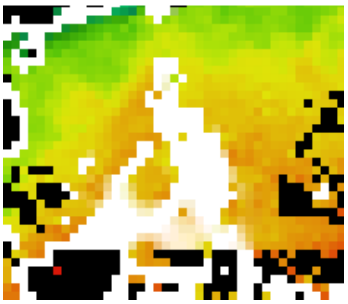		

Appendix H.
PAGASA-DOST Typhoon Tracks 2019

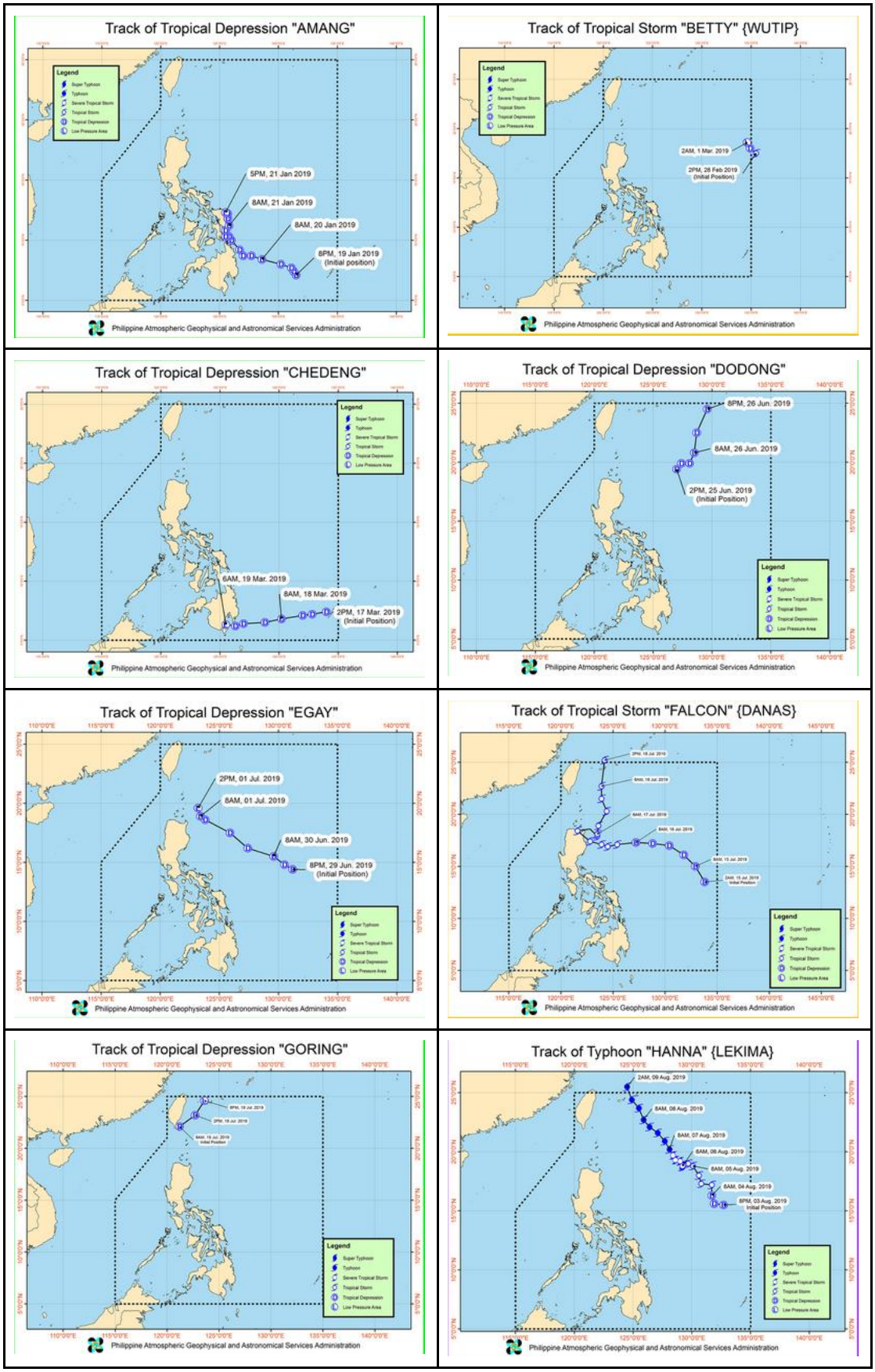

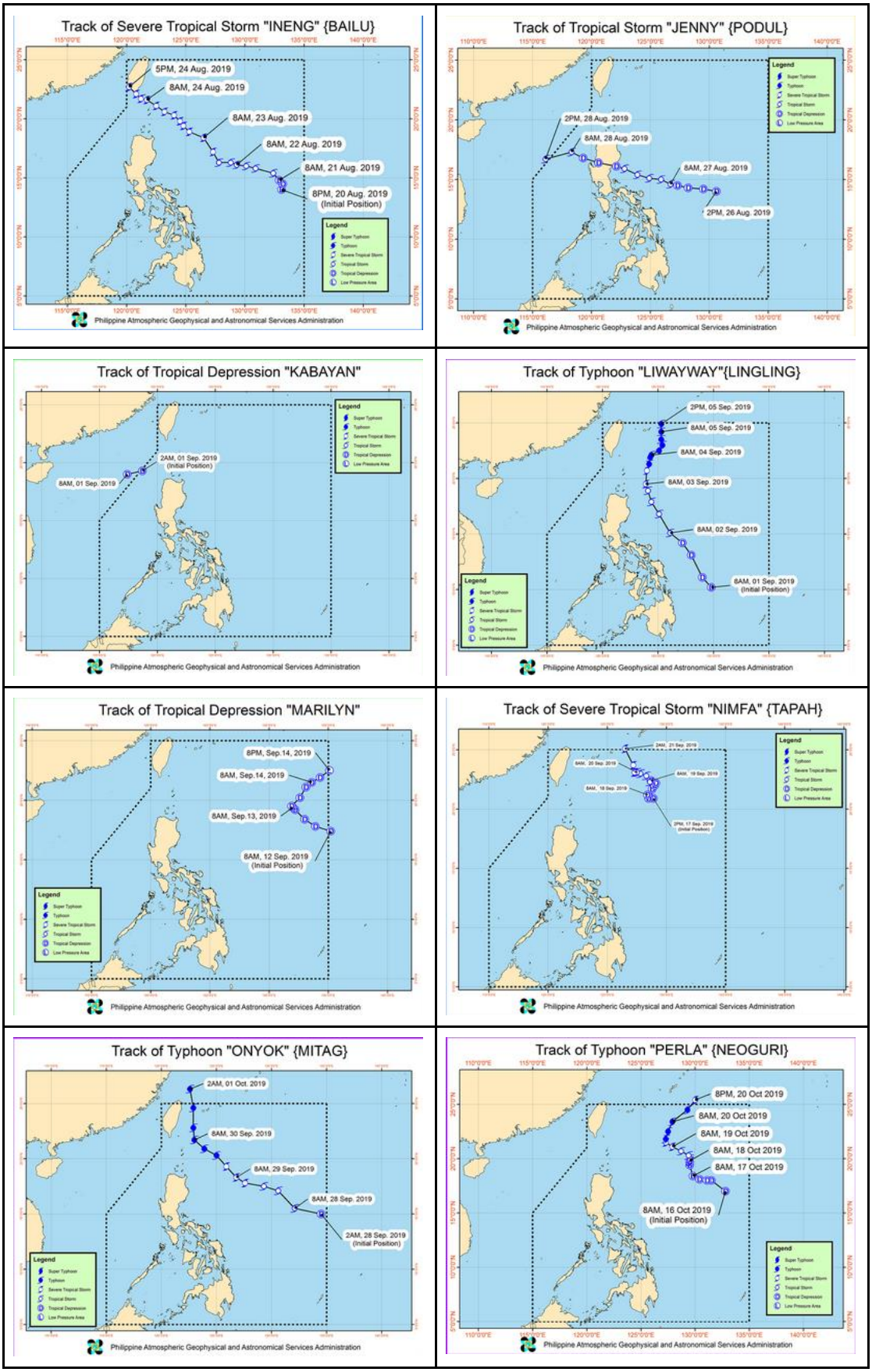
Track of Severe Tropical Storm "INENG" {BAILU}
5PM, 24 Aug. 2019
8AM, 24 Aug. 2019
8AM, 23 Aug. 2019
8AM, 22 Aug. 2019
8AM, 21 Aug. 2019
8PM, 20 Aug. 2019 (Initial Position)
Legend
Philippine Atmospheric Geophysical and Astronomical Services Administration
Track of Tropical Storm "JENNY" {PODUL}
2PM, 28 Aug. 2019
8AM, 28 Aug. 2019
8AM, 27 Aug. 2019
2PM, 26 Aug. 2019
Legend
Philippine Atmospheric Geophysical and Astronomical Services Administration
Track of Tropical Depression "KABAYAN"
2AM, 01 Sep. 2019 (Initial Position)
8AM, 01 Sep. 2019
Legend
Philippine Atmospheric Geophysical and Astronomical Services Administration
Track of Typhoon "LIWAYWAY"{LINGLING}
2PM, 05 Sep. 2019
8AM, 05 Sep. 2019
8AM, 04 Sep. 2019
8AM, 03 Sep. 2019
8AM, 02 Sep. 2019
8AM, 01 Sep. 2019 (Initial Position)
Legend
Philippine Atmospheric Geophysical and Astronomical Services Administration
Track of Tropical Depression "MARILYN"
8PM, Sep.14, 2019
8AM, Sep.14, 2019
8AM, Sep.13, 2019
8AM, 12 Sep. 2019 (Initial Position)
Legend
Philippine Atmospheric Geophysical and Astronomical Services Administration
Track of Severe Tropical Storm "NIMFA" {TAPAH}
Legend
Philippine Atmospheric Geophysical and Astronomical Services Administration
Track of Typhoon "ONYOK" {MITAG}
2AM, 01 Oct. 2019
8AM, 30 Sep. 2019
8AM, 29 Sep. 2019
8AM, 28 Sep. 2019
2AM, 28 Sep. 2019 (Initial Position)
Legend
Philippine Atmospheric Geophysical and Astronomical Services Administration
Track of Typhoon "PERLA" {NEOGURI}
8PM, 20 Oct 2019
8AM, 20 Oct 2019
8AM, 19 Oct 2019
8AM, 18 Oct 2019
8AM, 17 Oct 2019
8AM, 16 Oct 2019 (Initial Position)
Legend
Philippine Atmospheric Geophysical and Astronomical Services Administration

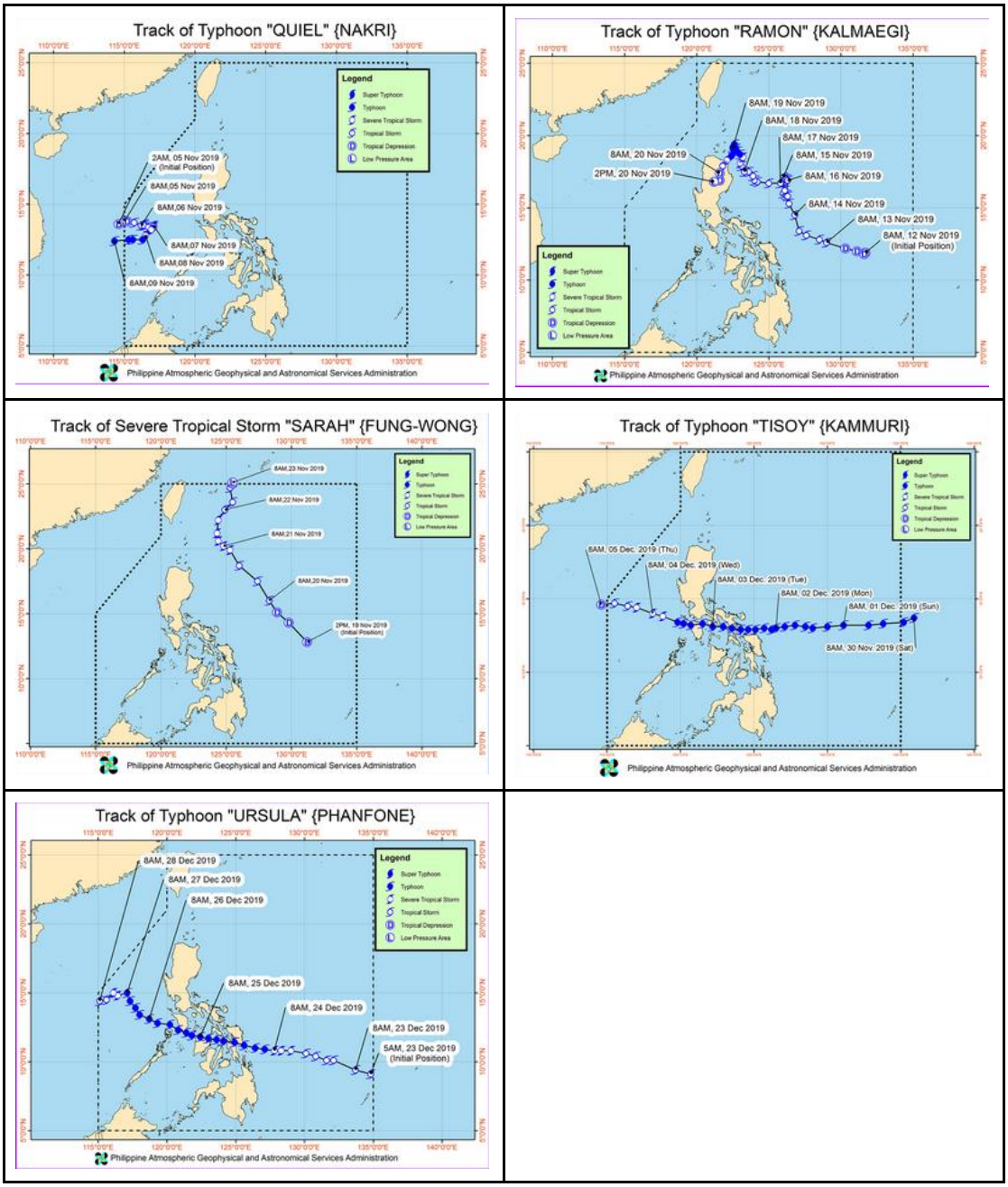
Track of Typhoon "QUIEL" {NAKRI}
Legend
Super Typhoon
Typhoon
Severe Tropical Storm
Tropical Storm
Tropical Depression
Low Pressure Area
2AM, 05 Nov 2019 (Initial Position)
8AM,05 Nov 2019
8AM,06 Nov 2019
8AM,07 Nov 2019
8AM,08 Nov 2019
8AM,09 Nov 2019
Philippine Atmospheric Geophysical and Astronomical Services Administration
Track of Typhoon "RAMON" {KALMAEGI}
8AM, 19 Nov 2019
8AM, 18 Nov 2019
8AM, 17 Nov 2019
8AM, 20 Nov 2019
8AM, 15 Nov 2019
2PM, 20 Nov 2019
8AM, 16 Nov 2019
8AM, 14 Nov 2019
8AM, 13 Nov 2019
8AM, 12 Nov 2019 (Initial Position)
Philippine Atmospheric Geophysical and Astronomical Services Administration
Track of Severe Tropical Storm "SARAH" {FUNG-WONG}
8AM,23 Nov 2019
8AM,22 Nov 2019
8AM,21 Nov 2019
8AM,20 Nov 2019
2PM, 19 Nov 2019 (Initial Position)
Philippine Atmospheric Geophysical and Astronomical Services Administration
Track of Typhoon "TISOY" {KAMMURI}
8AM, 05 Dec 2019 (Thu)
8AM, 04 Dec 2019 (Wed)
8AM, 03 Dec 2019 (Tue)
8AM, 02 Dec 2019 (Mon)
8AM, 01 Dec 2019 (Sun)
8AM, 30 Nov 2019 (Sat)
Philippine Atmospheric Geophysical and Astronomical Services Administration
Track of Typhoon "URSULA" {PHANFONE}
8AM, 28 Dec 2019
8AM, 27 Dec 2019
8AM, 26 Dec 2019
8AM, 25 Dec 2019
8AM, 24 Dec 2019
8AM, 23 Dec 2019
5AM, 23 Dec 2019 (Initial Position)
Philippine Atmospheric Geophysical and Astronomical Services Administration

Appendix I.
DOST Typhoon Tracks 2020

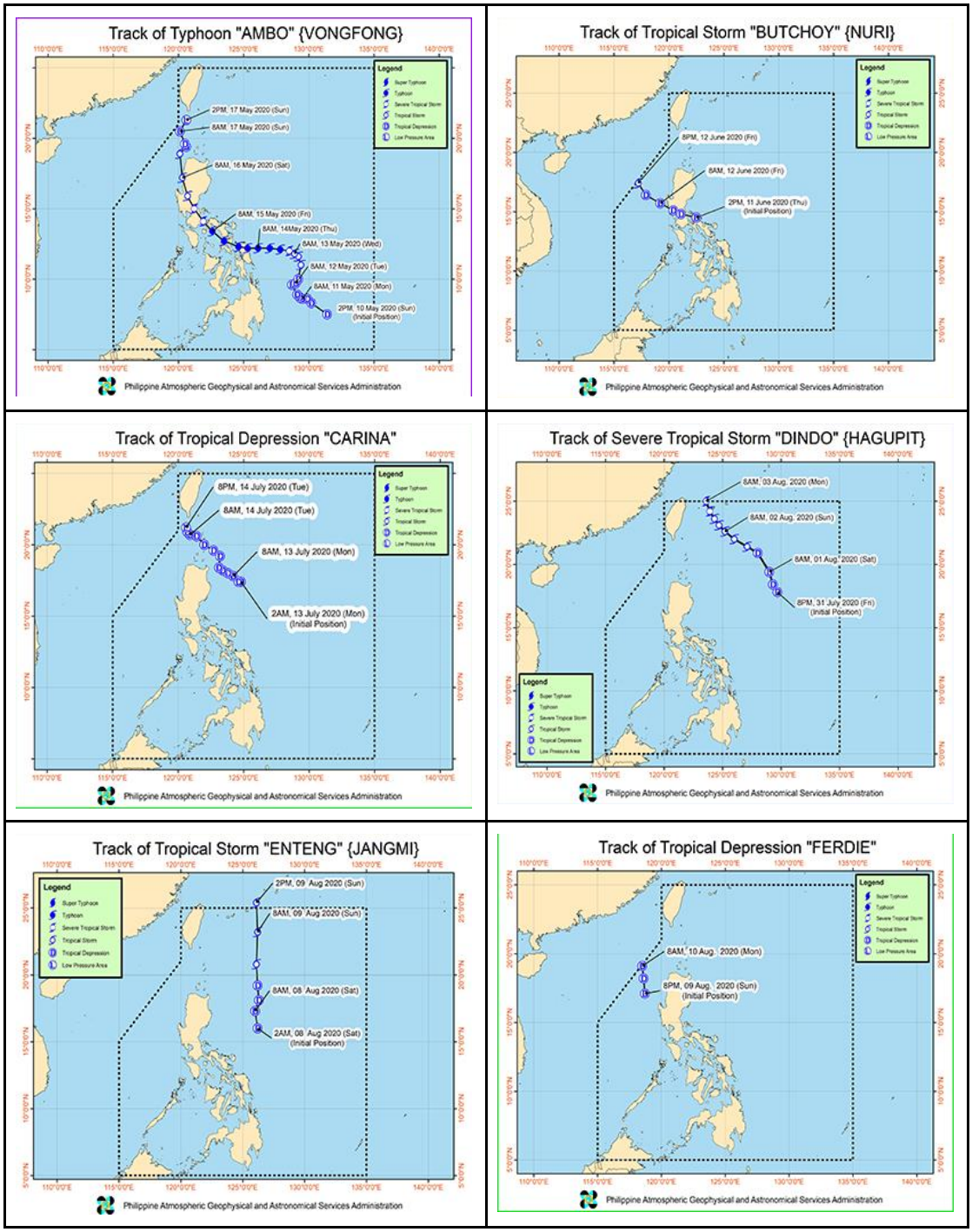

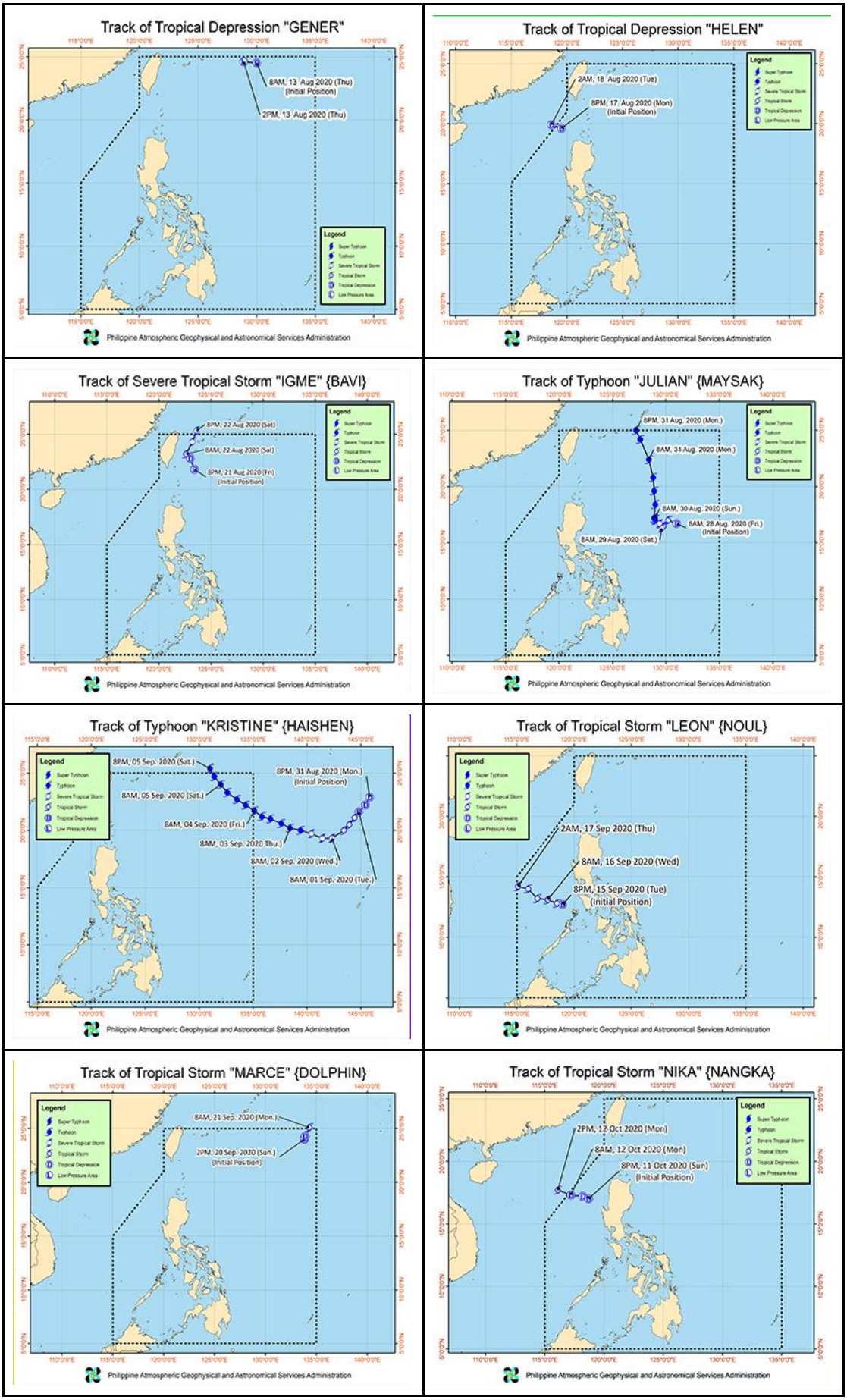
Track of Tropical Depression "GENER"
8AM, 13 Aug 2020 (Thu)
(Initial Position)
2PM, 13 Aug 2020 (Thu)
Legend
Philippine Atmospheric Geophysical and Astronomical Services Administration
Track of Tropical Depression "HELEN"
2AM, 18 Aug 2020 (Tue)
8PM, 17 Aug 2020 (Mon)
(Initial Position)
Legend
Philippine Atmospheric Geophysical and Astronomical Services Administration
Track of Severe Tropical Storm "IGME" {BAVI}
8PM, 22 Aug 2020 (Sat)
8AM, 22 Aug 2020 (Sat)
8PM, 21 Aug 2020 (Fri)
(Initial Position)
Legend
Philippine Atmospheric Geophysical and Astronomical Services Administration
Track of Typhoon "JULIAN" {MAYSAK}
8PM, 31 Aug 2020 (Mon.)
8AM, 31 Aug 2020 (Mon.)
8AM, 30 Aug 2020 (Sun.)
8AM, 28 Aug 2020 (Fri.)
(Initial Position)
8AM, 29 Aug 2020 (Sat.)
Legend
Philippine Atmospheric Geophysical and Astronomical Services Administration
Track of Typhoon "KRISTINE" {HAISHEN}
8PM, 05 Sep 2020 (Sat.)
8AM, 05 Sep 2020 (Sat.)
8PM, 31 Aug 2020 (Mon.)
(Initial Position)
8AM, 04 Sep 2020 (Fri.)
8AM, 03 Sep 2020 Thu.)
8AM, 02 Sep 2020 (Wed.)
8AM, 01 Sep 2020 (Tue.)
Legend
Philippine Atmospheric Geophysical and Astronomical Services Administration
Track of Tropical Storm "LEON" {NOUL}
2AM, 17 Sep 2020 (Thu)
8AM, 16 Sep 2020 (Wed)
8PM, 15 Sep 2020 (Tue)
(Initial Position)
Legend
Philippine Atmospheric Geophysical and Astronomical Services Administration
Track of Tropical Storm "MARCE" {DOLPHIN}
8AM, 21 Sep 2020 (Mon.)
2PM, 20 Sep 2020 (Sun.)
(Initial Position)
Legend
Philippine Atmospheric Geophysical and Astronomical Services Administration
Track of Tropical Storm "NIKA" {NANGKA}
2PM, 12 Oct 2020 (Mon)
8AM, 12 Oct 2020 (Mon)
8PM, 11 Oct 2020 (Sun)
(Initial Position)
Legend
Philippine Atmospheric Geophysical and Astronomical Services Administration

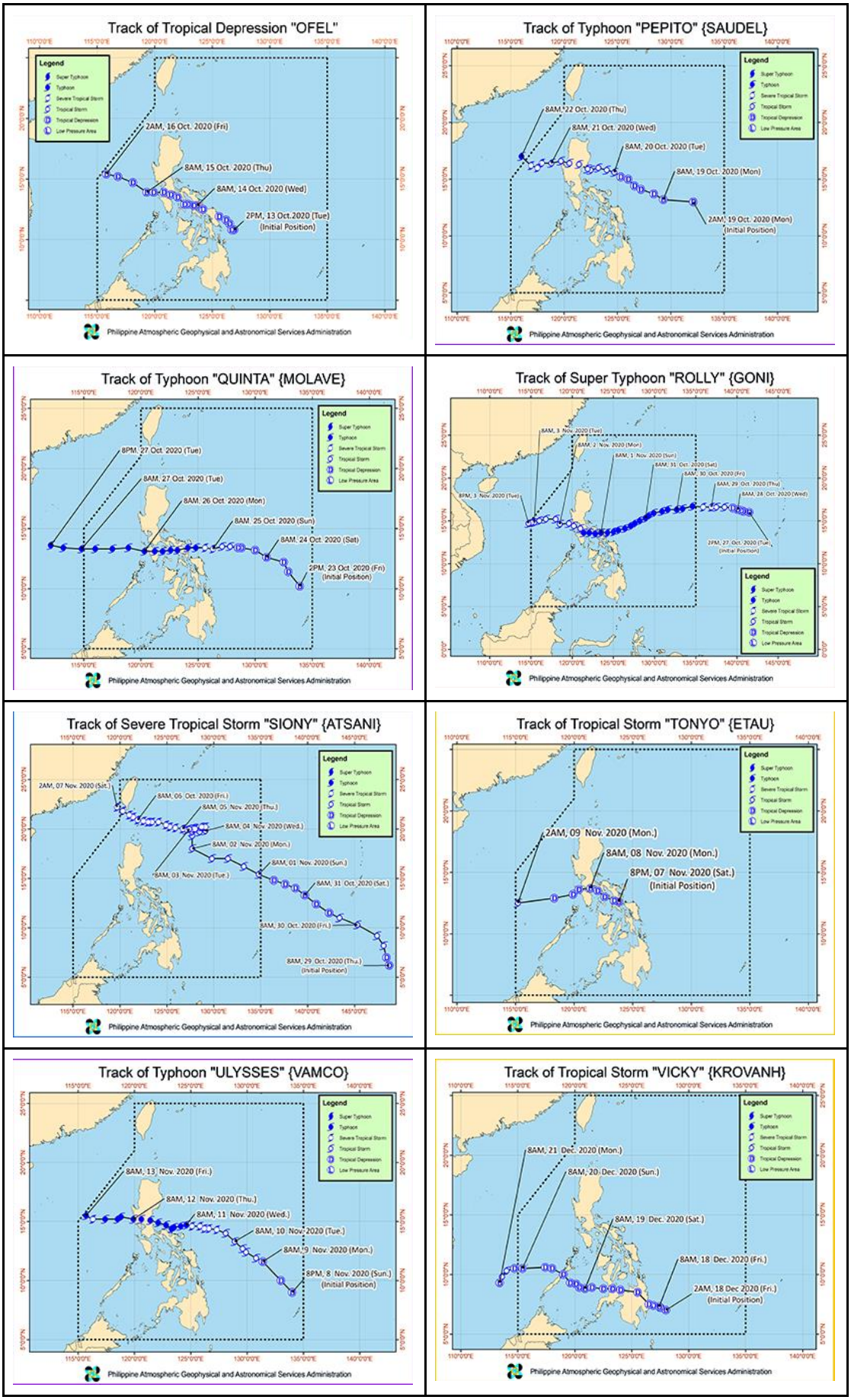
Track of Tropical Depression "OFEL"
2AM, 16 Oct. 2020 (Fri)
8AM, 15 Oct. 2020 (Thu)
8AM, 14 Oct. 2020 (Wed)
2PM, 13 Oct.2020 (Tue)
(Initial Position)
Track of Typhoon "PEPITO" {SAUDEL}
8AM, 22 Oct. 2020 (Thu)
8AM, 21 Oct. 2020 (Wed)
8AM, 20 Oct. 2020 (Tue)
8AM, 19 Oct. 2020 (Mon)
2AM, 19 Oct. 2020 (Mon)
(Initial Position)
Track of Typhoon "QUINTA" {MOLAVE}
8PM, 27 Oct. 2020 (Tue)
8AM, 27 Oct. 2020 (Tue)
8AM, 26 Oct. 2020 (Mon)
8AM, 25 Oct. 2020 (Sun)
8AM, 24 Oct. 2020 (Sat)
2PM, 23 Oct. 2020 (Fri)
(Initial Position)
Track of Super Typhoon "ROLLY" {GONI}
Track of Severe Tropical Storm "SIONY" {ATSANI}
2AM, 07 Nov. 2020 (Sat.)
8AM, 06 Oct. 2020 (Fri.)
8AM, 05 Nov. 2020 (Thu.)
8AM, 04 Nov. 2020 (Wed.)
8AM, 02 Nov. 2020 (Mon.)
8AM, 01 Nov. 2020 (Sun.)
8AM, 03 Nov. 2020 (Tue.)
8AM, 31 Oct. 2020 (Sat.)
8AM, 30 Oct. 2020 (Fri.)
8AM, 29 Oct. 2020 (Thu.)
(Initial Position)
Track of Tropical Storm "TONYO" {ETAU}
2AM, 09 Nov. 2020 (Mon.)
8AM, 08 Nov. 2020 (Mon.)
8PM, 07 Nov. 2020 (Sat.)
(Initial Position)
Track of Typhoon "ULYSSES" {VAMCO}
8AM, 13 Nov. 2020 (Fri.)
8AM, 12 Nov. 2020 (Thu.)
8AM, 11 Nov. 2020 (Wed.)
8AM, 10 Nov. 2020 (Tue.)
8AM, 9 Nov. 2020 (Mon.)
8PM, 8 Nov. 2020 (Sun.)
(Initial Position)
Track of Tropical Storm "VICKY" {KROVANH}
8AM, 21 Dec. 2020 (Mon.)
8AM, 20 Dec. 2020 (Sun.)
8AM, 19 Dec. 2020 (Sat.)
8AM, 18 Dec. 2020 (Fri.)
2AM, 18 Dec 2020 (Fri.)
(Initial Position)
Philippine Atmospheric Geophysical and Astronomical Services Administration

Appendix J.
PAGASA-DOST Typhoon Tracks 2021

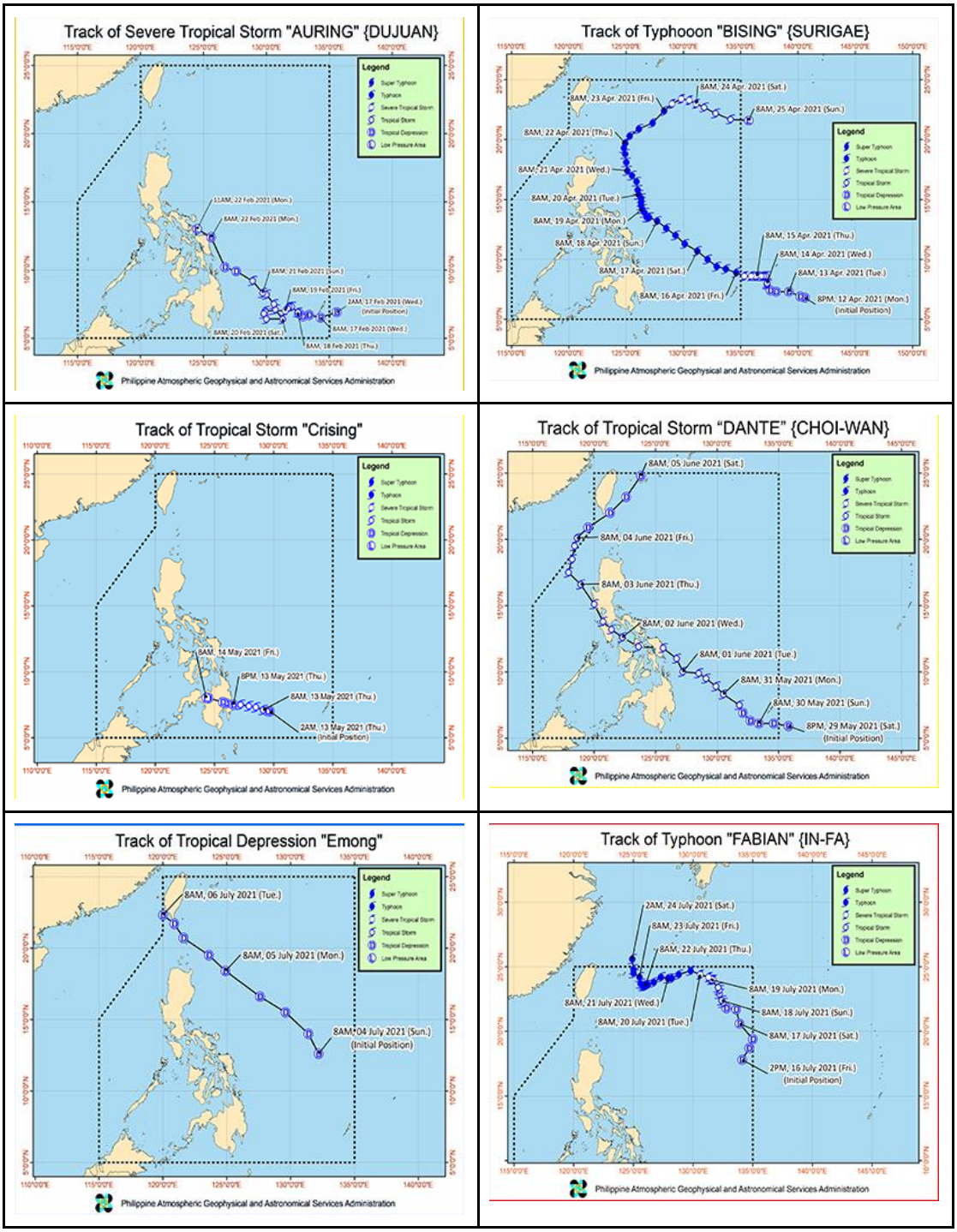

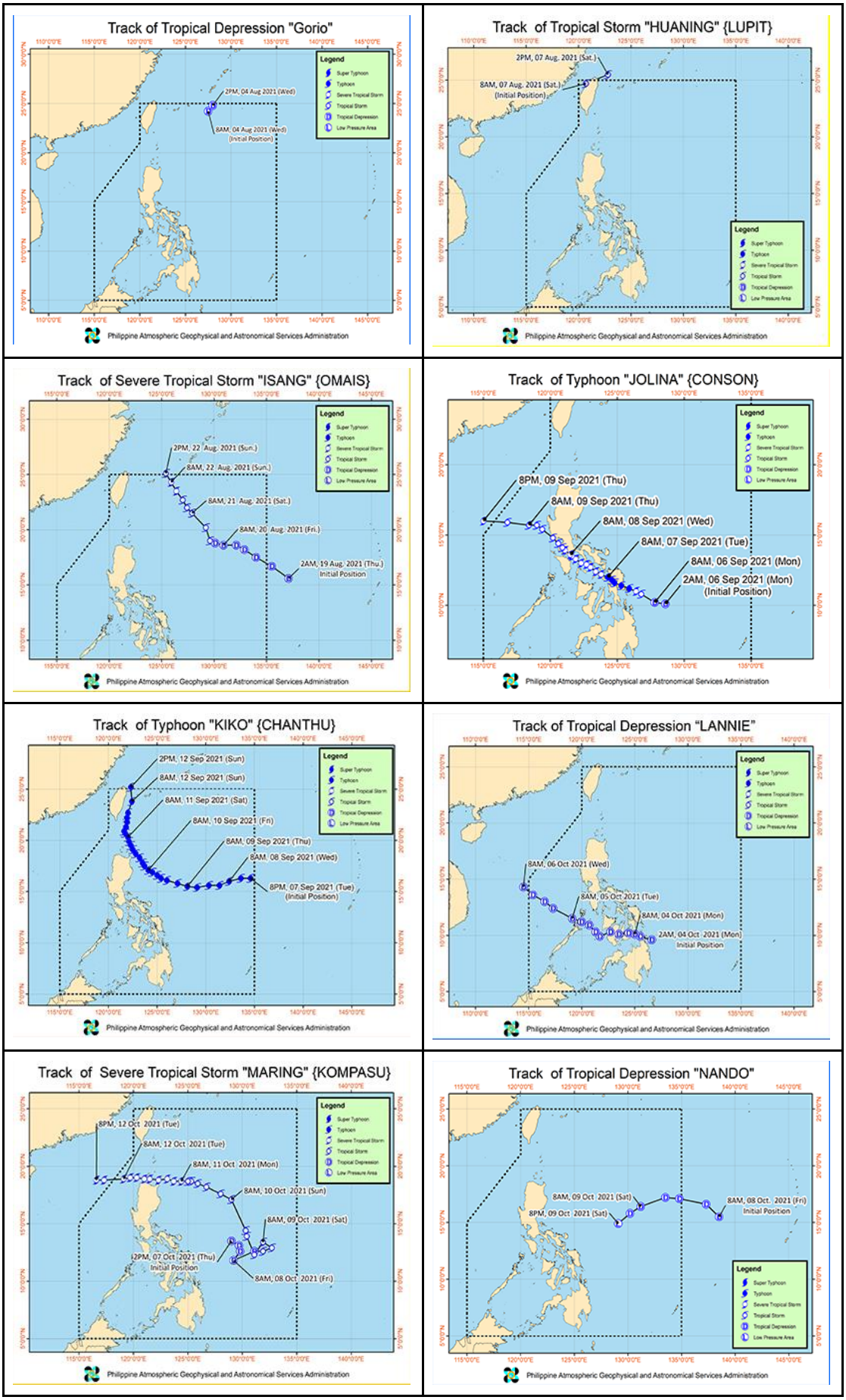
Track of Tropical Depression "Gorio"
2PM, 04 Aug 2021 (Wed)
8AM, 04 Aug 2021 (Wed)
(Initial Position)
Legend
Philippine Atmospheric Geophysical and Astronomical Services Administration
Track of Tropical Storm "HUANING" {LUPIT}
2PM, 07 Aug. 2021 (Sat.)
8AM, 07 Aug. 2021 (Sat.)
(Initial Position)
Legend
Philippine Atmospheric Geophysical and Astronomical Services Administration
Track of Severe Tropical Storm "ISANG" {OMAIS}
2PM, 22 Aug. 2021 (Sun.)
8AM, 22 Aug. 2021 (Sun.)
8AM, 21 Aug. 2021 (Sat.)
8AM, 20 Aug. 2021 (Fri.)
2AM, 19 Aug. 2021 (Thu.)
Initial Position
Legend
Philippine Atmospheric Geophysical and Astronomical Services Administration
Track of Typhoon "JOLINA" {CONSON}
8PM, 09 Sep 2021 (Thu)
8AM, 09 Sep 2021 (Thu)
8AM, 08 Sep 2021 (Wed)
8AM, 07 Sep 2021 (Tue)
8AM, 06 Sep 2021 (Mon)
2AM, 06 Sep 2021 (Mon)
(Initial Position)
Legend
Philippine Atmospheric Geophysical and Astronomical Services Administration
Track of Typhoon "KIKO" {CHANTHU}
2PM, 12 Sep 2021 (Sun)
8AM, 12 Sep 2021 (Sun)
8AM, 11 Sep 2021 (Sat)
8AM, 10 Sep 2021 (Fri)
8AM, 09 Sep 2021 (Thu)
8AM, 08 Sep 2021 (Wed)
8PM, 07 Sep 2021 (Tue)
(Initial Position)
Legend
Philippine Atmospheric Geophysical and Astronomical Services Administration
Track of Tropical Depression "LANNIE"
8AM, 06 Oct 2021 (Wed)
8AM, 05 Oct 2021 (Tue)
8AM, 04 Oct 2021 (Mon)
2AM, 04 Oct 2021 (Mon)
Initial Position
Legend
Philippine Atmospheric Geophysical and Astronomical Services Administration
Track of Severe Tropical Storm "MARING" {KOMPASU}
8PM, 12 Oct 2021 (Tue)
8AM, 12 Oct 2021 (Tue)
8AM, 11 Oct 2021 (Mon)
8AM, 10 Oct 2021 (Sun)
8AM, 09 Oct 2021 (Sat)
2PM, 07 Oct 2021 (Thu)
Initial Position
8AM, 08 Oct 2021 (Fri)
Legend
Philippine Atmospheric Geophysical and Astronomical Services Administration
Track of Tropical Depression "NANDO"
8AM, 09 Oct 2021 (Sat)
8PM, 09 Oct 2021 (Sat)
8AM, 08 Oct. 2021 (Fri)
Initial Position
Legend
Philippine Atmospheric Geophysical and Astronomical Services Administration

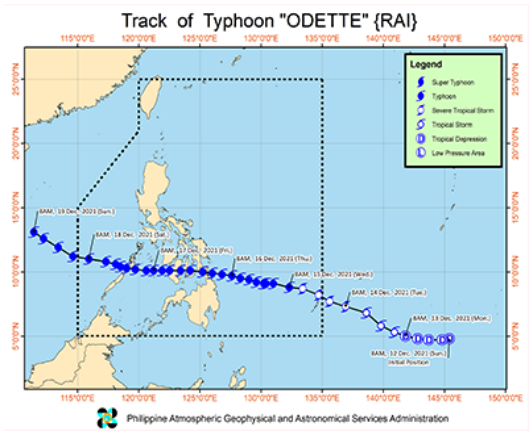
Track of Typhoon "ODETTE" {RAI}
Legend
Super Typhoon
Typhoon
Severe Tropical Storm
Tropical Storm
Tropical Depression
Low Pressure Area
Philippine Atmospheric Geophysical and Astronomical Services Administration

Appendix K.
Image Processing Code


```
#mount google drive
from google.colab import drive

drive.mount('/content/gdrive')
```

Import Train Data (CHL)

This code generates a coresponding value matrix of CHL from RGB transect colors

```
#Import Gsheets in Colab

from google.colab import auth
auth.authenticate_user()

import gspread
from google.auth import default
creds, _ = default()

gc = gspread.authorize(creds)

worksheet = gc.open('enrm290-ML-CHL').sheet1

# get_all_values gives a list of rows.
crows = worksheet.get_all_values()

# Convert to a DataFrame and render.
import pandas as pd
CHL=pd.DataFrame.from_records(crows)

#add columns in the data frame
CHL.columns = [
    "Red",
    "Green",
    "Blue",
    "ValCHL"
    ]

print(CHL)
#show the information of the data
CHL.info()
```

Save the X and Y into vectors

```
#independent var
cX = CHL.drop("ValCHL", axis=1) #remove the ValCHL column ##but the dataframe now is a string
cX = cX.values
#dependent var
cy = CHL["ValCHL"]
cy = cy.values

cX = cX.astype(float)
print(cX)

cy = cy.astype(float)
print(cy)
```

Import Train Data (SST)

This code generates a coresponding value matrix SST from RGB transect colors

```
#Import Gsheets in Colab

from google.colab import auth
auth.authenticate_user()

import gspread
```

```
from google.auth import default
creds, _ = default()

gc = gspread.authorize(creds)

worksheet = gc.open('enrm290-ML-SST').sheet1

# get_all_values gives a list of rows.
srows = worksheet.get_all_values()

# Convert to a DataFrame and render.
import pandas as pd
SST=pd.DataFrame.from_records(srows)

#add columns in the data frame
SST.columns = [
    "Red",
    "Green",
    "Blue",
    "ValSST"
    ]

print(SST)
#show the information of the data
SST.info()
```

Save the X and Y into vectors

```
#independent var
sX = SST.drop("ValSST", axis=1) #remove the ValCHL column ##but the dataframe now is a string
sX = sX.values
#dependent var
sy = SST["ValSST"]
sy = sy.values

sX = sX.astype(float)
print(sX)

sy = sy.astype(float)
print(sy)
```

Input Actual Data

```
#Import Gsheets in Colab CHL RGB DATA

from google.colab import auth
auth.authenticate_user()

import gspread
from google.auth import default
creds, _ = default()

gc = gspread.authorize(creds)

worksheet = gc.open('enrm290-ML-CHL-RGB').sheet1

# get_all_values gives a list of rows.
c_rgb_rows = worksheet.get_all_values()

# Convert to a DataFrame and render.
import pandas as pd
CHL_RGB=pd.DataFrame.from_records(c_rgb_rows)

#add columns in the data frame
CHL_RGB.columns = [
    "Index",
    "Transect",
    "Red",
    "Green",
    "Blue",
    ]
```

```
#print(SST_RGB)
#show the information of the data
CHL_RGB.info()


#Import Gsheets in Colab SST RGB DATA

from google.colab import auth
auth.authenticate_user()

import gspread
from google.auth import default
creds, _ = default()

gc = gspread.authorize(creds)

worksheet = gc.open('enrm290-ML-SST-RGB').sheet1

# get_all_values gives a list of rows.
s_rgb_rows = worksheet.get_all_values()

# Convert to a DataFrame and render.
import pandas as pd
SST_RGB=pd.DataFrame.from_records(s_rgb_rows)

#add columns in the data frame
SST_RGB.columns = [
    "Index",
    "Transect",
    "Red",
    "Green",
    "Blue",
    ]

#print(SST_RGB)
#show the information of the data
SST_RGB.info()
```

knn CHL

```
#print(CHL_RGB)
cdX = CHL_RGB.drop(["Index","Transect"], axis=1) #remove the Index column ##but the dataframe now is a string
cdX = cdX.values
cdX = cdX.astype(float)
print(cdX)


import numpy as np

CHL_rowsize=int(CHL_RGB.size/5)
a=[0]

for x in range(0,CHL_rowsize):
    new_data_point = cdX[x,:] #[start:end:step]
    #print(new_data_point)

    distances = np.linalg.norm(cX - new_data_point, axis=1)
    k = 3
    nearest_neighbor_ids = distances.argsort()[:k]
    nearest_neighbor_ids
    #array([4045, 1902, 1644], dtype=int32)
    nearest_neighbor_CHL = cy[nearest_neighbor_ids]
    nearest_neighbor_CHL
    #MODE not MEAN
    import scipy.stats
    #class_neighbors = np.array(["A", "B", "B", "C"])
    mode=scipy.stats.mode(nearest_neighbor_CHL)
    #print(mode[0])

    CHL_dataval = np.array(mode[0])
    b=np.vstack((a, CHL_dataval))
    a=b

val=b[1:]
```

knn SST

```
#print(SST_RGB)
sdX = SST_RGB.drop(["Index","Transect"], axis=1) #remove the Index & Transect column
sdX = sdX.values
sdX = sdX.astype(float)
print(sdX)


import numpy as np

SST_rowsize=int(SST_RGB.size/5)
a=[0]

for x in range(0,SST_rowsize):
    new_data_point = sdX[x,:] #[start:end:step]
    #print(new_data_point)

    distances = np.linalg.norm(sX - new_data_point, axis=1)
    k = 3
    nearest_neighbor_ids = distances.argsort()[:k]
    nearest_neighbor_ids
    #array([4045, 1902, 1644], dtype=int32)
    nearest_neighbor_SST = sy[nearest_neighbor_ids]
    nearest_neighbor_SST
    #MODE not MEAN
    from scipy import stats
    #class_neighbors = np.array(["A", "B", "B", "C"])
    mode=stats.mode(nearest_neighbor_SST, keepdims=False)
    print(mode[0])

    SST_dataval = np.array(mode[0])
    b=np.vstack((a, SST_dataval))
    a=b

val=b[1:]
```

Write to File

```
#%pwd

#change the directory to google desktop

%cd '/content/gdrive/Othercomputers/My Laptop/PhD/others/upou'

#check the working directory
#%pwd

import pandas as pd
pd.DataFrame(val).to_csv('SST-1-2021.csv')
```

Appendix L.
Linear Regression Results

SUMMARY OUTPUT

Regression Statistics	
Multiple R	0.650791805
R Square	0.423529973
Adjusted R Square	0.419227958
Standard Error	0.010920877
Observations	136

ANOVA

	df	*SS*	*MS*	*F*	*Significance F*
Regression	1	0.011741599	0.011741599	98.44920602	9.81594E-18
Residual	134	0.015981585	0.000119266		
Total	135	0.027723184			

	Coefficients	*Standard Error*	*t Stat*	*P-value*	*Lower 95%*	*Upper 95%*	*Lower 95.0%*	*Upper 95.0%*
Intercept	0.364919418	0.027242776	13.39508955	1.70254E-26	0.311037955	0.418800881	0.311037955	0.418800881
SST	-0.010383431	0.001046489	-9.922157327	9.81594E-18	-0.012453205	-0.008313658	-0.012453205	-0.008313658

a) 2019-2021

SUMMARY OUTPUT

Regression Statistics	
Multiple R	0.705231009
R Square	0.497350775
Adjusted R Square	0.485926929
Standard Error	0.010314718
Observations	46

ANOVA

	df	*SS*	*MS*	*F*	*Significance F*
Regression	1	0.004631964	0.004631964	43.53619393	4.44793E-08
Residual	44	0.00468131	0.000106393		
Total	45	0.009313273			

	Coefficients	*Standard Error*	*t Stat*	*P-value*	*Lower 95%*	*Upper 95%*	*Lower 95.0%*	*Upper 95.0%*
Intercept	0.452741011	0.054533264	8.302107327	1.49173E-10	0.342836439	0.562645583	0.342836439	0.562645583
SST	-0.013868681	0.00210189	-6.598196263	4.44793E-08	-0.018104761	-0.009632601	-0.018104761	-0.009632601

b) 2019

SUMMARY OUTPUT

Regression Statistics	
Multiple R	0.901926579
R Square	0.813471554
Adjusted R Square	0.809133683
Standard Error	0.003874051
Observations	45

ANOVA

	df	*SS*	*MS*	*F*	*Significance F*
Regression	1	0.002814469	0.002814469	187.5278412	2.79474E-17
Residual	43	0.000645356	1.50083E-05		
Total	44	0.003459825			

	Coefficients	*Standard Error*	*t Stat*	*P-value*	*Lower 95%*	*Upper 95%*	*Lower 95.0%*	*Upper 95.0%*
Intercept	0.309913534	0.016158191	19.17996429	1.07267E-22	0.277327436	0.342499633	0.277327436	0.342499633
SST	-0.008470018	0.000618517	-13.69408052	2.79474E-17	-0.009717375	-0.00722266	-0.009717375	-0.00722266

c) 2020

SUMMARY OUTPUT

Regression Statistics	
Multiple R	0.648243193
R Square	0.420219238
Adjusted R Square	0.407042402
Standard Error	0.011789143
Observations	46

ANOVA

	df	*SS*	*MS*	*F*	*Significance F*
Regression	1	0.004432301	0.004432301	31.89075537	1.11073E-06
Residual	44	0.006115291	0.000138984		
Total	45	0.010547592			

	Coefficients	*Standard Error*	*t Stat*	*P-value*	*Lower 95%*	*Upper 95%*	*Lower 95.0%*	*Upper 95.0%*
Intercept	0.358274458	0.045348764	7.900423963	5.6094E-10	0.266880031	0.449668886	0.266880031	0.449668886
SST	-0.009830167	0.001740718	-5.647190042	1.11073E-06	-0.013338354	-0.00632198	-0.013338354	-0.00632198

d) 2021

Appendix M.
NPP Estimation

```
fchl="CHL-Q4-2021.csv";
fsst="SST-Q4-2021.csv";
fdayL="DayLength.xls";

tab_chl=readtable(fchl);
tab_sst=readtable(fsst);
tab_dayL=readtable(fdayL);

npp0=0;
%let's compute per quadrant
for i=2:47 %47/46/47
    chl=tab_chl{i,2};
    sst=tab_sst{i,2};
    dayL=tab_dayL{i,4}; %change by year (2-4)
    %pb_opt
    if sst < -10.0
        pb_opt = 0.00;
    elseif sst <  -1.0
        pb_opt = 1.13;
    elseif sst >  28.5
        pb_opt = 4.00;
    else
        pb_opt = 1.2956 + (2.749*10^-1)*sst + (6.17*10^-2)*(sst^2) - (2.05*10^-2)*(sst^3)↙
+ (2.462*10^-3)*(sst^4) - (1.348*10^-4)*(sst^5) + (3.4132*10^-6)*(sst^6) - (3.27*10^-8)*↙
(sst^7);
    end
    %PAR
    irr=69;
    irrFunc = 0.66125*irr/(irr+4.1);
    %z_eu
   if (chl <  1.0)
     chl_tot = 38.0*(chl^0.425);
   else
     chl_tot = 40.2*(chl^0.507);
   end
    z_eu = 200.0*(chl_tot^-.293);
    if (z_eu <= 102.0)
        z_eu = 568.2*(chl_tot^-.746);
    end
    z_euf=z_eu;
    %NPP Proper
    npp = chl*pb_opt * dayL * irrFunc * z_euf;
    npp0=vertcat(npp0,npp);
end

nsize=size(npp0,1);
nppf=npp0(2:nsize,:);
```

```
%Plot NPP

%load NPP mats

%PLOT

nexttile
plot(nq1_2019, 'color','#EDB120')
hold on
plot(nq1_2020, 'color','#7E2F8E')
plot(nq1_2021, 'color','#77AC30')
hold off
ax.XLim = [0 46];
title("Quadrant 1")
xlabel('Month','FontWeight','bold')
legend('2019','2020','2021')
xticks([1 23])
xticklabels({'Jan 1','Jul 1'})
ylabel('npp mgC m-2 day-1',"Color",'k')

nexttile
plot(nq2_2019, 'color','#EDB120')
hold on
plot(nq2_2020, 'color','#7E2F8E')
plot(nq2_2021, 'color','#77AC30')
ax.XLim = [0 46];
title("Quadrant 2")
xlabel('Month','FontWeight','bold')
xticks([1 23])
xticklabels({'Jan 1','Jul 1'})
legend('2019','2020','2021')
hold off

nexttile
plot(nq3_2019, 'color','#EDB120')
hold on
plot(nq3_2020, 'color','#7E2F8E')
plot(nq3_2021, 'color','#77AC30')
hold off
ax.XLim = [0 46];
title("Quadrant 3")

xlabel('Month','FontWeight','bold')
xticks([1 23])
xticklabels({'Jan 1','Jul 1'})
legend('2019','2020','2021')

nexttile
plot(nq4_2019, 'color','#EDB120')
hold on
plot(nq4_2020, 'color','#7E2F8E')
plot(nq4_2021, 'color','#77AC30')
hold off
ax.XLim = [0 46];
title("Quadrant 4")
xlabel('Month','FontWeight','bold')
xticks([1 23])
xticklabels({'Jan 1','Jul 1'})
legend('2019','2020','2021')
```